

# **Develop and Implement a Freeze Thaw Model Based Seasonal Load Restriction Decision Support Tool**

**Final Report**

**Report Number: OR16-009**

Michigan Department of Transportation  
Office of Research Administration  
8885 Ricks Road  
Lansing, MI 48909

By

Zhen (Leo) Liu, Ting Bao, Michael Billmire, Stanley Vitton, John Bland, and Min Wang

Michigan Technological University  
1400 Townsend Drive  
Houghton, MI 49931

**August 2019**

## Technical Report Documentation Page

|  |   |   |                         |
|--|---|---|-------------------------|
| <b>1. Report No.</b><br>OR16-009   | <b>2. Government Accession No.</b><br>N/A                 | <b>3. MDOT Project Manager</b><br>Melissa Longworth   |                         |
| <b>4. Title and Subtitle</b><br>Develop and Implement a Freeze Thaw Model Based Seasonal Load Restriction Decision Support Tool  |   | <b>5. Report Date</b><br>August 2019  |                         |
|  |   | <b>6. Performing Organization Code</b><br>N/A   |                         |
| <b>7. Author(s)</b><br>Zhen (Leo) Liu, Stanley Vitton, Michael Billmire, and Min Wang  |   | <b>8. Performing Org. Report No.</b><br>N/A   |                         |
| <b>9. Performing Organization Name and Address</b><br>Michigan Technological University<br>1400 Townsend Drive<br>Houghton, MI 49931   |   | <b>10. Work Unit No. (TRAIS)</b><br>N/A   |                         |
|  |   | <b>11. Contract No.</b><br>2016-0067  |                         |
|  |   | <b>11(a). Authorization No.</b><br>Z9   |                         |
| <b>12. Sponsoring Agency Name and Address</b><br>Michigan Department of Transportation Research Administration<br>8885 Ricks Rd.<br>P.O. Box 30049<br>Lansing MI 48909   |   | <b>13. Type of Report &amp; Period Covered</b><br>Final Report<br>5/01/2017 to<br>3/1/2020  |                         |
|  |   | <b>14. Sponsoring Agency Code</b><br>N/A  |                         |
| <b>15. Supplementary Notes</b>   |   |   |                         |
| <b>16. Abstract</b><br>This report summaries a study on the development and implementation of a freeze thaw model based Seasonal Load Restriction (SLR) decision support tool. A multivariable prediction approach for freezing and thawing depths were proposed. The approach was implemented with input from weather data and Road Weather Information System (RWIS) data, leading to statistical models for site-specific predictions. Predictions made with the approach were validated against freezing and thawing depths calculated with subsurface temperatures measured by temperature sensors at the MDOT RWIS sites. A detailed procedure was proposed for predicting the start and end dates of the SLR policy, and this procedure was evaluated and validated with frost tube measurements and recorded SLR dates. The above freezing and thawing depth predictions and SLR date predictions were automated in a web-based app, i.e., <a href="http://www.mdotslr.org">www.mdotslr.org</a> , which is available to the public. For app, weather and RWIS data starting from 2013 and Geographic Information System (GIS) data covering Michigan were imported and managed as local databases on the backend server. In addition, daily weather and RWIS data including weather 5-day forecast were imported via APIs in real time for real-time for predictions of freezing and thawing depths and SLR dates. The app provides functions for predicting and visualizing temperature, freezing/thawing indices, degree of SLR, and SLR dates in terms of curves and contour maps. Maximum freezing depth contours can also be generated for any given period of time for pavement design and other purposes. All the data is available via the data portal of the app and can be downloaded. The study provides high-accuracy methods for predicting freezing and thawing depths and SLR dates and a convenient web-based tool for road engineers and users. |   |   |                         |
| <b>17. Key Words</b><br>Freeze-Thaw, Spring Load Restriction, Freezing Index, Frost Depth, Thawing Index, Thawing Depth, Road Weather Information System, Web-Based App  |   | <b>18. Distribution Statement</b><br>No restrictions. This document is available to the public through the Michigan Department of Transportation. |                         |
| <b>19. Security Classification - report</b><br>Unclassified  | <b>20. Security Classification - page</b><br>Unclassified | <b>21. No. of Pages</b>   | <b>22. Price</b><br>N/A |



## **Acknowledgment**

The authors like to thank the Michigan Department of Transportation (MDOT) for the financial support and the MDOT staff for their cooperation and for offering training, data, access to MDSS, feedback on preliminary results. In addition, the authors gratefully acknowledge the Minnesota Department of Transportation (MNDOT) for providing the MnROAD and SLR data and for its assistance. The authors want to extend their appreciation to the Transportation Research Board technical committee AFP50 Seasonal and Climatic Effects on Transportation Infrastructure for the feedback and technical support.

## **Research Report Disclaimer**

“This publication is disseminated in the interest of information exchange. The Michigan Department of Transportation (hereinafter referred to as MDOT) expressly disclaims any liability, of any kind, or for any reason, that might otherwise arise out of any use of this publication or the information or data provided in the publication. MDOT further disclaims any responsibility for typographical errors or accuracy of the information provided or contained within this information. MDOT makes no warranties or representations whatsoever regarding the quality, content, completeness, suitability, adequacy, sequence, accuracy or timeliness of the information and data provided, or that the contents represent standards, specifications, or regulations.”

## **App Disclaimer**

“This website is a prototype application under development to evaluate various seasonal load restriction models for Michigan roadways. It is a product of an ongoing joint research project between the [Michigan Department of Transportation \(MDOT\)](#) and [Michigan Technological University](#). This is an evolving prototype and is not used for the placement and removal of seasonal load restrictions.”

## **Executive Summary**

This report summarizes a study on the development and implementation of a freeze thaw model based Seasonal Load Restriction (SLR) decision support tool. A multivariable prediction approach for freezing and thawing depths were proposed. The approach was implemented with input from weather data and Road Weather Information System (RWIS) data, leading to statistical models for site-specific predictions. Predictions made with the approach were validated against freezing and thawing depths calculated with subsurface temperatures measured by temperature sensors at the MDOT RWIS sites. A detailed procedure was proposed for predicting the start and end dates of the SLR policy, and this procedure was evaluated and validated with frost tube measurements and recorded SLR dates. The above freezing and thawing depth predictions and SLR date predictions were automated in a web-based app, i.e., [www.mdotslr.org](http://www.mdotslr.org), which is available to the public. For app, weather and RWIS data starting from 2013 and Geographic Information System (GIS) data covering Michigan were imported and managed as local databases on the backend server. In addition, daily weather and RWIS data including weather 5-day forecast were imported via APIs in real time for real-time for predictions of freezing and thawing depths and SLR dates. The app provides functions for predicting and visualizing temperature, freezing/thawing indices, degree of SLR, and SLR dates in terms of curves and contour maps. Maximum freezing depth contours can also be generated for any given period of time for pavement design and other purposes. All the data is available via the data portal of the app and can be downloaded. The study provides high-accuracy methods for predicting freezing and thawing depths and SLR dates and a convenient web-based tool for road engineers and users.

# Table of Contents

|  |             |
|--|-------------|
| <b>Technical Report Documentation Page</b> .....                       | <b>ii</b>   |
| <b>Acknowledgment</b> .....  | <b>iv</b>   |
| <b>Research Report Disclaimer</b> .....                                | <b>iv</b>   |
| <b>App Disclaimer</b> .....  | <b>iv</b>   |
| <b>Executive Summary</b> .....   | <b>v</b>    |
| <b>List of Figures</b> .....   | <b>ix</b>   |
| <b>List of Tables</b> .....  | <b>xiii</b> |
| <b>Chapter 1 Introduction</b> .....                                    | <b>14</b>   |
| 1.1 Statement of the Problem.....                                      | 14          |
| 1.2 Objectives of the Study.....                                       | 16          |
| 1.3 Research Plan.....   | 17          |
| 1.4 Organization of This Report.....                                   | 21          |
| <b>Chapter 2 Literature Review</b> .....                               | <b>25</b>   |
| 2.1 Overview of SLR Practice.....                                      | 25          |
| 2.2 Relationship between SLR Practice and Freezing/Thawing.....        | 28          |
| 2.3 Prediction of Freezing and Thawing Depths.....                     | 31          |
| 2.4 Popular SLR Procedures based on Simple Weather Data.....           | 34          |
| 2.4.1 FHWA-WSDOT.....  | 34          |
| 2.4.2 MnDOT.....   | 35          |
| 2.4.3 MIT.....   | 37          |
| 2.4.4 SDDOT.....   | 38          |
| 2.4.5 USDA/FS-NHDOT.....   | 39          |
| <b>Chapter 3 Acquisition, Processing, and Evaluation of Data</b> ..... | <b>42</b>   |
| 3.1 Data Acquisition.....  | 42          |
| 3.1.1 Weather Data.....  | 42          |
| 3.1.2 Acquisition of RWIS Data.....                                    | 44          |
| 3.1.3 Integration of GIS and Soil Data.....                            | 46          |
| 3.2 Data Processing.....   | 49          |
| 3.2.1 Air and Pavement Surface Temperatures.....                       | 49          |

|  |   |           |
|--|---|-----------|
| 3.2.2  | Subsurface Temperatures .....   | 51        |
| 3.2.3  | Freezing and Thawing Depths .....   | 52        |
| 3.2.4  | Freezing and Thawing Indices .....  | 55        |
| 3.3  | Data Evaluation.....  | 58        |
| 3.3.1  | Issues in the RWIS Data .....   | 58        |
| 3.3.2  | Data Mapping (vRWIS) for Site-Specific Predictions.....                           | 60        |
| 3.3.3  | Data Selection via Correlation Analysis .....                                     | 61        |
| <b>Chapter 4 Multivariate Freezing-Thawing Depth Prediction Model .....</b>  |   | <b>64</b> |
| 4.1  | Overview .....  | 64        |
| 4.2  | Field Measurements .....  | 64        |
| 4.3  | A New Freezing-Thawing Depth Prediction Model.....                                | 66        |
| 4.4  | Prediction and Evaluation of Freezing-Thawing Depth Model .....                   | 70        |
| 4.5  | Discussions .....   | 76        |
| 4.5.1  | Calculations of FI and TI via Surface Temperature Rather than Air Temperature ..  | 76        |
| 4.5.2  | Prediction Improvement.....   | 78        |
| 4.6  | Conclusions.....  | 80        |
| <b>Chapter 5 Freezing-Thawing Depth Prediction with Constrained Optimization for Applications of Spring Load Restriction .....</b> |   | <b>81</b> |
| 5.1  | Overview .....  | 81        |
| 5.2  | Introduction.....   | 81        |
| 5.3  | Theory and Method.....  | 83        |
| 5.3.1  | Field Measurements and SLR Determination Method .....                             | 83        |
| 5.3.2  | Freeze-Thaw Depth Prediction Model with Constrained Optimization .....            | 86        |
| 5.4  | Results.....  | 89        |
| 5.4.1  | Site Measurements .....   | 89        |
| 5.4.2  | Application of Constrained Optimization for FD/TD Predictions.....                | 94        |
| 5.5  | Discussions .....   | 98        |
| 5.5.1  | Advantages of Using Constrained Optimization for FD/TD Predictions .....          | 98        |
| 5.5.2  | Feasibility of Using Year Cycle 1 Fitting Constants to Predict Year Cycle 2 FD/TD |           |
|  | 99  |           |

|   |   |            |
|---|---|------------|
| 5.5.3   | FD/TD Prediction Models are Better than a TI/FI Ratio for SLR Decision-Making | 100        |
| 5.6   | Conclusions.....  | 102        |
| <b>Chapter 6 Development of Web-Based Spring Load Restriction Decision Support Tool</b> |   |            |
| <b>104</b>  |   |            |
| 6.1   | Abstract.....   | 104        |
| 6.2   | Goals for the App Development.....  | 105        |
| 6.2.1   | Objectives.....   | 105        |
| 6.2.2   | Features and Benefits.....  | 105        |
| 6.3   | Models and Data.....  | 107        |
| 6.3.1   | Models.....   | 107        |
| 6.3.2   | Composite Data Mapping Service.....   | 109        |
| 6.3.3   | Optimization of MongoDB Queries.....  | 110        |
| 6.4   | Functions and Organization of the APP.....                                    | 110        |
| 6.5   | Construction of the App.....  | 115        |
| 6.5.1   | Data Transfer and Workflow.....   | 115        |
| 6.5.2   | Development of the Web-Based App.....   | 116        |
| 6.5.3   | Freezing/Thawing Index Acquisition on Backend.....                            | 117        |
| 6.5.4   | Freezing/Thawing Depth Acquisition on Backend.....                            | 119        |
| 6.5.5   | Refactoring.....  | 122        |
| 6.5.6   | Map Binary Search.....  | 124        |
| 6.6   | Conclusions.....  | 126        |
| <b>References.....</b>  |   | <b>135</b> |

## List of Figures

|  |    |
|--|----|
| Figure 1.1 Major components of the planned research product.....   | 22 |
| Figure 2.1 SLR practices in the U.S. and Canada.....   | 26 |
| Figure 2.2 SLR decisions based on freezing/thawing depth predictions (modified after (Baiz et al. 2008)).....                        | 28 |
| Figure 2.3 Maximum predicted TDs vs measured TDs from measurement sites in Michigan (data is from (Baladi and Rajaei 2015)).....     | 30 |
| Figure 2.4 Statistical models for data from MDOT Project RC1609 .....  | 33 |
| Figure 3.1 Average air temperatures and pavement surface temperatures for the five selected sites .....                              | 50 |
| Figure 3.2 Pavement base temperatures for the five selected sites.....   | 52 |
| Figure 3.3 Calculation of freezing and thawing depths based on subsurface temperature measurements.....                              | 53 |
| Figure 3.4 Calculations of measured FDs and TDs for the five selected sites .....  | 55 |
| Figure 3.5 Calculation of freezing and thaw indices .....  | 56 |
| Figure 3.6 FI/TI calculated with the pavement surface temperature: (a) Harvey and (b) Michigamme .....                               | 57 |
| Figure 3.7 Pavement temperature calculation with measurements from nearby RWIS sites.....  | 60 |
| Figure 3.8 Correlation analysis for data selection in predictions of freezing and thawing depths and SLR dates (Site Fife Lake)..... | 62 |
| Figure 3.9 Correlation analysis for data selection in predictions of freezing and thawing depths and SLR dates (Site Eastport).....  | 63 |

|   |                                     |
|---|-------------------------------------|
| Figure 3.10 Correlation analysis for data selection in predictions of freezing and thawing depths and SLR dates (Site Cadillac South).....  | 63                                  |
| Figure 4.1 Overview of monitored sites with ESSs in Michigan .....  | 65                                  |
| Figure 4.2 Field measurement results of TI-FD relationships from ten sites in Michigan.....   | 67                                  |
| Figure 4.3 Schematic of 3D model and its project on the FD plane <b>Error! Bookmark not defined.</b>  |                                     |
| Figure 4.4 Schematic of 3D model and its project on the TD plane <b>Error! Bookmark not defined.</b>  |                                     |
| Figure 4.5 Fitting surfaces for Harvey: (a) FD fitting, (b) TD fitting with the whole TD data, (c) TD fitting with the thawing cycle data .....   | <b>Error! Bookmark not defined.</b> |
| Figure 4.6 Fitting surfaces for FD and TD: (a) Michigamme, (b) Seney, (c) Charlevoix, and (d) Glennie .....   | <b>Error! Bookmark not defined.</b> |
| Figure 4.7 Locations of additional sites in Michigan .....  | 75                                  |
| Figure 4.8 Comparisons of FI/TI calculated with the pavement surface temperature and the average air temperature: (a) Harvey and (b) Michigamme .....                                     | 77                                  |
| Figure 4.9 Fitting lines for Harvey: (a) FD fitting, (b) TD fitting with the thawing cycle data ...   | 78                                  |
| Figure 4.10 Comparison of the maximum measured TDs and predicted TDs .....  | 79                                  |
| Figure 5.1 Measured vs predicted data for FD and TD [data is from (Baiz et al. 2008)]. Note that predicted TD and FD trends are obtained using the thawing season fitting constants. .... | 82                                  |
| Figure 5.2 Monitoring sites in Michigan and selected sites location for analyses. Data is from the Michigan SLR website ( <a href="https://mdotslr.org">https://mdotslr.org</a> ) .....   | 84                                  |
| Figure 5.3 Schematic of a test road pavement cross section.....   | 85                                  |
| Figure 5.4 SLR decision-making based on the theory proposed by (Baiz et al. 2008) .....   | 85                                  |
| Figure 5.5 Conceptual flowchart of the FD/TD prediction model implementation for SLR .....  | 86                                  |

|   |     |
|---|-----|
| Figure 5.6 Measured air and pavement surface temperatures for Year Cycle 2017-2018 .....  | 90  |
| Figure 5.7 Measured air and pavement surface temperatures for Year Cycle 2018-2019 .....  | 91  |
| Figure 5.8 Measured FDs and TDs with FI/TI calculated using the pavement surface temperature for Year Cycle 2017-2018. Data within circles will be excluded in the fitting analysis ..... | 92  |
| Figure 5.9 Measured FDs and TDs with FI/TI calculated using the pavement surface temperature for Year Cycle 2018-2019. Data within circles will be excluded in the fitting analysis ..... | 93  |
| Figure 5.10 Predictions of FD and TD with the measured data for Year Cycle 2017-2018. Circled data Fig. 7 are excluded .....  | 94  |
| Figure 5.11 Predictions of FD and TD with the measured data for Year Cycle 2018-2019. Circled data Fig. 8 are excluded .....  | 95  |
| Figure 5.12 Comparison of FD/TD predictions with non-constrained and constrained optimization for Seney during 2017-2018 .....  | 98  |
| Figure 5.13 Comparison of FD/TD predictions with non-constrained and constrained optimization in Michigamme and Seney for Year Cycle 2017-2018 .....                                      | 100 |
| Figure 6.1 SLR decisions with freezing/thawing depth predictions (Baiz et al. 2008) .....   | 108 |
| Figure 6.2 Homepage of MDOT SLR App .....   | 111 |
| Figure 6.3 Page of temperature, F/T indices & SLR prediction .....  | 111 |
| Figure 6.4 Maps of freezing indices (a), thawing indices (b), and RWIS stations (c).....  | 112 |
| Figure 6.5 SSURGO soil data of the selected station (a) and daily weather data of the selected station (b) .....  | 114 |
| Figure 6.6 Predicted variation of freezing/thawing depth .....  | 114 |
| Figure 6.7 Measured variation of freezing/thawing depth.....  | 115 |
| Figure 6.8 The calculation framework of the web-based tool .....  | 116 |

|   |     |
|---|-----|
| Figure 6.9 Variation of freezing and thawing depth with time.....   | 122 |
| Figure 6.10 The first picture shows the re-factored code, it is all on one indent and uses await calls instead of callbacks ..... | 124 |
| Figure 6.11 Schematic of map binary search: original map .....  | 124 |
| Figure 6.12 Schematic of map binary search: one box.....  | 125 |
| Figure 6.13 Schematic of map binary search: refined boxes .....   | 125 |

## List of Tables

|  |     |
|--|-----|
| Table 1.1 Relationship between research tasks, chapters, and research products .....           | 23  |
| Table 2.1 Critical thawing index for SLR placement in SDDOT procedure.....                     | 39  |
| Table 2.2 Critical thawing index for SLR placement in SDDOT procedure.....                     | 39  |
| Table 3.1 Part of the historical data at RWIS Site Seney .....                                 | 58  |
| Table 3.2 Gaps in the historical data at RWIS Site Trout Creek Ess.....                        | 59  |
| Table 4.1 Needed parameters for analyses .....   | 66  |
| Table 4.2 Fitting results for the five selected sites.....                                     | 74  |
| Table 4.3 Prediction results for additional sites.....   | 75  |
| Table 5.1 Fitting results for FD and TD .....  | 96  |
| Table 5.2 Site SLR determination.....  | 96  |
| Table 5.3 Ratios between TI and FI on the SLR removal date.....                                | 101 |
| Table 5.4 SLR removal dates at three additional sites in the Superior region in Michigan ..... | 101 |

# Chapter 1 Introduction

## 1.1 Statement of the Problem

Spring (or Seasonal) Load Restriction (SLR) policies that limit the axle loads of trucks have been implemented in many states of the United States and other countries to minimize costly roadway damage that occurs in seasonally frozen areas during the annual spring thaw and strength recovery period (Zarrillo et al. 2012). This is because concrete and asphalt, though look indestructible, can actually be quite fragile in late winter as frost comes out of the ground (CRAM 2019). The frost accumulates during the freezing season (Baiz et al. 2008) due to the sub-freezing air temperatures leads to accumulated ice in the pavement structure and subgrade soils (Liu et al. 2012; Liu and Yu 2011). This ice results from the phase change of both the in-situ pore water and that sucked from deeper locations such as the phreatic zone below the groundwater table, depending on the frost susceptibility of the soils (Baladi and Rajaei 2015; Konrad and Morgenstern 1982; Konrad and Shen 1996). In the following thawing stage in spring, i.e., March, April, and May in Michigan (michigan.gov), thawing starts from both above and below the frozen layer. The resultant liquid water on the top of the frozen layer may not efficiently drain out of the soil, as the surrounding soil remains frozen and impermeable (C-SHRP 2000). The soil then becomes temporarily saturated with water, appears “spongy”, and loses its strength to support the above pavement, leading to thaw-weakening. Paved roads with thin overlays may lose more than 50 percent of their bearing capacity in spring whereas a gravel road, built without sufficient base course thickness, may lose 70 percent (Isotalo 1993). When trucks and heavy equipment travel over a layer of concrete or asphalt that is not well supported from beneath due to this thawing weakening, lots of permanent cracks can occur and water pumping through cracks in the roadway can be observed (Marquis 2008). Therefore, the SLR and the associated pavement issues are closely related to the freeze-thaw cycles and the status of the pavement and subgrade soils. Such issues are especially obvious in secondary (low volume) roads, e.g., county roads, city streets, and farm-to-market roads, the majority of which are not designed with layer thicknesses to provide adequate protection against freezing as those in interstate and primary roads (Baladi and Rajaei 2015).

Road commissions such as DOTs and local road agencies use SLR policies to preserve the public’s investment in the existing pavement structure by both reducing the costs of road repair for damages

occurring in the spring thaw season (Isotalo 1993) and elongating the service life of the roads (C-SHRP 2000). However, the SLR policy needs to be applied by striking a balance between “business as usual” and protecting the roads (CRAM 2019). The SLR usually involves mandatory reductions in the maximum axle load and in the maximum travel speeds for certain vehicles. When an SLR sign is active in a specific area, taking Michigan for example, the maximum axle load allowable on concrete pavements or pavements with a concrete base is reduced by 25% from the maximum axle load, and the maximum axle loads allowable on all other types of roads are reduced by 35% from the maximum, except as provided in several other conditions (<http://www.legislature.mi.gov>, Section 257.722(8)).

Such SLR policies, which can effectively protect the roads, however, can increase the cost to the industry due to the increasing trucking costs of hauling multiple, lighter loads on the highway system, or delaying delivery until the movement of oversize/overweight goods are allowed. A report published by the World Bank (Ray et al. 1992) established that the estimated savings associated with the implementation of SLRs are substantial, ranging from 40% up to 92%, with an average of 79% for the countries analyzed. The United States Federal Highway Administration (FHWA) also investigated the benefits of SLRs in 1990. The results indicated that SLRs can significantly extend the useful pavement life, e.g., a 20% and 50% of pavement load reduction lead to 62% and 95% of pavement life increase, respectively (FHWA 1990). The cost of SLRs includes direct costs to road users due to reductions of speeds and increases in traveling distance and indirect costs to the economy due to lower utilization of vehicle capacity and disturbed business, both of which are hard to quantify. An economic study sponsored by MnDOT (Smalkoski and Levinson 2003) reported an increase of 30.4%, 30.9%, and 6.3% in truck distance traveled in Lyon, Olmsted, and Clay counties, respectively, if SLR is implemented strictly on all 5, 7, and 9-ton roads.

Regardless of the benefits and costs of the SLR policy, one key to the success of the SLR placement is accurate timing for setting and removing the SLR to maximize industry’s time to prepare for the restrictions and minimize the time to lift the restrictions. This study is proposed to provide an SLR decision support tool for MDOT and local road agencies. The tool is developed based on the existing SLR practices in other states, a scientific understanding of the physical processes, existing models for freezing/thawing depth predictions, and available criteria and protocols for placing and

lifting SLRs. All of these are detailed in the following chapter for literature review. The proposed work will also be built on the PI team' expertise (frozen soil, MDOT pavement work, statistics, and software development), existing resources of MDOT (RWIS information, MDOT Report RC1619, experience of MDOT engineers and local experts), and other significant Weather and GIS data resources (NOAA, AccuWeather; MDEQ GeoWebFace, USDA Web Soil Survey).

## **1.2 Objectives of the Study**

The overall objective of the project is to establish a thawing model and a process for setting and removing SLRs in a manner that will give industry the most amount of time to prepare for the restrictions and minimize the time to lift the restrictions based on the MDOT Project RC 1619. The overall objective will be accomplished through a series of objectives and tasks leveraging existing research, technology, and resources that MDOT already has in place. The objectives of this research proposal matching MDOT's priorities as stated in the request for proposal are as follows.

1. Evaluate existing thawing/freezing depth prediction models, practice for SLR in state DOTs and MDOT's needs and available resources, and based on that, determine if existing thawing depth models suffice for application as a decision support tool for Michigan or if a refined model would be prudent. **(Task 1)**
2. Identify the type, sources, and format of the soil and weather information used for analysis by the decision support tool. **(Task 2)**
3. Building on this project and the research of RC 1619, develop a thawing depth prediction model that utilizes the existing data sources in Objective 2. **(Task 3)**
4. Explore and evaluate the data from the Road Weather Information System (RWIS) sites of the Michigan Department of Transportation with virtual Road Weather Information System (RWIS) sites. **(Tasks 6)**

5. Develop a user-friendly decision support tool that could be easily utilized by public and private sector in estimating potential thaw conditions and setting of SLRs for any location on the MDOT road network. **(Task 5)**
6. Recommend processes for predicting the time to post and remove SLR signs to protect the pavement structures from excessive damage during the spring thaw season. **(Tasks 4)**
7. Identify opportunities to collect, present, and apply data to help refine pavement designs in Michigan. **(Task 6)**
8. Develop professional training materials and course for training MDOT staff in the use of the decision support tool. **(Task 7)**

The above eight objectives will be achieved via seven tasks, which are marked accordingly in the parentheses after each objective.

### **1.3 Research Plan**

This section outlines the research tasks and the major objectives and action items for each task.

#### **Task 1 A Comprehensive Survey on Thaw Depth Predictions, DOT SLR Practices, and MDOT's Needs and Resources**

The objective of the first task is threefold.

- ❖ Conduct a detailed review of existing freezing/thawing depth prediction models: origin, way of application, and performance especially in pavement applications to better guide the later statistical model development
- ❖ Obtain a detailed documentation and comparison of DOT SLR practices in the U.S. and Canada: theory, procedure, technical difficulties, usefulness and acceptance in local agencies, land users and field engineers, plans for further improvement will be collected via communications with these DOTs (Kestler et al. 1998)

- ❖ Acquire a clear understanding of the MDOT's needs and resources via communications with MDOT officials, field engineers, and county road commission engineers

### **Task 2 Data Type Selection for the Freeze/Thaw Depth Prediction Model**

Task 2 is proposed to find out 1) what will be the input for the freeze/thaw prediction models, and 2) what will be the sources and formats of such input data.

- ❖ The task is conducted on the basis of the widely-adopted air-temperature-based practices for freezing/thawing depth and SLR date predictions including MDOT project **RC 1619**.

- ❖ Three categories of data are considered:

1. Weather: air temperature (1), wind speed (2), and solar irradiation (3);
2. Soil: thermal diffusivity (4), hydraulic conductivity, saturation (5), susceptibility, water table;
3. Pavement: type (6), layers, thickness (7), snow coverage, surface (absorptivity, convective heat transfer).

Items 1, 2 and 3 will come from weather websites; Items 4 and 5 will be estimated with soil types and groundwater information from GIS sites; Items 6 and 7 will come from MDOT, local agencies or the users.

- ❖ The data evaluation and selection are carried out with the automatic data acquisition by means of Application Programming Interfaces (APIs) in Task 6.

### **Task 3 Development and Validation of the Freeze/Thaw Depth Prediction Model**

- ❖ The development of models will be performed based on the major conclusions of MDOT Project RC 1619: statistical models are preferred over mechanistic models

- ❖ Data in Task 2 will be split into two parts: training and validation. Employ cross-validation study to quantitatively measure the accuracy of the model with the selected important predictors.
- ❖ Site-specific models are attempted. The models are created for MDOT RWIS sites where valid data is available for more accurate predictions at different geographic locations.

#### **Task 4 Development and Validation of SLR Decision Procedure**

- ❖ The establishment of the procedure will start from existing models: Mahoney et al. (1986) model for WSDOT and FHWA, the Berg model (Berg et al. 2006), and (Kestler et al. 2007) for the US Forest Service which was initially used by the NH DOT, the MnDOT Models (Van Deusen et al. 1998), and the MIT method (Bradley et al. 2012).
- ❖ The proposed procedure is evaluated against available Michigan data
  - If yes, choose the best model
  - If no, adjust the model(s) with Michigan-specific data
- ❖ Validate the suggested model against independent data: historical data, field data from other sources and additional frost tube data (if needed) for specific locations

#### **Task 5 Development of a Web-Based SLR Decision Support Tool**

A web-based tool will be developed based on the above model for assisting SLR decisions to allow MDOT, local road agencies, and road users to better predict the dates for SLR placement and lifting. The tool will be developed as a web-based app that will be accessible from any electronic device with Internet access and a web browser.

- ❖ Front-end: Write web pages using HTML5 and CSS3. The adaptive web design approach for all major types of electronic devices, i.e., desktops, tablets, and mobile phones. JQuery,

a JavaScript library, will be used to enhance the functionality and user-friendliness of the front-end webpages.

- ❖ Front-end Back-end Communication: Data transfer between the front-end and the server will be conducted via JSON. Node.js and Python are used to manage the data retrieval from weather and GIS sites.
- ❖ Back-end: The calculation process will be programmed on the server side using Python to shorten the development cycle. Weather and GIS information is obtained via the APIs and stored as local databases.
- ❖ The calculation results are shown as charts and tables on the webpages using open-source third-party JavaScript libraries such as JFreeChart or D3.js.

#### **Task 6 Potential RWIS Sites and Pavement Design**

- ❖ Evaluate the current RWIS data based on predictions of freezing and thawing depths and SLR dates. Identify a way to make site-specific predictions via the concept of virtual RWIS (vRWIS).
- ❖ The maximum historical freezing depth is one of the most critical parameters for pavement design in seasonal-frozen areas such as Michigan. This task aims to find a way to calculate and illustrate the maximum freezing depth in Michigan over a given period of time.

#### **Task 7 Final Report and Training Materials**

The final task is for writing the final report and preparing the training materials for MDOT.

- ❖ Final report
  - Takes 6 to 8 weeks
- ❖ Training Materials

- Take 4-6 weeks
- For a half-day event
- Part 1: a general introduction to freezing/thawing depth predictions and SLR and the project work; Part 2: a demonstration session for the web-based tool in various typical scenarios using different electronic devices; Part 3: several practice cases; Part 4: suggestions for vRWIS sites and better pavement design.

## **1.4 Organization of This Report**

This report is organized into 6 chapters and an appendix. The contents of each chapter can be seen in the Table of Contents. The titles of the chapters are listed below.

Chapter 1 Introduction

Chapter 2 Literature Review

Chapter 3 Acquisition, Processing, and Evaluation of Data

Chapter 4 Multivariate Freezing-Thawing Depth Prediction Model

Chapter 5 Freezing-Thawing Depth Prediction with Constrained Optimization for Applications of Spring Load Restriction

Chapter 6 Development of Web-Based Spring Load Restriction Decision Support Tool

The major objective of the project is to develop a web-based app to assist MDOT engineers and road users in SLR decisions. Therefore, the app is a major research product. To produce a functional and useful tool, the app needs to be running on models that guide the predictions of SLR dates in a convenient and accurate way. As the SLR dates rely on the freezing and thawing depths, models for the accurate predictions of freezing and thawing depths are also needed. Due to this reason, models including those for both freezing and thawing depths and SLR dates are sought to support the establishment and operation of the app. Data are needed for the development of the models. Hence, data should be another significant component of the planned research. Especially,

we will need to collect the data to be used, process the data for the model development and validation, evaluate the data for possible issues, and select appropriate data types for creating and running implementable models. In summary, as shown in Figure 1.1, the major research products consist of three components: app, data, and models. By analogy, the app is the body, by which an intelligent creature interacts with the environment and realizes its major functions; models are the brain, which determines how the body (app) interact with the environment; data are the food, which helps build up the brain (models). The app can become more and more robust as models are improved with more and more data, and the data can be obtained, processed, and managed by the app, leading to a closed loop and a healthy research and development ecosystem.

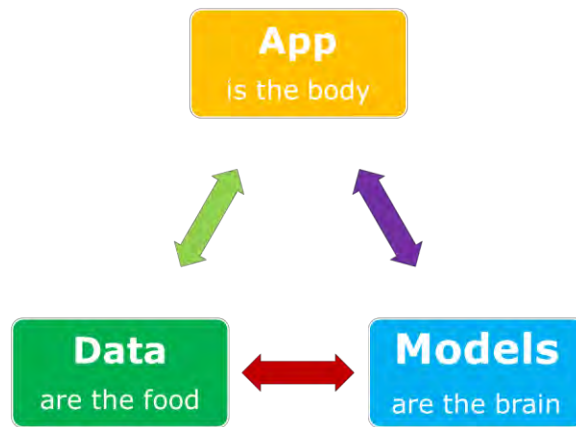


Figure 1.1 Major components of the planned research product

There are also clear relationships between the research tasks, chapters, and the above major components of the research products. A clear mapping as illustrated as Table 1.1 can be used to understand these relationships. Chapter 1 offers an overview of the whole project, laying down the statement of the problem, objectives of the study, research plan with detailed research tasks, and organization of the report. The effort made in Task 1 is detailed in Chapter 2, leading to a literature review on SLR practices, the relationship between SLR practice and freezing and thawing depths, predictions of the depths, and popular SLR procedures based on simple weather data. The data work in Task 3, including acquisition, preprocessing, evaluation, and selection, is detailed in Chapter 3. The data work in Task 2 (Chapter 3) includes both data analysis research associated with model development and data operations associated with app development, so it is entangled

with model development work in Chapter 4 and Chapter 5 and app development work in Chapter 6. Chapter 4 and Chapter 5 presents the research for developing the models for the predictions of freezing and thawing depths and SLR dates. While Chapter 4 discusses a basic model for freezing and thawing depth predictions, Chapter 5 introduces how to advance the basic model in Chapter 4 and apply this model for the prediction of SLR dates. The app uses the models in Chapter 5, though Chapter 4 is needed to understand these models. Finally, the development of the app is introduced in Chapter 6. Task 7 is about the development of reports and training materials.

Table 1.1 Relationship between research tasks, chapters, and research products

| Task   | Chapter          | Major Products |
|--------|------------------|----------------|
| Task 1 | Chapter 2        | Preparation    |
| Task 2 | Chapter 3        | Data           |
| Task 3 | Chapters 4&5     | Models         |
| Task 4 | Chapters 4&5     | Models         |
| Task 5 | Chapter 6        | App            |
| Task 6 | Chapters 3,4&5,6 | Models & App   |
| Task 7 |                  |                |

As can be seen, different tasks do not take equal space in this report. This is due to the following reasons.

- ❖ Some tasks are more labor-intensive and less intellectually challenging and thus demands less explanation such as Task 2 and Task 6, while some others require more original research work but requires less labor such as Task 3 and Task 4 and consequently take more space for their explanations.
- ❖ Tasks are not totally independent of each other. For example, the development of freezing/thawing depth prediction models and SLR date predictions models are closely related. Therefore, introductions to the research work for Task 4 and Task 5 are housed in both Chapter 4 and Chapter 5.
- ❖ Tasks may not correspond to an independent piece of work. For example, Task 6 includes vRWIS data mapping and work for pavement design and these correspond to multiple

pieces of work that are needed for the work introduced in Chapters 3-6 and they do not need a lot of effort to explain. Therefore, these pieces of work are introduced in these chapters instead of as an independent chapter.

## Chapter 2 Literature Review

### 2.1 Overview of SLR Practice

The use of SLR has a long history, for example, the SLR policy in Minnesota was enacted in 1937 (Minnesota Statute 169.87) and has been periodically updated. Traditional methods count on engineers' experience and visual observations in situ. For example, the SLRs in Maine were placed based on visual observations such as water pumping from cracks or roadway frost deformation (Marquis 2008). As summarized in the classic report of Mahoney et al. (1987), agencies initiated limits based on judgments, which could range from evidence of water at the surface (indicating a saturated base) to signs of cracking (which is too late) or simply relied on an established date. SLR is needed because thawing weakening can cause more than

- ❖ 50% loss in the bearing capacity for normal roads
- ❖ 70% loss for gravel roads (without sufficient base course thickness) (Isotalo 1993)
- ❖ more obvious in secondary roads

On the contrary, an unnecessarily long period for SLR will also cause an economic loss due to non-usage of the roads.

A survey (Kestler et al. 2007; Kestler et al. 1998) of the practices of 45 state DOTs and 3 forest service regional offices, as shown in Figure 2.1, revealed that 24% of the agencies used quantitative methods (FWD, frost tubes or thaw index) to impose SLR, while 45% of agencies used inspection and observation. The remaining 25% relied on a fixed date method. The removal of the SLR was made quantitatively in 14% of the agencies, 57% by inspection and observation and 29% by date. In Michigan, as described on the CRA website, the road commissions employ licensed Professional Engineers to make these decisions and also consult neighboring road agencies.

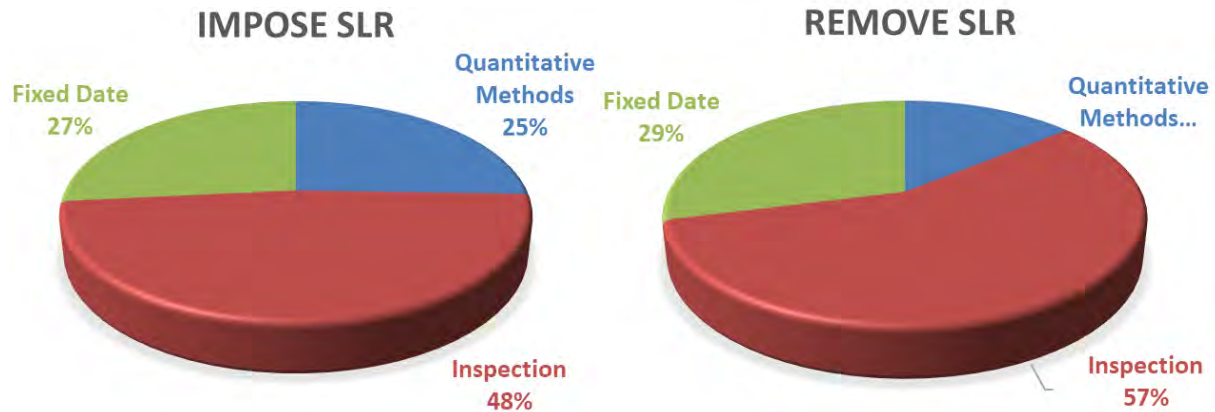


Figure 2.1 SLR practices in the U.S. and Canada

Despite the historical statistics, more and more agencies are switching to or plan to switch to quantitative SLR decision algorithms. Several agencies in the United States and Canada have performed research which addresses the question of monitoring roadways and posting SLRs (Eaton et al. 2009; Eaton et al. 2009; Embacher 2006; Hanek et al. 2001; Kestler et al. 2007; Marquis 2008; McBane and Hanek 1986; Ovik et al. 2000; Yesiller et al. 1996).

Typical approaches for determining SLR dates can be summarized as the following categories (Kestler et al. 2007; Kestler et al. 1998):

- ❖ Fixed dates
- ❖ Observations such as water seeping out of cracks (usually too late)
- ❖ Frost tube monitoring-SLR is set on and off according to critical depths
- ❖ Temperature measurement with thermistors/thermocouples: freezing and thawing depths can be inferred from the measurements and SLR dates can be determined similar to the methods using frost tubes.
- ❖ Moisture measurement: status of the pavement and subgrade is analyzed with measurements from Time Domain Reflectometry (TDR) or Frequency Domain (FD) sensors for the determination of SLR dates

- ❖ Deflection: stiffness of the pavement and subgrade is measured with Falling Weight Deflectometer (FWD) or Light Weight Deflectometer (LWD) for the determination of SLR dates
- ❖ Freezing/Thawing Index or other weather data: simple meteorological/weather data, e.g., air/pavement temperature or freezing/thawing indices calculated with the temperature, was used to analyze the accumulation of freezing or thawing in the pavement and subgrade for the determination of SLR dates
- ❖ Mechanistic Model such as MEPDG (Kestler et al. 2007), CHEVRON (Everseries suite)-USDA/FS , UNSAT-H (RC1619), ECIM/Clarus Initiative (Cluett et al. 2011): the behavior of pavement (and subgrade) is analyzed to obtain the SLR dates.

Among the above categories of methods, the existing efforts have produced several popular methods for the determination of the placement and removal dates or the duration of the SLR. The category is based on simple meteorological/weather data, especially air/pavement temperature or freezing/thawing indices calculated with the temperature, and has been adopted by many state transportation agencies and county engineers. The popularity of this category of methods is attributed to the simplicity and relatively good performance of such approaches. Many agencies in the U.S. and Canada are trying to adopt quantitative SLR decision algorithms using the Freezing Depth (FD) and the Thawing Depth (TD) predicted based on the Freezing Index (FI) and/or the Thawing Index (TI).

These include the method proposed by (Rutherford et al. 1985) and (Mahoney et al. 1987) for the State of Washington Department of Transportation and the Federal Highway Administration (FHWA), which was the first widely accepted analytical method. The method involved freezing and thawing index and set up a paradigm for following methods. (Berg et al. 2006) and (Kestler et al. 2007) described the procedure originally developed for the US Forest Service and initially used by the NHDOT. It was similar to the WSDOT and FHWA method, where SLR application and removal dates are determined using air freezing and thawing indices. (Van Deusen et al. 1998) revised the FHWA procedure to better apply to Minnesota conditions. MnDOT recommended applying the SLR based upon a cumulative thawing index (CTI) threshold of 25°F-days, which is calculated by following a specific calculation procedure. Manitoba Department of Infrastructure

and Transportation (MIT) in Canada recommended applying the SLR at a CTI threshold value of 27°F-days and they computed the CTI (°F-days) by taking into account the influence of pavement surface temperatures. MIT recommended an ending threshold set to the sooner of 56 days (8 weeks) from start of the SLR or when CTI reaches 630 °F-days. Further method and procedure details will be discussed in Task 4.

## 2.2 Relationship between SLR Practice and Freezing/Thawing

In order to determine the placement and removal dates of SLR, accurate predictions of FD and TD, especially the latter one, are essential to prevent the extensive damage to the pavement due to the late placement or early removal of SLR. As explained by Baiz et al. (2008), the SLR placement corresponds to the time when the continuous thawing starts in the subgrade soils, as illustrated by the yellow square in Figure 2.2. The SLR removal should take place after TD meets FD in the thawing season, i.e., the green square in Figure 2.2, which was also adopted by Chapin et al. (2012).

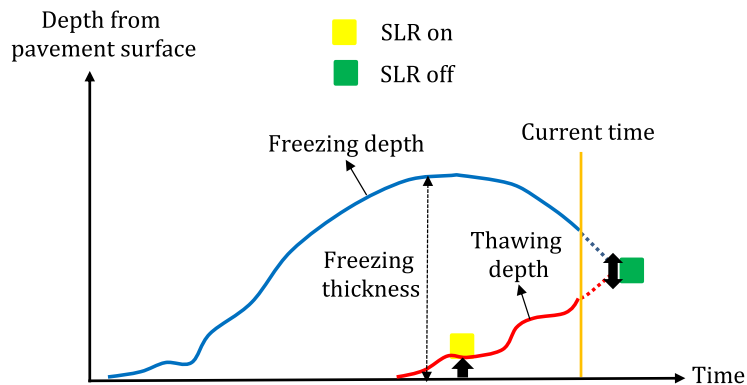


Figure 2.2 SLR decisions based on freezing/thawing depth predictions (modified after (Baiz et al. 2008))

For FD predictions, three major types of prediction models were widely utilized in the U.S. and Canada: the mechanistic model, the classic physico-empirical model, and the empirical model. The mechanistic models (Cluett et al. 2011; Fayer and Jones 1990) were usually developed based on

the physical process from a continuum mechanics perspective by considering heat transfer (Fourier's equation) and water movement (modified Richards' equation) in soils. The physico-empirical models, e.g., the Neumann' empirical model (Jiji and Ganatos 2009), the Stefan's equation (Jiji and Ganatos 2009), and the Modified Berggren equation (ACE-US 1984; Aldrich and Paynter 1953), were developed from the solution to a simplified case of the mechanistic model, in which FD is a function of the square root of FI and soil properties. The empirical models (Baiz et al. 2008; Tighe et al. 2007) further reduced the constraints by using FI only and lumping all the other terms in the physico-empirical models with suitable fitting constants.

For TD predictions, Chapin et al. (2012) demonstrated a prediction model based on the nonlinear regression analysis of field measurements, in which TD is a power function of TI. This power model, however, overlooked the physical process from a continuum mechanics perspective. Baiz et al. (2008) considered the physical process and predicted TD using exactly the same mathematical function (i.e., square root) and fitting constant numbers as those of FD based on TI and FI, in which two different TD models were developed, one for the freezing season and the other one for the thawing season. Efforts have also been made for predicting the maximum TD for the sites in Michigan using Stefan's equation (Baladi and Rajaei 2015). This Stefan's equation formulated TD as a square root of thermal properties of a pavement and its base/subbase soils, which thus shares the same mechanism when TD is a square root of TI. The maximum TD is very helpful to determine the removal of SLR (see Figure 2.2). However, it is seen in Figure 2.3 that the predicted maximum TDs in the existing study are significantly underestimated when compared to the measured TDs.

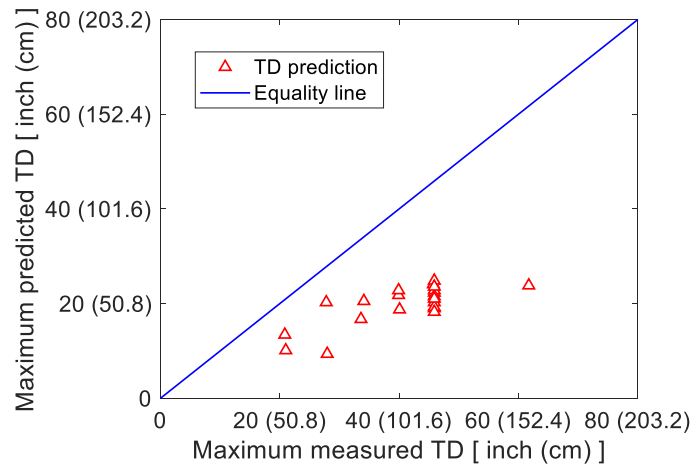


Figure 2.3 Maximum predicted TDs vs measured TDs from measurement sites in Michigan (data is from (Baladi and Rajaei 2015))

Despite the above progress, three key questions for predicting FD and TD still need to be addressed. First, most existing prediction models for TD use exactly the same mathematical formulation as that of FD. This, however, is site dependent and is not suitable for every case. The results in Fig. 2 clearly shows the large deviations of TD predictions for roadways in Michigan the same mathematical formulation for TD as that of FD is applied. Thus, a new TD prediction model is urgently needed to improve the TD prediction accuracy. Second, most existing prediction models, e.g., Chapin et al. (2012) and Baladi and Rajaei (2015), assume that FD can be predicted based on FI only (i.e., 2-dimensional line). In fact, FD is also highly correlated to TI (i.e., 3-dimensional surface) because intermittent thawing periods always exist in the freezing season. Baiz et al. (2008) included TI for predicting FD; however, FD in the freezing and thawing seasons is predicted separately using a piecewise function, which is inconvenient in practice. Therefore, no integrated FD and TD prediction model involving both FI and TI in the whole freeze-thaw cycle is available. Third, most existing prediction models, e.g., Baiz et al. (2008) and Chapin et al. (2012), are developed and validated against field data from only one or two sites due to the monetary and time constraints. Plenty of field data from 104 sites in Michigan alone are available, which have not yet been used. More discussions on the theory and conclusions from existing studies will be presented in the next section.

## 2.3 Prediction of Freezing and Thawing Depths

The key scientific and engineering question in determining the placement and removal dates of SLR is the predictions of freeze and thawing depths, especially the latter one. This is because the depth and thickness of the frost in the pavement determine the seasonal fluctuations in the bearing capacity of the road as explained in Section 1.1. Inaccurate predictions of these depths will lead to either extensive damage to the pavement due to late placement or early removal of the SLR, or economic loss of road users due to an unnecessarily long period for SLR. Accurate SLR decisions depending on the predictions of freezing/thawing depths are highly desirable because most agencies are required to notify the public of SLR postings at least 3 to 5 days in advance.

The MDOT Project RC 1619 provided a relatively comprehensive review on the prediction models for the freezing depth. The review gave detailed descriptions for one mechanistic model, i.e., UNSAT-H Modeler (Fayer 2000), three classic semi-empirical models, i.e., Neumann's empirical model (Jiji and Ganatos 2009), Stefan's equation (Jiji and Ganatos 2009) and the Modified Berggren equation (Aldrich and Paynter 1953), and empirical models including the models developed by Chisholm and Phang (1983) and Tighe et al. (2007).

In fact, there are much more mechanistic models. One significant effort was the freeze/thaw prediction using the Enhanced Integrated Climatic Model (EICM) funded under the FHWA *Clarus* initiative, which recently underwent a regional demonstration in Montana and North Dakota (Cluett et al. 2011). The mechanistic models were developed based on a comprehensive description of the physical process from a continuum mechanics perspective, for which the PI, Dr. Liu, has published many similar but more complicated works (Liu et al. 2012; Liu and Yu 2011; Liu et al. 2012; Liu et al. 2012; Liu et al. 2013). This type of model usually involves two governing equations for heat transfer (Fourier's equation) and water movement (modified Richards' equation) in soils. More about such models and the behavior of frozen soils can be found in the review paper published by Dr. Liu in the Soil Society of America Journal (Liu et al. 2012).

The semi-empirical models were developed from the solution to a simplified case of the mechanistic model. Models of this type share a common form of Aldrich and Paynter (1953),

$$FD = a \sqrt{\frac{48\lambda \cdot n \cdot FI}{L}} \quad \text{Eq. 2.1}$$

where  $FD$  is the freezing depth,  $\lambda$  is the thermal conductivity of the soil,  $a$  is a dimensionless correction factor considering initial freezing depression (Berg et al. 2006),  $n$  is a dimensionless parameter converting air index to surface index,  $FI$  is the freezing index (or called Cumulative Freezing Degree Days,  $CFDD$ ),  $L$  is the latent heat of water freezing. Different models may define the freezing index differently and add or drop constants for soil properties or other factors.

The empirical models further loosen the constraints by only keeping one term,  $FI$ , and lumping all the other terms with a physical meaning into two fitting constants. The fitting constants can be obtained by linear regression with measured data. Therefore, the empirical models are also statistical models. One major conclusion of MDOT project RC1619 is that statistical/empirical models are preferred over mechanical models for practical purposes. In detail, the mechanistic models tested in the study require materials properties that are hard to determine in field applications and the accuracy of the predictions made by the mechanistic models are not as compromising the statistical model proposed in RC1619.

One major feature of these statistical models is the linear relationship between the freezing depth and the square root of freezing index (Baiz et al. 2008; Miller et al. 2012):

$$FD = a + \sqrt{b \cdot FI} \quad (\text{or equivalently, } FD = a + (b \cdot FI)^{0.5}) \quad \text{Eq. 2.2}$$

In RC 1619, the above constraints were further loosened by removing the square root linearity:

$$FD = a \cdot FI^b \quad \text{Eq. 2.3}$$

As shown in Figure 2.4, both of the above two functions will yield very good curve fitting to the measured data used in RC 1619. However, we think Equation (2) makes more sense as it was proposed based on physical laws instead of random guesses. We thus will start from this one.

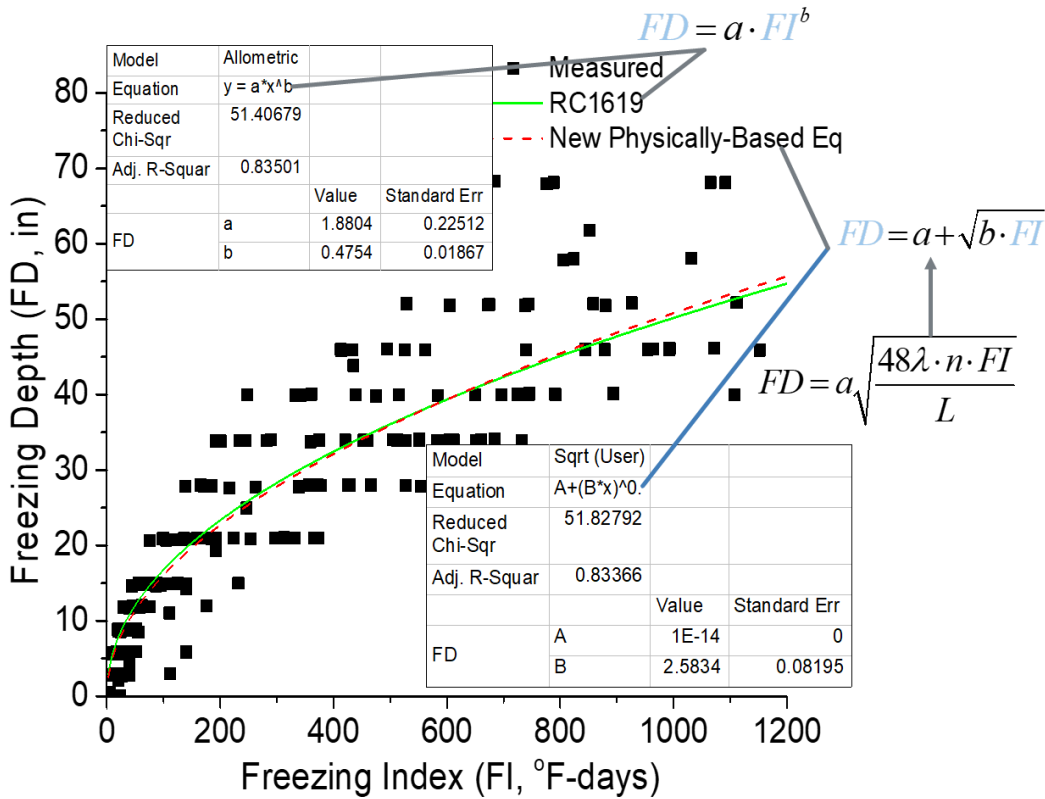


Figure 2.4 Statistical models for data from MDOT Project RC1609

One another thing that has been repeatedly proven in previous studies and needs clarification here is that freezing and thawing are two very similar processes. If the hysteresis is overlooked, they can be thought to be reverse processes. This is possibly why in many previous studies, the statistical relationship between the freezing depth and freezing index and that between the thawing depth and thawing index take exactly the same mathematical function ( Eq. 2.4 and Eq. 2.2 are similar):

$$TD = c + \sqrt{d \cdot TI} \tag{Eq. 2.4}$$

where  $c$  and  $d$  are fitting constants and  $TI$  is the (cumulative) thawing index. This viewpoint and method were tactically adopted in the majority of the previous freezing/thawing depth and SLR studies (Asefzadeh et al. 2016; Baiz et al. 2008; Marquis 2008; Miller et al. 2013). Therefore, in this project, we start from this mainstream viewpoint and discuss freezing and thawing depths

simultaneously by hypothesizing that they can have similar or at least related mathematical forms while the major differences between them are the fitting constants (i.e.,  $a$ ,  $b$ ,  $c$ , and  $d$  in Equations (2) & (4)). RC 1619 only tested one semi-empirical model (Nixon and McRoberts) for the thawing depth, which yielded unsatisfactory results. This is not surprising as mechanistic models can hardly provide satisfactory results, let alone semi-empirical models, which adopt further simplifications. Statistical models incorporating information from measurements, as proven in RC 1619, should present much better predictions in the geological locations where the measurements were taken. Unfortunately, empirical/statistical methods were not tried in RC 1619 for thawing depths. Based on the results of RC 1619, it seems that predictions using statistical models for thawing depth using either Eq. 2.3 or Eq. 2.4 can present comparable results or much worse results than that in freezing depth predictions in a few cases; while in most cases, a statistical model cannot be obtained because the TD curves are usually much further from a monotonic curve than the FD curves. The TD curves usually have many different peaks as the thawing front moves up and down due to the micro freeze-thaw cycles.

## 2.4 Popular SLR Procedures based on Simple Weather Data

### 2.4.1 FHWA-WSDOT

The FHWA-WSDOT SLR procedure was built on the use of the freezing and thawing indices. In this report, we will the freezing index and thawing index to refer to the cumulative indices if not otherwise specified. If needed, the daily index will be used to represent the increment gained over a day in a freezing or thawing index. In the FHWA-WSDOT SLR procedure, the freezing and thawing indices are defined using the following equations.

$$FI = \sum_{i=1}^N (0 - T_i) \quad \text{Eq. 2.5}$$

$$TI = \sum_{i=1}^N (T_i - T_{\text{ref}}) \quad \text{Eq. 2.6}$$

where  $T_{\text{ref}} = -1.67 \text{ } ^\circ\text{C}$  .

Though different definitions of FI and TI can also be found in some later literature, the above is still one of the most popular definitions for FI and TI.

The following rules were adopted as the criteria for the SLR placement:

Thin 5.6 °C-days (10 °F-days) 13.9 °C-days (40 °F-days)

Thick 22.2 °C-days (25 °F-days) 22.2 °C-days (25 °F-days)

The following rules were proposed to determine the date for the SLR removal:

$$D = 25 + 0.018 \cdot FI \text{ (days and } ^\circ\text{C-days)} \text{ or } TI = 4.154 + 0.256 \cdot FI \text{ or } TI = 0.3 \cdot FI$$

In theory, the “should date correlated to when the thaw front reaches the bottom of the base layer and the “must” date correlate to when the thaw front reaches 4” below the bottom of the base. Pavement is considered thin if the bituminous wearing surface is 2” or less and the base course is 6” or less. Pavements are considered thick if the wearing surface and base course are over 2” and 6”, respectively. The range of data for obtaining the above relationships is 204-1093 °C-days.

## 2.4.2 MnDOT

The Minnesota Department of Transportation (MnDOT) developed their SLR procedure based on the local weather conditions. This MnDOT procedure was updated multiples as it was applied to the field. These major versions are the 1998 version based on Van Deusen et al. (1998), 2000 version (MnDOT final report 2000-18), and 2004 version (MnDOT SLR memorandum).

In all the versions, the following are the basic rules:

- ❖ 25 °F-days is the criterion for SLR Placement.
- ❖ The whole state is divided into five different geographic zones. But 8 weeks is the maximum SLR duration for all frost zones when determining the SLR Removal date.

The following are the major points in the 2000 version.

- ❖ The range of data for obtaining the above relationships is 900-2100 °C-days.
- ❖ It is evident that the thaw in the pavement sections with sandy subgrades was out sooner than those with clay subgrades.
- ❖ The reference temperature in the FHWA model was revised to allow for the fact that the air temperature required for thawing actually decreases from January to March due to the declination of the sun during the spring. Based on historical data (1994-1997), reference temperature for Jan., Feb., and Mar. are -0.9, -2.3, and -4.3 The range of data for obtaining the above relationships is 204-1093 °C-days.
- ❖ Criteria for SLR date determination
  - SLR Placement  
15 °C-days for 30 °C-days different pavement types.
  - SLR Removal

$$D = 0.15 + 0.01 \cdot FI + 19.1 \cdot FD - 12090 \cdot \frac{FD}{FI} \quad \text{Eq. 2.7}$$

$$FD = -0.328 + 0.0578\sqrt{FI} \quad (\text{Chisholm and Phang, 1977, TRB}) \quad \text{Eq. 2.8}$$

when measurements are not available.

The above removal criterion was proposed based on the evaluation of the following two FHWA criteria,  $D = 25 + 0.018 \cdot FI$  and  $TI = 0.3 \cdot FI$

In the 2004 version, a major update is the adoption of a new method for calculating FI and TI, which is much more complicated than the FWHA model.

❖ New *FI*

$$\begin{cases} T_i > T_{\text{ref}} & TI_i = TI_{i-1} + (T_i - T_{\text{ref}}) \quad (\text{The pavement is thawing}) \\ T_i < T_{\text{ref}} & \begin{cases} TI_{i-1} \leq 0.5 \cdot (32^\circ F - T_i) & TI_i = TI_{i-1} \ \& \ FI_i = 0 \quad (\text{Significant thawing has not occurred}) \\ TI_{i-1} > 0.5 \cdot (32^\circ F - T_i) & TI_i = TI_{i-1} - 0.5 \cdot (32^\circ F - T_i) \ \& \ FI_i = 32^\circ F - T_i \quad (\text{Refreezing}) \end{cases} \end{cases}$$

$T_{\text{ref}}$  is 32 °F in January, then starting from February, it decreases from 29.3°F at a rate of 0.9 °F per week until 14.9 °F in the last week of May.

❖ SLR Placement

25 °F-days

❖ SLR Removal

$$D = 0.15 + 0.01 \cdot FI + 19.1 \cdot FD - 12090 \cdot \frac{FD}{FI} \quad \text{Eq. 2.9}$$

$$FD = -0.328 + 0.0578\sqrt{FI} \quad \text{Eq. 2.10}$$

The detailed equation for SLR removal is unclear. According to MnDOT, the end date of the SLR period for each frost zone is determined using measured frost depths, forecast daily air temperature, and other key indicators at several locations within each frost zone. The SLR restrictions last no more than 8 weeks.  $TI$  is set to 0 when turns negative.

$TI$  resets to zero on January 1. MnDOT does not provide a definitive suggestion for determining the end of SLR (Asefzadeh et al. 2016). The changes to the FI and TI calculations were proposed to 1) better eliminate the micro freeze-thaw cycles in the early freeze-thaw season, and 2) better consideration the influence of solar irradiation on the pavement surface temperature.

### 2.4.3 MIT

The MIT procedure proposed by the Manitoba Department of Infrastructure and Transportation, (Bradley et al. 2012) was also derived from the FHWA model. This procedure is based on  $TI$  only.  $TI$  follows the FHWA definition, but a varying  $T_{\text{ref}}$  is used.

$$TI = TI_{i-1} + (T_i - T_{\text{ref}}) \quad \text{Eq. 2.11}$$

$$\text{If } T_i < 32 \text{ °F, then } TI = TI_{i-1} + 0.5 \cdot (T_i - T_{\text{ref}}) \quad \text{Eq. 2.12}$$

$T_{ref}$  increases from 29 °F on March 1 and increases by 0.1 °F per day until May 31 and equals 32 °F in the rest of the year. As can be seen,  $T_{ref}$  varies in a way that is similar to the MnDOT procedure.

The following threshold TI values are adopted as the criteria for determining the SLR dates.

❖ **SLR Placement**

$$TI = 27 \text{ °F-days} \quad \text{Eq. 2.13}$$

❖ **SLR Removal**

$$TI = 630 \text{ °F-days} \quad \text{Eq. 2.14}$$

It is also worthwhile to mention that the SLR duration cannot exceed 8 weeks. In addition,  $TI$  is set to 0 when turns negative.

#### 2.4.4 SDDOT

The procedure developed by the South Dakota Department of Transportation (<https://sddot.clearpathweather.com/public/freztrax/help.html>) represents another significant deviation from the FHWA model.  $FI$  and  $TI$  use the original FHWA definitions, in which  $T_{ref}$  is 29 °F

The South Dakota Department of Transportation uses FrezTrax to determine the timing and duration of SLR. Instead of varying the thaw index equation as MnDOT does, SDDOT varies the threshold (critical) indices for the start and end of SLR. Both indices are dependent on the amount of precipitation from August to November of the previous year.

The critical values are expressed as a percentage of the maximum accumulated freeze index that occurs during the course of the winter. Once the thawing index at a given location reaches its critical percentage of the maximum accumulated freeze index at that location, restrictions can be removed.

For the SLR placement,

- ❖ Table 2.1 is used to determine the critical thawing index.

Table 2.1 Critical thawing index for SLR placement in SDDOT procedure

| Aug-Nov Precipitation | Critical Thawing Index |
|-----------------------|------------------------|
| 7.75"                 | 35                     |
| 6.25"                 | 40                     |
| 5.50"                 | 45                     |
| 4.75"                 | 50                     |

- ❖ For the SLR removal, Table 2.2 is used to determine the critical thawing index.

Table 2.2 Critical thawing index for SLR placement in SDDOT procedure

| Aug-Nov Precipitation | Removal Thawing Index (%) |
|-----------------------|---------------------------|
| 7.75"                 | 40                        |
| 7.00"                 | 35                        |
| 6.25"                 | 30                        |
| 4.75"                 | 25                        |

The following is an example. Suppose you live in the Pierre area and you want to determine when you should implement and remove spring road restrictions. For the sake of discussion, let's assume that Pierre observed exactly 4.75" of fall precipitation and accumulated a maximum freeze index of 1000 during the winter. Based upon the tables above, restrictions should be implemented at Pierre when the accumulated thaw index reaches 50. Restrictions should be lifted when the thawing index reaches 25% of the maximum freeze index, or 250 (25% of 1000).

#### 2.4.5 USDA/FS-NHDOT

The procedure adopted by the United States Department of Agriculture Forest Services and the New Hampshire Department of Transportation (USDA/FS-NHDOT) is a modification of the FHWA model. A major modification is the extra steps explained in the following for calculating the reference temperature by finding the difference between air temperature and asphalt pavement temperature.

1. Obtain the sinusoidal fit to the monthly air temperatures.

$$T = T_M + T_A \cdot \sin \left[ \frac{2\pi}{365} (t - L) \right] \quad \text{Eq. 2.15}$$

where  $T_M$  and  $T_A$  are the mean annual temperature and amplitude of temperature sinusoid, respectively;  $t$  is time (Julian days),  $L$  is the time lag (number of days) of the temperature sinusoid.

2. Obtain freezing and thawing index using a reference temperature of 32 °F. Then obtain the freezing and thawing of asphalt temperature based on the N factors of 0.5 and 1.7 for freezing and thawing, respectively.

$$FI \cdot N_f = AFI \quad \text{Eq. 2.16}$$

$$FI \cdot N_t = ATI \quad \text{Eq. 2.17}$$

where  $N_f$  and  $AFI$  are the freezing N-factor and freezing index of asphalt, respectively; and  $N_t$   $ATI$  are the thawing N-factor and thawing index of asphalt, respectively.

3. Then using the following two relationships obtain the amplitude,  $T_{A,as}$ , and mean annual temperatures,  $T_{M,as}$

$$T_{M,as} = \frac{-AFI + ATI}{365} \text{ in } ^\circ\text{C}; \quad \text{Eq. 2.18}$$

$$T_{M,as} = \frac{-AFI + ATI}{365} + 32 \text{ in } ^\circ\text{F} \quad \text{Eq. 2.19}$$

$$\frac{\pi \cdot |FI|}{365} = \sqrt{T_{A,as}^2 - T_{M,as}^2} - T_{M,as} \cdot \arccos \left( \frac{T_{M,as}}{T_{A,as}} \right), \text{ in } ^\circ\text{C}; \quad \text{Eq. 2.20}$$

$$\frac{\pi \cdot |FI|}{365} = \sqrt{T_{A,as}^2 - (T_{M,as} - 32)^2} - (T_{M,as} - 32) \cdot \arccos \left( \frac{T_{M,as} - 32}{T_{A,as}} \right), \text{ if in } ^\circ\text{F} \quad \text{Eq. 2.21}$$

4. Plot both the sinusoidal variation of air and asphalt temperature and obtain the temperature difference for each day.

$$T = T_{M,as} + T_{A,as} * \sin \left[ \frac{2\pi}{365} (t - L) \right]$$

Eq. 2.22

## **Chapter 3 Acquisition, Processing, and Evaluation of Data**

This chapter is devoted to the acquisition, processing, evaluation, and selection of for the development of the development and implementation of the freeze thaw model based SLR decision support tool. The data work in Task 2 (Chapter 3) includes both data analysis research associated with model development and data operations associated with app development, so this chapter is closely related to Chapter 4 and Chapter 5 for the model development and Chapter 6 for the app development. First, this chapter introduces the way to acquire data, i.e., weather, RWIS, and GIS data, that are possibly needed for developing the models and the app and their improved successors. Next, several key operations which are needed for processing the data for later model and app work are introduced. Followed are the evaluation of the data, including experience and issues collected when dealing with the data and knowledge gained in the selection of the data for the model development work to be discussed in the following chapter.

### **3.1 Data Acquisition**

The target app, MDOTSLR ([www.mdotslr.org](http://www.mdotslr.org)) is developed based on the existing SLR practices in other states, a scientific understanding of the physical processes, existing models for freezing/thawing depth predictions, and available criteria and protocols for placing and lifting SLR. RWIS, significant Weather and GIS data are being collected by this web-based tool to make SLR decisions. As of now weather and RWIS data have been partially implemented with data going back to 2013 while GIS soil data has been fully implemented.

#### **3.1.1 Weather Data**

Accurate air temperatures, both existing weather data and forecasts can be obtained from various websites for free, though historical weather data can be hard to find at best and unreliable at worst. We created the initial weather database with the weather API from APIXU (<https://www.apixu.com/>) for data going back to 2016 considering the low cost, good coverage, and excellent data integrity (no missing dates or regions). Other data APIs including those from

NOAA were also tested at the beginning of the project. Most of these APIs exhibit issues in the above three aspects to our intended research tasks. For data before 2016, we import data via the utilization of <https://mesowest.org/api/> since it is available for free and has a longer date range available but lacks complete coverage. The following is the sample code for fetching the data using JavaScript code.

```
// get the weather data stored in the database, handle any errors
[err, zipCode] = await to(
  ZipCode.findOne({
    zip: zip
  }, 'forecastDays'
).lean().populate('forecastDays.id', 'date day.avgtemp_c').exec());
if ( err ) throw {
  status: 500,
  error: err };
if ( !zipCode ) throw {
  status: 404,
  error: {
    message: 'ZIP code ${zip} not found'
  }
};
```

For forecast data, the wunderground weather API at <https://www.wunderground.com/weather/api/> is used for its free ten-day forecast. Forecast extends over a longer period of time such as thirty days are also possible with APIs such as the one from <http://www.accuweather.com/>. However, long-range forecasts beyond one week are very questionable due to significantly reduced accuracy. In the latest version of the API, an API provided by Iteris (<https://www.iteris.com/>), who is the contractor for the MDOT MDSS system, is used to replace APIXU weather data acquisition. The following is the sample code for getting the weather forecast data using JavaScript code.

```
// put the weather data into the averages variable
```

```

zipCode.forecastDays.forEach( function( day ) {
  if ( day.id && day.id.day && day.id.day.avgtemp_c ) {
    averages[ day.id.date ] = Number(day.id.day.avgtemp_c.toFixed(1));
  } else if ( day.id ) {
    averages[ day.id.date ] = null;
  }
} );

if ( testing ) return averages;

```

### 3.1.2 Acquisition of RWIS Data

In the early version of the app, RWIS data are acquired via an API provided by the Vaisala corporation, the RWIS contractor of MDOT from December 2016 to June 2019. The main area of interest in the data they had to provide was in the base temperatures, temperatures below ground, up to seventy-two inches for certain sensors. The main use of this data is the ability to directly measure freezing and thawing depths with a properly implemented algorithm, though the algorithm we have setup may still have some issues. The data provided by Vaisala’s API is expressed in fifteen-minute intervals and only provides data going back two days. This presents two problems as we are interested in looking at the entire day in aggregate, not just in 15-minute snapshots, and we want a long date range of data, not just three days. To solve these problems, a script is run at 1 a.m. every morning to capture and save the data from the API for the previous day into the MongoDB database. The script looks at all fifteen minute periods over the past twenty-four hours, organizes all values into arrays that are representative of each data field and each sensor. These arrays then have their values averaged and that average is stored in the database as the value for that sensor on that day. One issue early on was an assignment error for base temperature probes that weren’t reporting all their sensors every single time. Normally the probe used to record base temperature has either eight or sixteen sensors at various depths but some stations do not record every sensor value every time, resulting in a total number of sensors greater than eight but less than sixteen. As a result, the import script would treat the probe like an eight-sensor array but in actuality it was a sixteen sensor array. Stopping the problem was as simple as changing “sensor

length == 16” to “sensor length > 8”. The real problem was that the data already stored in the database was wrong and did not have the correct depth labels on the values. To fix this another script was used to find dates that lacked depth values, sort them by value and assign the depths based on this order. There are a number of problems with this, while the main one is that the sensor values may not have been linear. The values may have increased and decreased spontaneously. This may mean that certain dates towards the beginning of recording have incorrect depth and temperature values but the problem is at least stopped. The other source of RWIS data was historical data provided by Vaisala as csv and rpt files. The csv data has been fully imported to the MongoDB database in a fashion similar to the one described for the API. The rpt files unfortunately are proprietary and will require some extra time to turn into csvs that can be imported.

RWIS data come from MDOT RWIS sites, i.e., 104 RWIS sites distributed in different regions of data collect typical weather data and subsurface information. More sites will be built up in the field, whose data will be added via the API. As mentioned, an API prepared by Vaisala was adopted for real-time RWIS data import. As MDOT switched the RWIS contractor in July 2019, a TerraFormManager (TFM) API provided by Mixonhill ([www.mixonhill.com](http://www.mixonhill.com)) was adopted to replace the Vaisala API. The historical data are stored in our local database as well to ensure fast load times. The following sample code can be used to obtain the weather data.

```
// get the STATION at the id and fill its rwisDays, mukey and zipCode
```

```
    [err, station] = await to(
      Station.findOne(
        {
          id: id },
        'rwisDays.id mukey zipCode'
      ).populate( 'rwisDays.id' ).lean().exec() );
    if ( err ) throw {
      status: 500,
      error: err };
    if ( !station ) throw { status: 404, error: {
      message: 'RWIS station ( ' + id + ' ) not found'
    }};
```

```

// add query data to the result object's rwisData field
station.rwisDays.forEach( function( day ) {
    // reduce decimal precision of outputs, to reduce size of return
    // to client
    Object.keys(day.id).forEach(function(key) {
        if (day.id[key].constructor === Array) {
            day.id[key].forEach(function(st,i) {
                var v = day.id[key][i].value;
                delete day.id[key][i]._id; // delete unnecessary id while at it
                if (typeof(v) === 'number') {
                    day.id[key][i].value = Number(v.toFixed(2));
                }
            });
        }
    });
});

result.rwisData.push( day.id );

});

```

### 3.1.3 Integration of GIS and Soil Data

GIS soil data is available for free from the USDA's soil mart database (<https://websoilsurvey.sc.egov.usda.gov/App/HomePage.htm>). Typical material properties for the two soil layers, i.e., six feet, can be obtained via the websoilsurvey API. All needed GIS data have been imported from the GIS site using an API. The data are indexed using the RWIS sites and zip codes and are stored in a local database. The soil data is available via the data portal module of the app to be introduced in Chapter 6. However, it is worthwhile to mention that, the soil data is included in the current information to assist the model development but is not used in the operation of the models in the app. This is because most of the state highways managed by MDOT was built

with excavation to depth more than six feet. That means, the base and subgrade material can be different from that marked in the GIS for the same location. Therefore, the GIS soil information was just for reference when developing the models. But we also want to point out that such GIS information may still be very useful for low volume and unpaved roads, which are laid over the natural soil. The GIS data can be utilized for more accurate site-specific models.

The soil mart database is an enormous collection of soil data all throughout the world. Our interest is confined to Michigan, specifically the water content of the soil, the clay, silt and sand content of the soil and the depth to the water table. The soil data system uses relational databases, so some consideration had to be made when trying to find the data we wanted. The water and soil content data was found in the horizon table which, though it does not state this in the documentation, we believe, means the component horizon since each record relates back to one item in the components table. The problem is that the components do not have any geographical mapping but they do relate to a map unit which does have a geographical mapping. The issue with that is that the relationship is many components to one map unit. Thus, the data from the components are averaged and we use those averages to represent the values of the map unit which we can then represent geographically. One challenge in the geographical mapping is that each map unit has multiple polygons that represent it. If you look at [mdot.slr.org/services/gis-test](https://mdot.slr.org/services/gis-test), you can see that each map unit is represented by many polygons that look like a grouping of islands. Our best guess for this is that each polygon is actually one component, though we would need to test this to confirm. This raises the question of “if each polygon does represent a component, why don’t they just relate to the components and not the map units?” Even if the polygons do represent a component, we do not see a way to figure out which polygon matches which component so it would not do us any good in any way. Getting back on track, in this way any geographical point that is within one of these map unit polygons, and the polygons seem to cover the whole state, can be linked to its proper soil data. The following is some sample for fetching typical soil data from the remote GIS system.

```
// get the soil TYPE content data for the station's mukey from the
// soil mart database
[err, body] = await to(
  request.post({
```

```

url: 'https://sdmdataaccess.sc.egov.usda.gov/Tabular/post.rest',
form: {
  query:
    `SELECT co.cokey,
      ch.hzname,
      ch.sandtotal_l, ch.sandtotal_h,
      ch.silttotal_l, ch.silttotal_h,
      ch.claytotal_l, ch.claytotal_h,
      ch.wsatiated_l, ch.wsatiated_h
    FROM chorizon ch
    INNER JOIN component co ON ch.cokey = co.cokey
    AND co.mukey = '${station.mukey
      }'
    WHERE ch.sandtotal_l IS NOT NULL
      OR ch.sandtotal_h IS NOT NULL
      OR ch.silttotal_l IS NOT NULL
      OR ch.silttotal_h IS NOT NULL
      OR ch.claytotal_l IS NOT NULL
      OR ch.claytotal_h IS NOT NULL
      OR ch.wsatiated_l IS NOT NULL
      OR ch.wsatiated_h IS NOT NULL
    ORDER BY co.cokey, ch.hzname;`,
  format: 'JSON'
},
json: true
})
);
if ( err ) throw {
  status: 500,
  error: { message: 'Soil Data Server Error'
  }
}

```

```
};  
  
soilContent = {  
};
```

## 3.2 Data Processing

The raw data acquired from the remote data sources need to be processed before it can be used for developing the prediction models of the freezing and thawing depths and SLR dates as well as the supporting many functions of the app. This section describes several of the most significant data processing operations in this project: air and surface temperatures, base (subsurface) temperatures, freezing and thawing depths, and freezing and thawing indices.

### 3.2.1 Air and Pavement Surface Temperatures

The daily average temperature and daily pavement temperature are two major data types used in the model and app developments. In the app, such data can be fetched and visualized in the app for any given time period. But for the model development, we usually selected the data that cover a full freeze-thaw season. In the model development practice to be introduced in the following two chapters, we usually process the data for one or multiple freeze-thaw seasons for selected sites.

The daily average air temperature and daily pavement surface temperature for five selected sites are presented in Figure 3.1, which shows the measurements from August 1<sup>st</sup> 2017 to June 1<sup>st</sup> 2018 covering the entire freeze-thaw cycle. The pavement surface temperature in general is greater than the average air temperature, in particular, for the periods before October 2017 and after April 2018. It is also seen that the pavement surface temperature tends to be below 0 °C starting from the middle of November 2017 for all the sites, while it tends to be above 0 °C starting from March 2018. This indicates that freezing likely starts in the pavement layers from the middle of November 2017 and thawing likely begins occurring from March 2018 for all the selected sites. In Figure

3.1c, the data for the site Seney is missing from September 26<sup>th</sup> 2017 to November 14<sup>th</sup> 2017, probably due to the lost connection between the sensors and the ESS at the site during the data transmission. However, the missing data have a negligible effect because the complete freeze-thaw cycle is included in the collected data in Figure 3.1c. All the data can be obtained at the data portal of the app easily, so here we only show typical data in Figure 3.1.

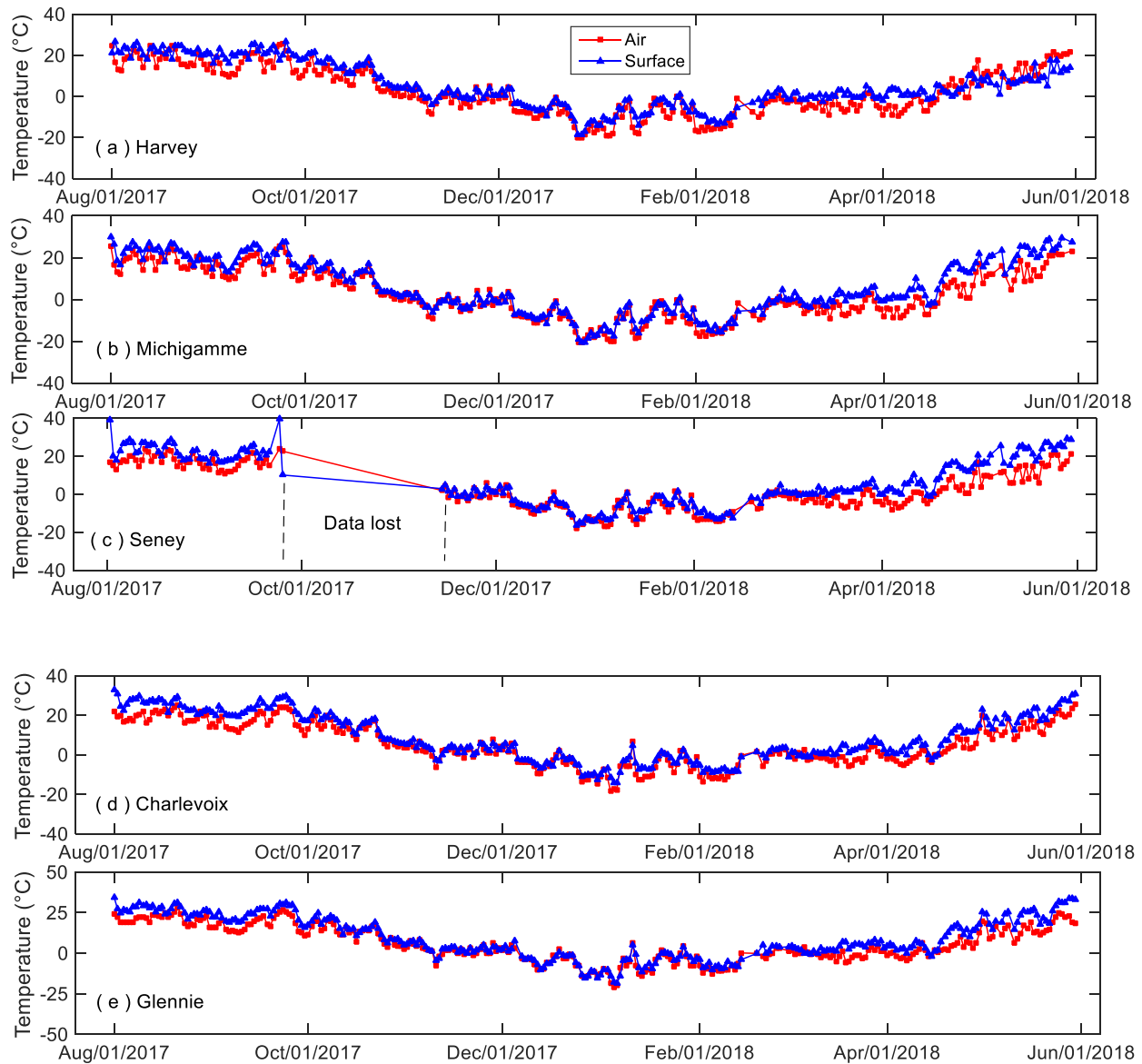
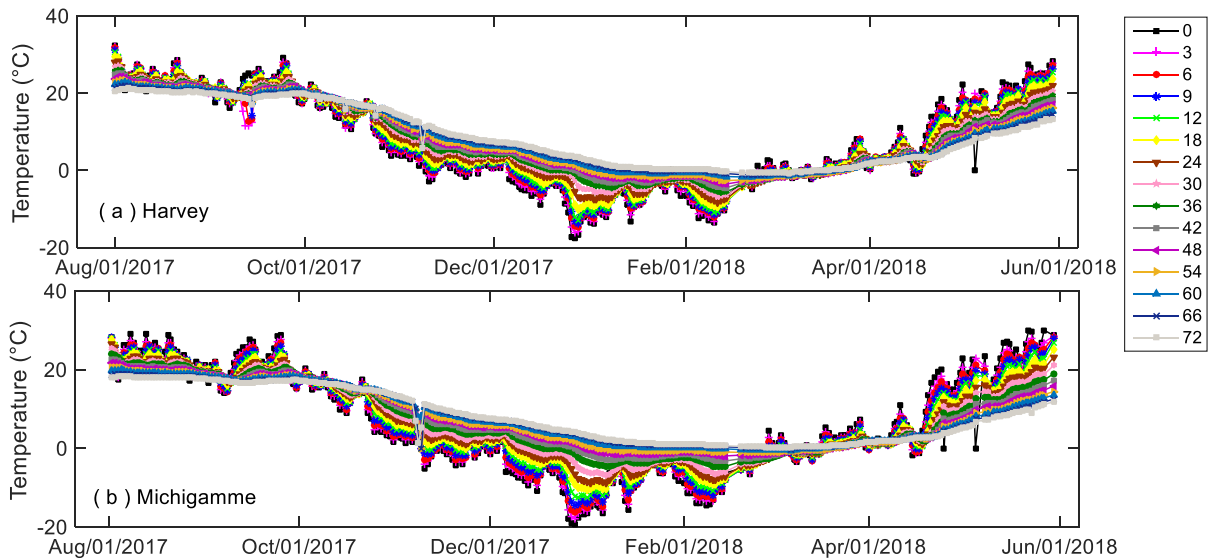


Figure 3.1 Average air temperatures and pavement surface temperatures for the five selected sites

### 3.2.2 Subsurface Temperatures

The subsurface temperatures (or called based temperatures) reflect the freezing and thawing penetration of the base and is used to determine FD and TD in the pavement layers. Figure 3.2 shows the measured base temperatures for all 15 locations from 0 to 72 inches (0-1.83 m) in Table 1. Similar to the air temperature and the pavement surface temperature in Fig. 6c, the base temperature data collected at the site Seney are not available from September 26<sup>th</sup>, 2017 to November 14<sup>th</sup>, 2017. It can be clearly seen in Figure 3.2 that from the middle of November 2017 to March 2018, the temperature measured in the base layer at different depths increases as the depth increases for all the sites. Among them, the measured temperatures at the bases, whose depths are less than 24 inches (60.96 cm), are below 0 °C. Starting from March 2018, the reverse temperature trend is observed, especially after April 2018, where the measured temperature decreases as the depth increases. These observations further confirm that for these sites, the thawing period starts around the beginning of March 2018. The freezing period is from the middle of November 2017 to the end of February 2018.



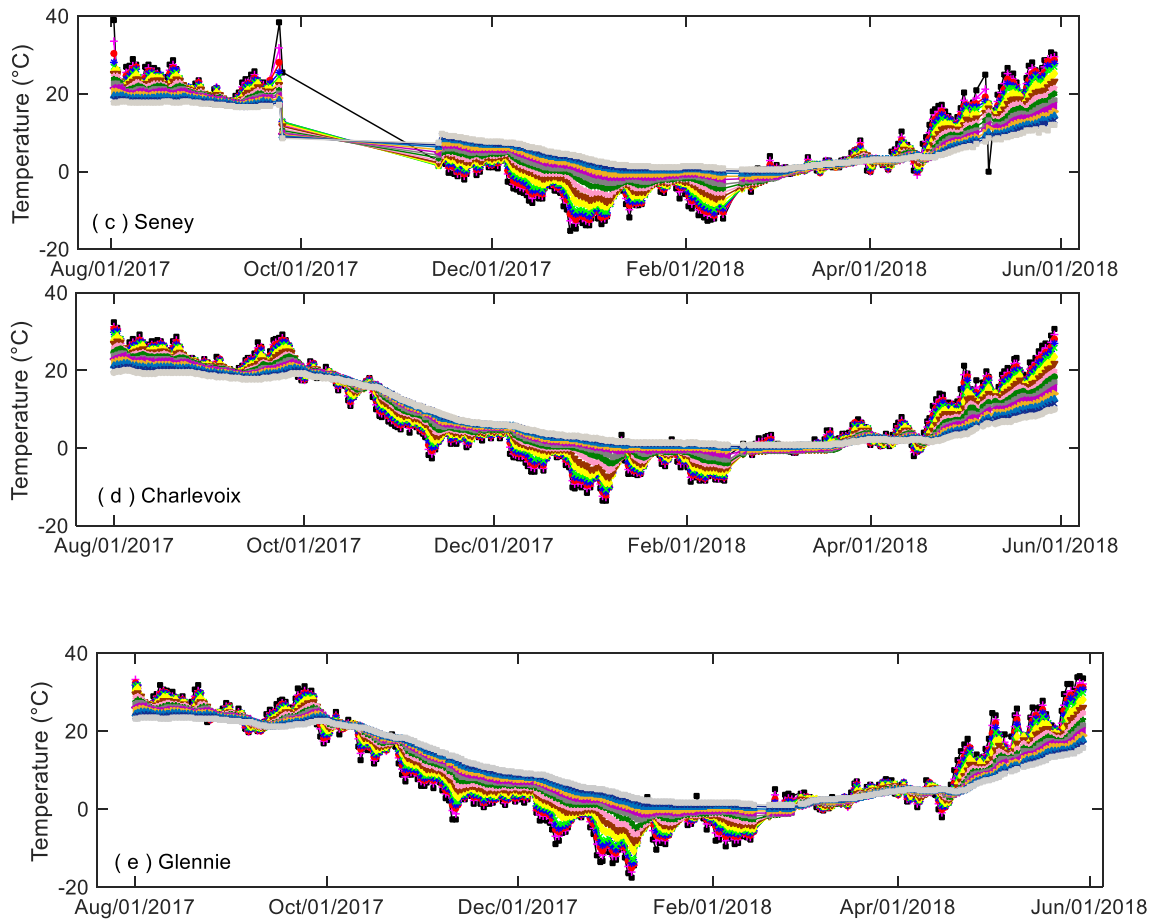


Figure 3.2 Pavement base temperatures for the five selected sites

### 3.2.3 Freezing and Thawing Depths

Freezing Depth (FD) and Thawing Depth (TD) are two of the most significant types of data that are needed for the development and validation of models. Such data can be measured using frost tubes or other similar devices directly. However, frost tube measurements are not available at MDOT RWIS sites, which is possibly very common in most RWIS systems. Frost tube measurements are only available for some sites at locations different from the RWIS sites. Considering the situation, an effort was made to obtain FD and TD based on subsurface temperatures. The limited frost tube data is excluded in the current app and only used for the development and validation of DLR date prediction models.

To exhibit the way to calculate the FD and TD from subsurface temperatures, the subsurface temperatures in Figure 3.2 are used to compute the variations of FD and TD at the selected sites. As shown in Figure 3.3, the rightmost curve represents a typical temperature distribution when the temperature at all the depth within the base and subgrade layers are above zero, e.g., a constant positive value. In early winter, the temperature decrease starts from the top, leading to the leftmost curve. The point of intersection between this curve and the freezing point curve corresponds to the freezing front. The depth of this point is the freezing depth. In spring, warm air temperatures trigger thawing from the top, which will bend the temperature curve into something like the middle curve. This curve intersects with the freezing point curve at two points. While the lower intersection point corresponds to the freezing depth, the upper intersection points represent the thawing depth. During calculation, these two curves can be differentiated by the change in the sign when passing the intersection point from top to bottom: a switch from the positive sign to the negative indicates the thawing depth whereas one from the negative to positive indicates the freezing point.

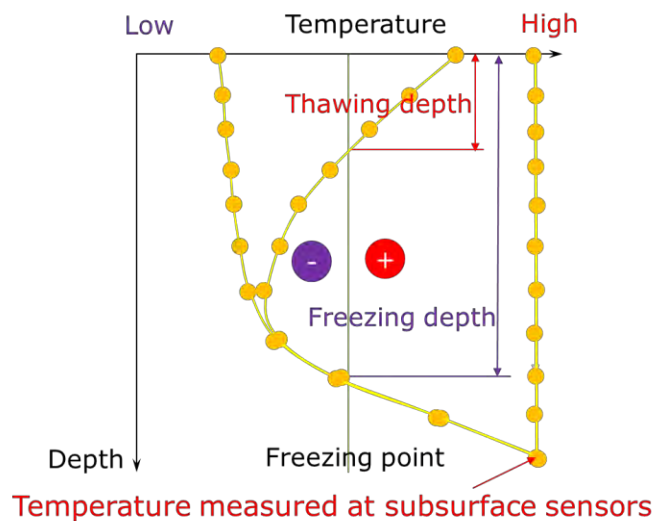


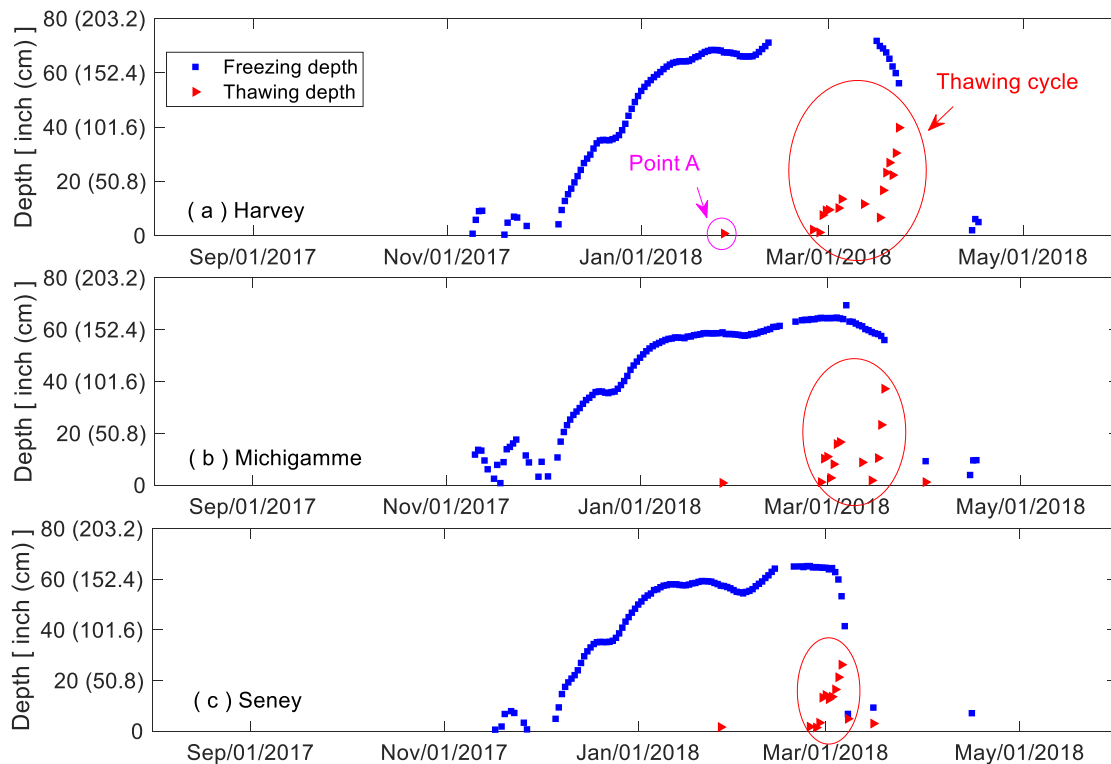
Figure 3.3 Calculation of freezing and thawing depths based on subsurface temperature measurements

For this purpose, two adjacent base temperatures from 0 to 72 inches (0-1.83 m) were compared. FD occurs if the previous base temperature is negative and the next one is positive, while TD appears if the previous base temperature is positive and the next one is negative. To calculate FD

and TD, linear interpolation was used and the base surface (i.e., base depth=0) was assumed as a datum. All calculated FDs and TDs below the datum are positive.

The measured FDs and TDs for the five selected sites are presented in Figure 3.4. We can see that FD occurs around the middle of November 2017 and starts decreasing significantly at the beginning of March 2018, which corresponds to the freezing and thawing starting dates seen in Figure 3.2. During the freezing period, FD decreases somewhat, especially at the beginning of the freezing period. This is because there were several warm days to thaw the pavement base, leading to a decrease in FD.

For all the sites, TD increases starting from March 2018, which agrees well with Figure 3.2. However, there are a few TD points before March 2018, e.g., Point A in Figure 3.4a. This could be because of some warm days during the freezing period. For some sites, as shown in Figure 3.4b and Figure 3.4c, there are also a few TD points when one freeze-thaw cycle is complete, where FD meets TD. This is again due to some warm days after the freeze-thaw cycle ends.



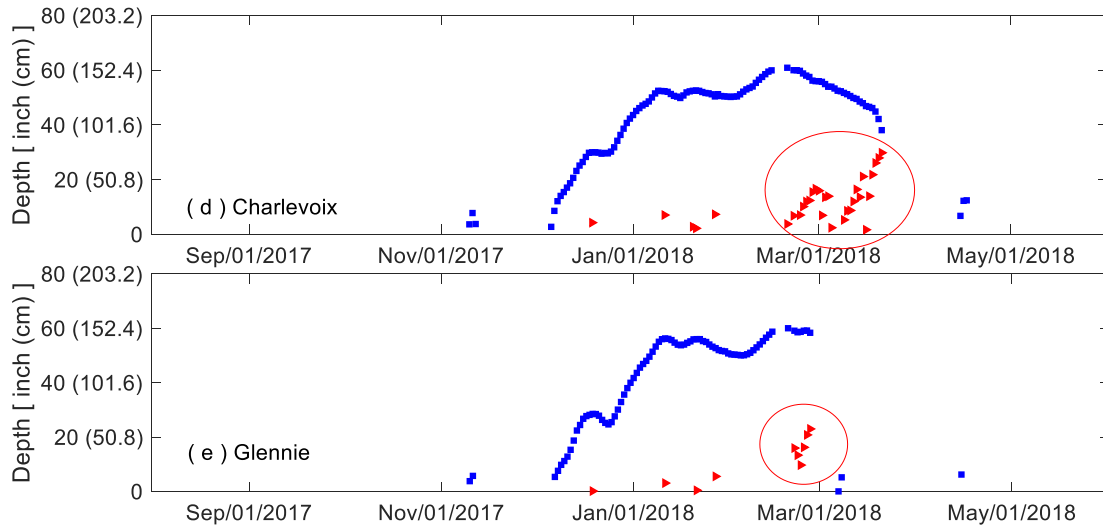


Figure 3.4 Calculations of measured FDs and TDs for the five selected sites

### 3.2.4 Freezing and Thawing Indices

As introduced in Section 2.4, there many different ways for calculating the Freezing Index (FI) and Thawing Index (TI), represented by the original way in the FHWA procedure and following deviations in the MnDOT procedure and MIT procedure. In fact, we can understand FI and TI as one way to process the temperature data, usually daily average air temperature, for understanding and predicting the amount of freezing and thawing. A simple way to understand the FI and TI is illustrated in Figure 3.5: FI and TI can be understood as the areas above and below a reference temperature. A straightforward choice of the reference temperature is the freezing point of bulk water, i.e., 0 °C or 32 °F, which separate freezing temperatures from thawing temperatures. However, reference temperature other than the freezing point is more frequently used due to a variety of considerations. Among them, the difference between the air temperature and the pavement surface temperature is the most common one. Such consideration can also be affected by other factors such as solar irradiation, location, pavement and soil conditions, and so on. Other considerations can also come into play to process the temperature data so that the data can better serve for the purpose of developing and running better freezing and thawing depth and SLR date prediction models.

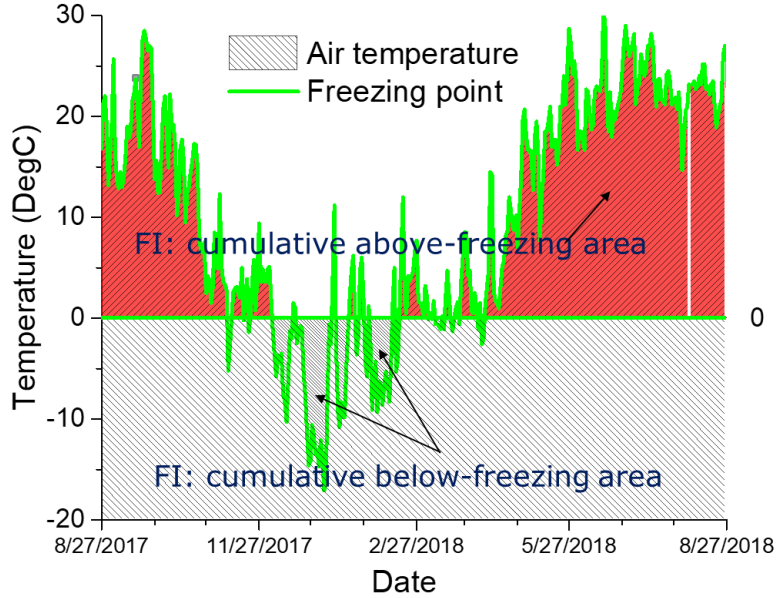


Figure 3.5 Calculation of freezing and thaw indices

In this project, the FD and TD are calculated in the way similar to the original FHWA model for simplicity. The cumulative freezing index is calculated based on  $T_0 = 0\text{ }^{\circ}\text{C}$  during a given period by the following expression

$$\begin{cases} FI = \sum(T_0 - T_s) \\ T_0 - T_s < 0 \Rightarrow T_0 - T_s = 0 \end{cases} \quad \text{Eq. 3.1}$$

where  $T_s$  is the pavement surface temperature. The cumulative thawing index is computed by

$$\begin{cases} TI = \sum(T_s - T_{ref}) \\ T_s - T_{ref} < 0 \Rightarrow T_s - T_{ref} = 0 \end{cases} \quad \text{Eq. 3.2 where } T_{ref} \text{ is the reference temperature to consider the}$$

amount of solar radiation and thermal properties of pavement materials.  $T_{ref} = -1.67\text{ }^{\circ}\text{C}$  is often utilized according to the guideline in Mahoney et al. (1987).

One major difference from the FHWA model is that the FI and TI used in the later model and app development are calculated with the pavement surface temperature instead of the air temperature for more accurate FD, TD and SLR date predictions. That is also the reason that complicated FI

and TI calculations adopted in MnDOT and MIT procedures are not needed in this study. The reason for using the pavement surface temperature will be discussed in detail in Section 4.5.1. Taking the Harvey and Michigamme sites for example, Fig. 9 shows the variations of FI and TI for these two sites, in which the corresponding FD and TD are also plotted. FI and TI were calculated starting from the first FD and ending by the last FD or TD. The rest of the FI and TI were treated as zero.

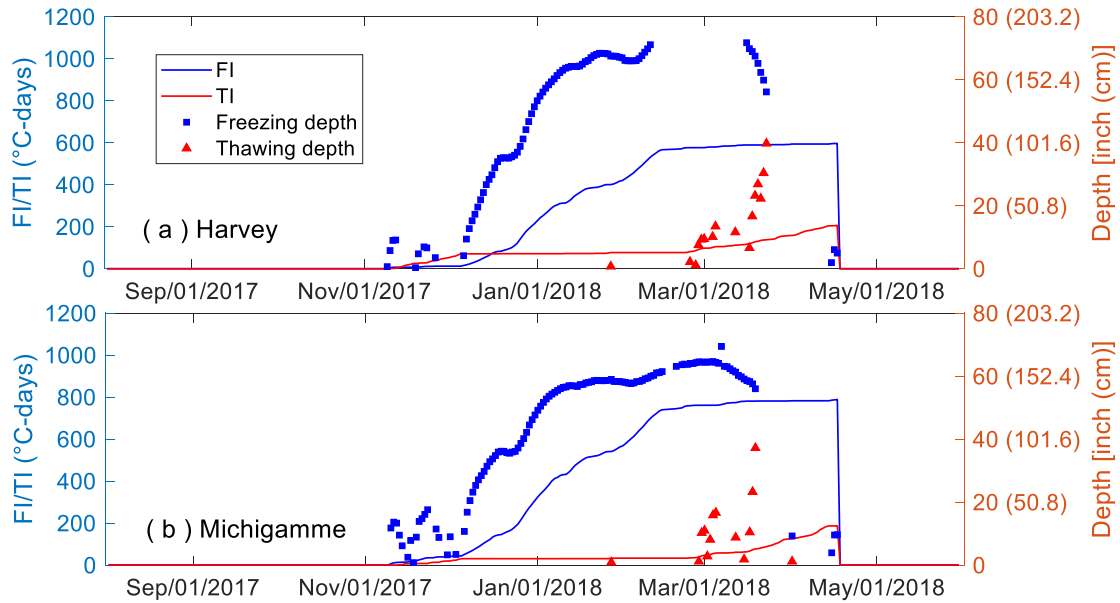


Figure 3.6 FI/TI calculated with the pavement surface temperature: (a) Harvey and (b) Michigamme

Another major difference is the introduction of one extra index called Freezing Index after Thaw starts (FIT). FIT is the FI cumulation after the first thaw temperature appears. FIT can be calculated using Eq. 3.1 starting from the date when the first TD data point occurs in the thawing season only.

### 3.3 Data Evaluation

#### 3.3.1 Issues in the RWIS Data

It requires a lot of effort to understand the structure of the data, find the most efficient way to deal with the data, and remove issues in the data. Among the three major categories of data, the weather data from external sources such as APIXU and Iteris are usually well managed, as a result, the data has seldom generated issues. In earlier attempts, weather data obtained using free APIs such as that from NOAA exhibit missing data for some zip codes. However, APIXU data and API are very reliable. The switch to Iteris app gave out a few problems at the beginning and soon become reliable. For the GIS data, as mentioned, the data is acquired and stored as local databases and can be accessed by MDOTSLR users via the data portal. However, the GIS data is excluded from the models. Due to this reason, the GIS data does not cause issues. Instead, the mapping the GIS data to the zip code, county, and RWIS sites, by the weather and RWIS data is indexed, poses a technical challenge, which will be discussed in Section 6.5.6.

The data from MDOT RWIS generated a lot of issues. First, the sensors and communication equipment of RWIS can easily generate problematic data if any of them malfunction. RWIS sites are usually installed below or not far from the shoulders at locations that are far from populated areas. Due to the reason, environmental factors such as aging caused by sun and rainwater, disturbance from traffic, limited attendance, and unreliable power source can more frequently cause issues. Such issues usually cannot be easily identified because they can only be manually identified by human users. One major issue in the MDOT RWIS data for our model and app developments reside in the historical RWIS data, i.e., data before December 2016. In detail, most subsurface temperature measurements do not appear meaningful. Taking the data for Site Seney for example, the subsurface temperatures at different depth did not change with time as shown in Table 3.1. Therefore, it is clear that the data are wrong. The same issue observed on the historical data for most of the RWIS sites.

Table 3.1 Part of the historical data at RWIS Site Seney

| Stationid | DisplayName                | DtTM                       | SubSurfT | SubSurfT2 | Depth2 | SubSurfT3 | Depth3 | SubSurfT4 | Depth4 | SubSurfT5 | Depth5 |
|-----------|----------------------------|----------------------------|----------|-----------|--------|-----------|--------|-----------|--------|-----------|--------|
| MX0858    | MI-01<br>SENEY<br>(705005) | 2013-01-24<br>03:35:00.000 | NULL     | 3.2       | 9.62   | 3.9       | 17.24  | 4.5       | 24.86  | 4.8       | 32.48  |



### 3.3.2 Data Mapping (vRWIS) for Site-Specific Predictions

The project aims to make site-specific predictions. Therefore, the success of this project relies on accurate information from RWIS sites; therefore, the insufficient physical RWIS infrastructure could be an obstacle. To clear this obstacle and also to improve the current MDOT RWIS, we will test the concept of virtual RWIS (vRWIS) with the freeze thaw model based SLR decision application and recommend a methodology for obtaining weather and pavement conditions at the vRWIS sites, and based on that, identify locations for potential vRWIS sites. A vRWIS will consist of both weather and pavement temperature information. However, this GIS information is excluded in the model development, the mapping the pavement data to any point of interest is not discussed. For weather, multiple techniques exist for extrapolating weather conditions from known locations to “virtual” sites: interpolation, climatological extrapolation, two-dimensional field analyses, and three-dimensional field analyses. This project adopts the interpolation technique. As shown in Figure 3.7, the data at any given point can be obtained by interpolating the data at the three nearest sites with known data. This interpolation is conducted based on the geographic locations of the sites. For the purpose, the latitudes and longitudes of the sites will be used to calculate the distance between any two sites.

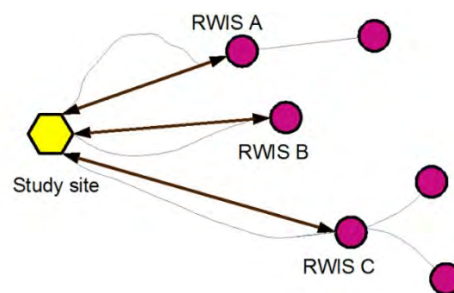


Figure 3.7 Pavement temperature calculation with measurements from nearby RWIS sites

In addition to vRWIS, another type of mapping is introduced to enable site-specific predictions for not only any RWIS site, but also any county and zip code. In the app, the data can be indexed by RWIS site, county, or zip code. That is, the data for any location associated with one type of index can be converted to any of the other indices. The conversion can be done with the mappings. In

the app, the mapping between them is achieved via tables. For example, the predictions for a given county can be obtained by averaging the predictions for the zip codes belonging to the county.

### 3.3.3 Data Selection via Correlation Analysis

As introduced in the previous section of this chapter, three types of data can be obtained. In theory, any type of data can be employed for the predictions of freezing and thawing depths and SLR dates as long as the data is related. For example, in an initial assessment, the following data types were included to be related to the intended predictions: 1. air temperature (freezing/thawing indices), 2. wind speed, 3. solar irradiation, 4. degree of saturation, 5. saturated thermal diffusivity 6. pavement type (cement and concrete) and thickness, and 7. thickness of the base (if any). However, it was found that it would be unrealistic to use all the information due to several reasons. First, some parameters such as pavement and soil information cannot be easily or/and accurately determined. Second, the establishment of a multivariate model with a lot of input variables could be difficult and computationally expensive. Third, not all the parameters are equivalently relevant; as a result, the inclusion of some parameters in the model not only could be unworthy but also cause unexpected issues both in the creation and operation of the models.

In the previous studies on freezing and thawing depth predictions and SLR dates predictions, engineers usually assume some parameters are significant, either based on observations or intuitions, and then construct prediction models based on the assumption. This project attempts to establish models using a more rational approach. That is, we resort to correlation analysis to quantify the correlation between different types of data and the freezing/thawing depth that we are trying to predict. Based on the results of the correlation analysis, we select the most relevant data types as the input of the prediction models to be developed. The most common formula for correlation is Pearson's correlation formula.

$$\rho_{X,Y} = \frac{cov(X,Y)}{\sigma_X\sigma_Y} \quad \text{Eq. 3.3}$$

where  $X$  and  $Y$  are the two variables whose correlation is computed,  $cov(X, Y)$  is the covariance of  $X$  and  $Y$ ,  $\sigma_X$  is the standard deviation of  $X$ ,  $\sigma_Y$  is the standard deviation of  $Y$ . The covariance is calculated using the following equation:

$$cov(X, Y) = E[(X - \mu_X)(Y - \mu_Y)] \tag{Eq. 3.4}$$

where  $E$  is the expectation,  $\mu_X$  is the mean of  $X$ , and  $\mu_Y$  is the mean of  $Y$ .

Shown in Figure 3.8 to Figure 3.10 are the correlation analysis results for selected data types at typical RWIS sites. As can be seen, the correlation coefficient between any variable and itself is one. The correlation coefficients of interest are the correlation coefficients between the FD/TD and other data types. It is not difficult to conclude that the pavement temperature has the highest correlation coefficient with both FD and TD in most cases, followed by the air temperature, freezing index, and thawing index. Due to this fact, the prediction models for freezing and thawing depth and SLR dates are built with freezing and thawing indices calculated with the pavement surface temperature, which is available as an RWIS data type.

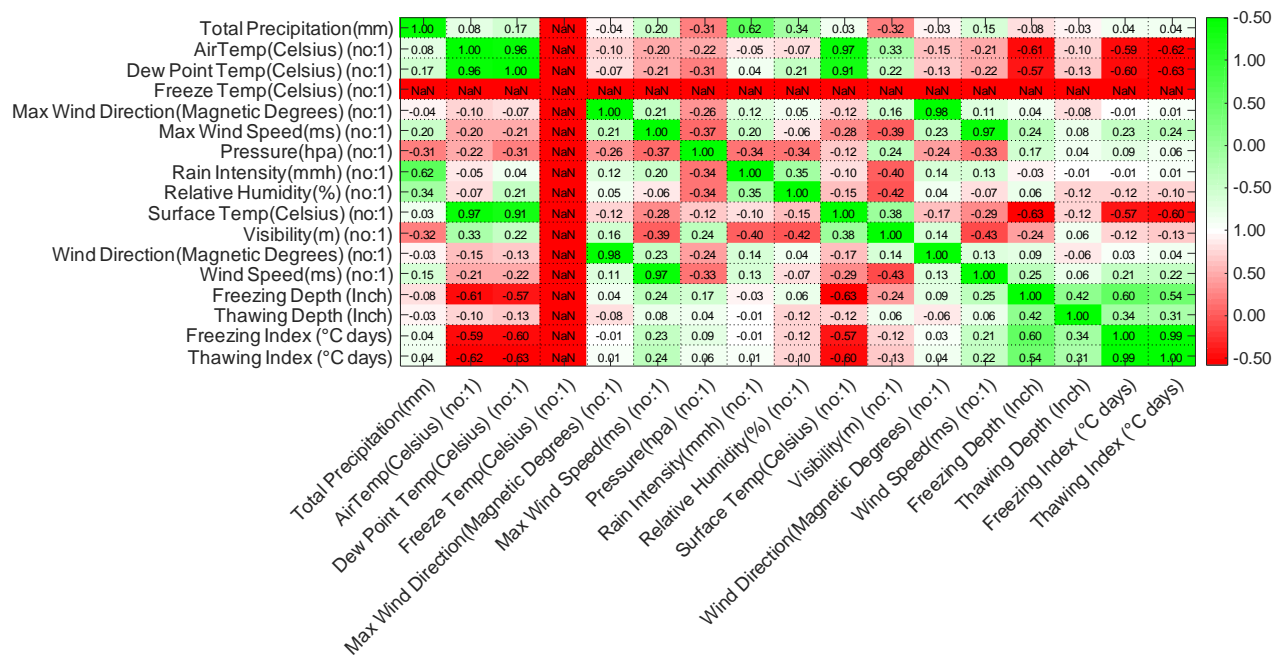


Figure 3.8 Correlation analysis for data selection in predictions of freezing and thawing depths and SLR dates (Site Fife Lake)

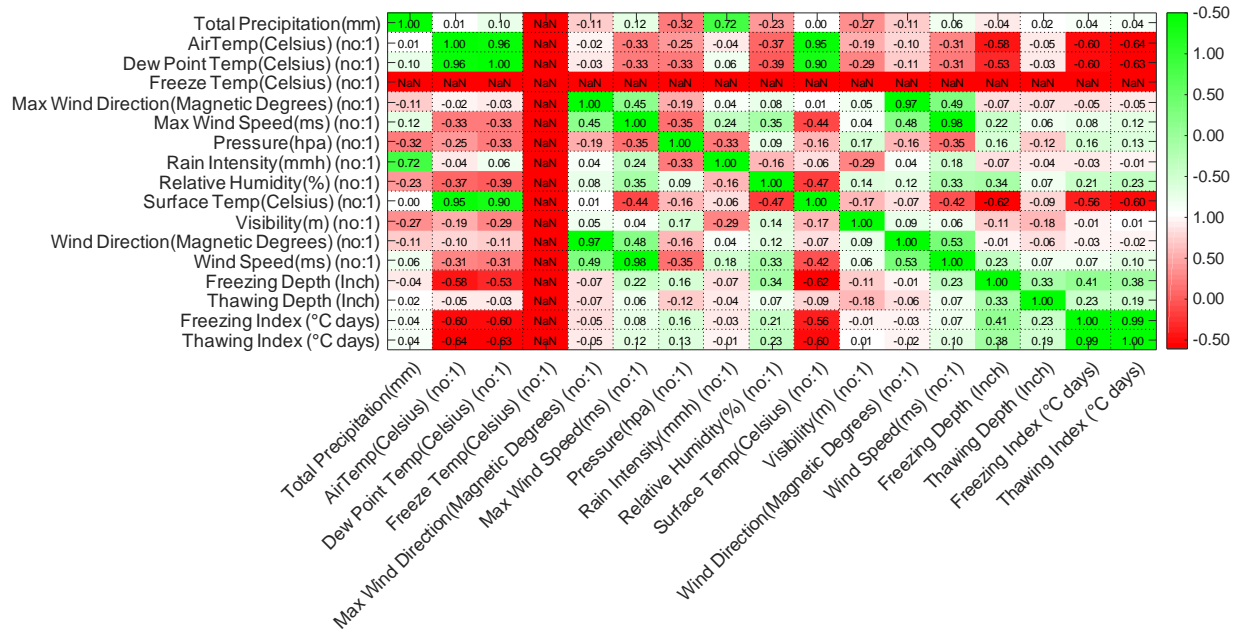


Figure 3.9 Correlation analysis for data selection in predictions of freezing and thawing depths and SLR dates (Site Eastport)

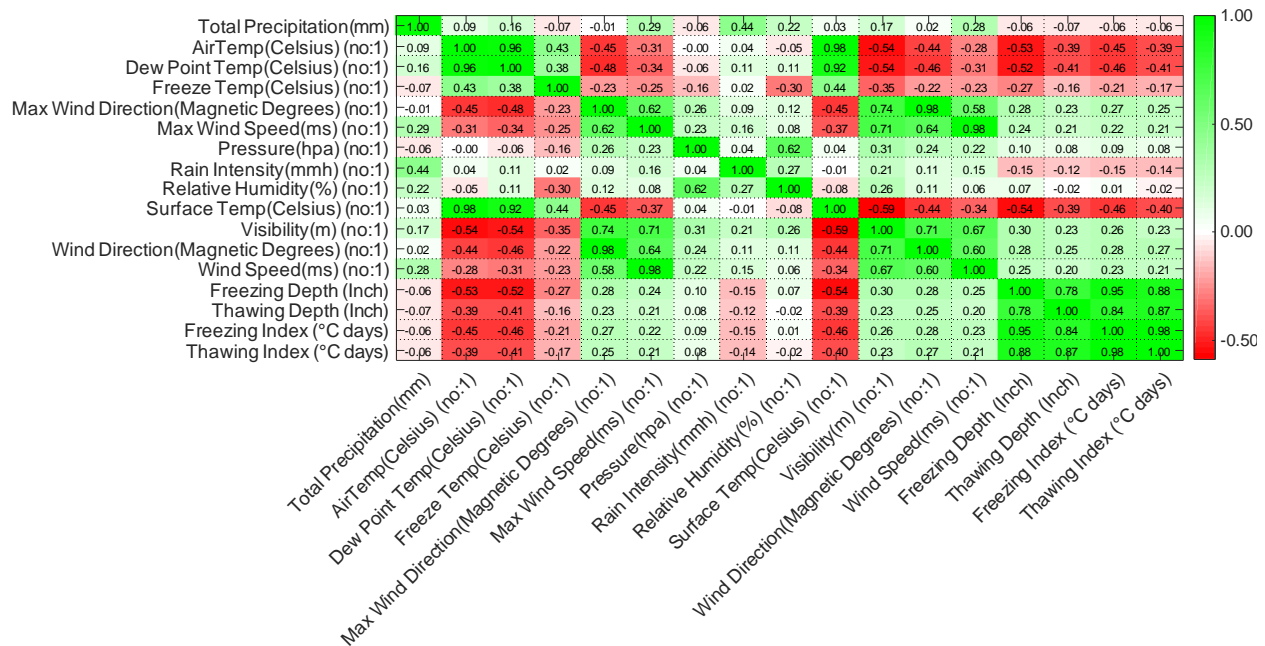


Figure 3.10 Correlation analysis for data selection in predictions of freezing and thawing depths and SLR dates (Site Cadillac South)

## **Chapter 4 Multivariate Freezing-Thawing Depth Prediction Model**

### **4.1 Overview**

Road damages induced by heavily loaded truck traffic during the spring thaw are major road distress in cold regions. To minimize these damages, Spring Load Restriction (SLR) is widely applied in the U.S., Canada, and other countries during the early thawing season by controlling the movement of freight-carrying trucks and heavy equipment travel until the thawing ends. Most SLR policies rely on the Freezing Depth (FD) and Thawing Depth (TD), especially the latter one. Therefore, accurate predictions of FD and TD are important to prevent both the extensive damage to the pavement due to the late placement or early removal of SLR and the economic loss of road users due to an unnecessarily long SLR period. Here, we propose a new multivariate model for predicting FD and TD in support of SLR decision-making. The model gives a curving surface of FD and TD in a 3-dimensional space, instead of 2-dimensional in traditional methods, by considering both the freezing and thawing indices in the entire freeze-thaw cycle. For model evaluations, yearly field data measured at five typical sites from 104 sites in Michigan were adopted. The evaluation results showed that the proposed model is accurate in predicting FD and TD for most sites. Compared to the previous TD predictions in the existing study, the TD predictions with the proposed model have been significantly improved. In addition, this study provides field data that have not been reported earlier in the literature and that can be used for validating other prediction models. The reported work is ready for practice for roadways in cold regions to support SLR decision-making.

In this chapter, we propose a new multivariate FD/TD prediction model, which is easily implementable for supporting SLR decision-making. The proposed model is primarily evaluated using field data measured at five typical sites in Michigan. The evaluation results for FD and TD based on both FI and TI in a 3-dimensional space are presented and discussed.

### **4.2 Field Measurements**

Michigan Department of Transportation (MDOT) deployed a Road Weather Information System (RWIS) to measure road and weather conditions on highways and communicate this information

to users in a maintenance facility. Through a series of strategically placed Environmental Sensor Stations (ESSs) in the RWIS, key road and weather conditions (e.g., humidity, wind speed, average air temperature, and temperatures of the pavement surface and subsurface) are measured in real-time. To share yearly RWIS data in public, we developed the MDOT SLR website (<https://mdotslr.org/>). As of now, there are 104 sites implemented with ESSs in Michigan as shown in Figure 4.1. The RWIS data for these sites can be freely downloaded from the MDOT SLR website.

In this study, we primarily selected five typical sites for analyses, three from the Upper Peninsula and two in the Lower Peninsula.

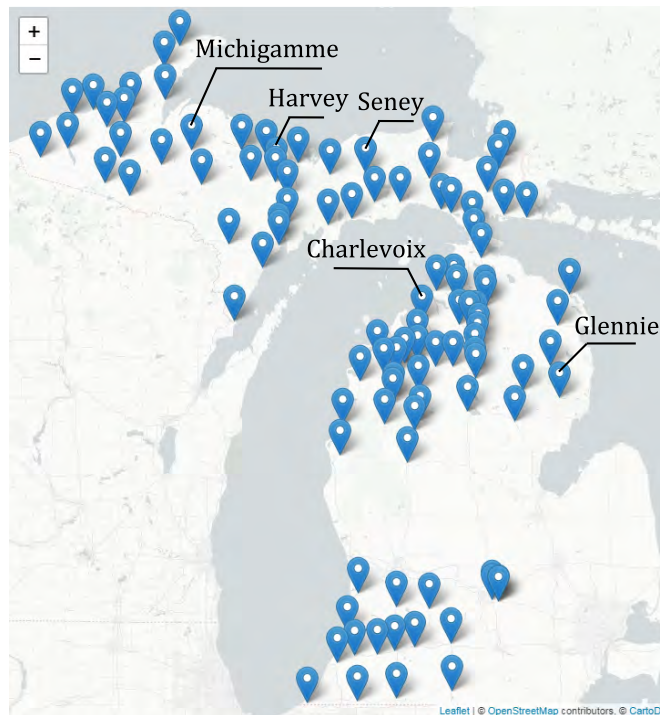


Figure 4.1 Overview of monitored sites with ESSs in Michigan

The pavement structure of the five selected sites primarily consists of an asphalt/concrete surface, a granular base, and a soil sub-base. Details of the pavement structure, soil types, and properties can be found in Baladi and Rajaei (2015). Table 4.1 shows all the measured temperatures needed for this study. The air temperature was measured by the air temperature sensor, while the pavement

surface and base temperatures were measured by surface and subsurface sensors, respectively. For base temperatures, 15 subsurface sensors were used to measure the temperatures from the base surface to a depth of 72 inches (1.83 m), which can be used to calculate FD and TD.

Table 4.1 Needed parameters for analyses

| Material |                       | Measured temperature           |   |   |   |    |    |    |    |    |    |    |    |    |    |
|----------|-----------------------|--------------------------------|---|---|---|----|----|----|----|----|----|----|----|----|----|
| Air      |                       | Average temperature (°C)       |   |   |   |    |    |    |    |    |    |    |    |    |    |
|          |                       | Surface temperature (°C)       |   |   |   |    |    |    |    |    |    |    |    |    |    |
| Pavement | Base temperature (°C) | Depth from base surface (inch) |   |   |   |    |    |    |    |    |    |    |    |    |    |
|          |                       | 0                              | 3 | 6 | 9 | 12 | 18 | 24 | 30 | 36 | 42 | 48 | 54 | 60 | 66 |

Note: 1 inch=2.54 cm

### 4.3 A New Freezing-Thawing Depth Prediction Model

Calculations of FD and TD are related to the solution to a phase-change (ice-liquid) problem of heat transfer. In a pioneering study, Neumman solved FD by analyzing the 1D heat transfer in a semi-infinite soil (Jiji and Ganatos 2009). FD in the Neumman's equation is a function of the surface temperature, time, and thermal conductivities of both the frozen and unfrozen soils (see details in Baladi and Rajaei (2015)). A special case of the Neumman's equation was further solved by assuming no heat transfer in the liquid (Baladi and Rajaei 2015), in which FD is formulated by

$$FD = \sqrt{\frac{2\lambda_f}{\rho l} (T_0 - T_{s,s})t} \quad \text{Eq. 4.1}$$

where  $\lambda_f$  is the thermal conductivity of a frozen soil (W/(m °C)),  $\rho$  is the soil density (kg/m<sup>3</sup>),  $l$  is the latent heat of fusion (J/kg),  $T_0$  is the freezing point of bulk water (=0 °C),  $T_{s,s}$  is the soil surface temperature, and  $t$  is the time (day). Based on Eq. 4.1, many physico-empirical models were further developed. These physico-empirical models share a common form of Eq. 4.2 to calculate FD (Aldrich and Paynter 1953)

$$FD = a_o \sqrt{\frac{48\lambda_f n FI}{L}} \quad \text{Eq. 4.2}$$

where  $L$  is the volumetric latent heat of fusion ( $\text{J/m}^3$ ),  $n$  is a dimensionless parameter converting the air temperature index to the surface temperature index,  $a_o$  is a dimensionless correction factor considering the initial freezing depression (Berg et al. 2006).

The recent physico-empirical models (Asefzadeh et al. 2016; Baiz et al. 2008; Marquis 2008; Miller et al. 2012) further loosened the constraints in Eq. 4.2 by only keeping FI and lumping all the other terms with physical meanings into one or two fitting constants. The fitting constants can be obtained by linear regression with measured data. Therefore, physico-empirical models are also statistical models. One major feature of these physico-empirical models is the linear relationship between FD and the square root of FI. The above existing studies have proved that satisfactory predictions for FD can be made using the square root of FI. This study also uses this method for the FD prediction with the square root of FI. In addition, results from the field measurements for the five selected sites and additional sites, shown in Fig. 4, clearly indicate that FD follows a square root function decay as TI increases.

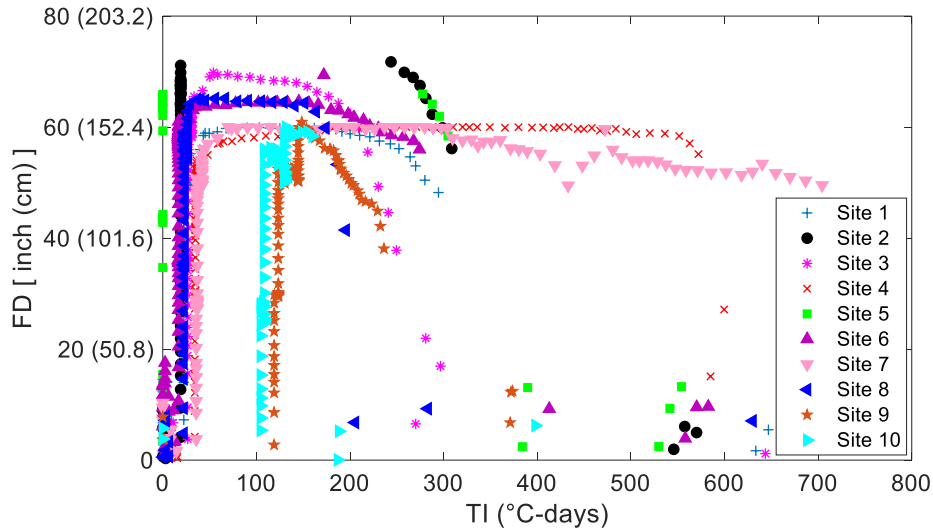


Figure 4.2 Field measurement results of TI-FD relationships from ten sites in Michigan

Considering the above facts, the following model is proposed for FD involving both FI and TI

$$FD = a\sqrt{FI} + \sqrt{c - bTI} + d \quad \text{Eq. 4.3}$$

where  $a$ ,  $b$ ,  $c$ , and  $d$  are fitting constants, the first three always positive. It is known that freezing and thawing processes are similar (Konrad 1989); as a result, the mathematical formulations for TD and FD are similar

$$TD = -e\sqrt{FIT} - \sqrt{g - fTI} + h \quad \text{Eq. 4.4}$$

where  $e$ ,  $g$ ,  $f$ , and  $h$  are fitting constants, the first three always positive. FIT is the cumulative freezing index in the thawing period only. FI is not adopted here for TD, as FI mainly represents the cumulative frost in the pavement base during the freezing period, which in fact is irrelevant to TD. Therefore, FIT is adopted, which can appropriately consider the cumulative freezing index when the thawing starts. The fitting constants for FD and TD reflect the real situation for the depth and duration of the freeze and/or thaw penetration in the pavement base. The fitting constants can be obtained using the nonlinear least-squares method on each site. It is noted that  $c - bTI > 0$  and  $g - fTI > 0$  should be ensured (i.e., the principal square root of a positive number) in the nonlinear regression analysis.

The cumulative freezing index during the freezing period can be calculated based on  $T_0 = 0^\circ\text{C}$  over a given period

$$\begin{cases} FI = \sum(T_0 - T_s) \\ T_0 - T_s < 0 \Rightarrow T_0 - T_s = 0 \end{cases} \quad \text{Eq. 4.5}$$

where  $T_s$  is the pavement surface temperature. Similarly, FIT can be calculated using Eq. 4.5 starting from the date when the first TD occurs in the thawing period. The cumulative thawing index is computed by

$$\begin{cases} TI = \sum(T_s - T_{ref}) \\ T_s - T_{ref} < 0 \Rightarrow T_s - T_{ref} = 0 \end{cases} \quad \text{Eq. 4.6}$$

where  $T_{ref}$  is the reference temperature to account for the amount of solar radiation and thermal properties of the pavement material. In this study,  $T_{ref} = -1.67\text{ }^{\circ}\text{C}$  was used according to the guideline of FHWA-WSDOT (Mahoney et al. 1987). Eq. 4.5 and Eq. 4.6 use the pavement surface temperature instead of the average air temperature. This is due to the fact that FI and TI calculated with the average air temperature failed to correlate FD and TD in the freeze-thaw cycle (see **Error! Reference source not found.**), which will be discussed later in detail.

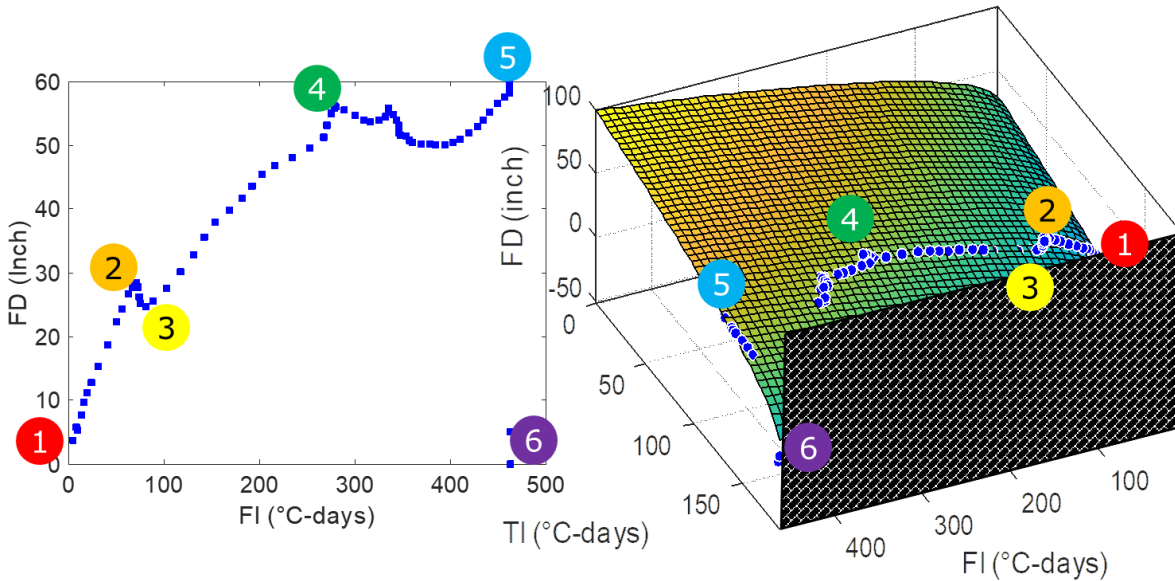


Figure 4.3 Schematic of 3D model and its project on the FD plane

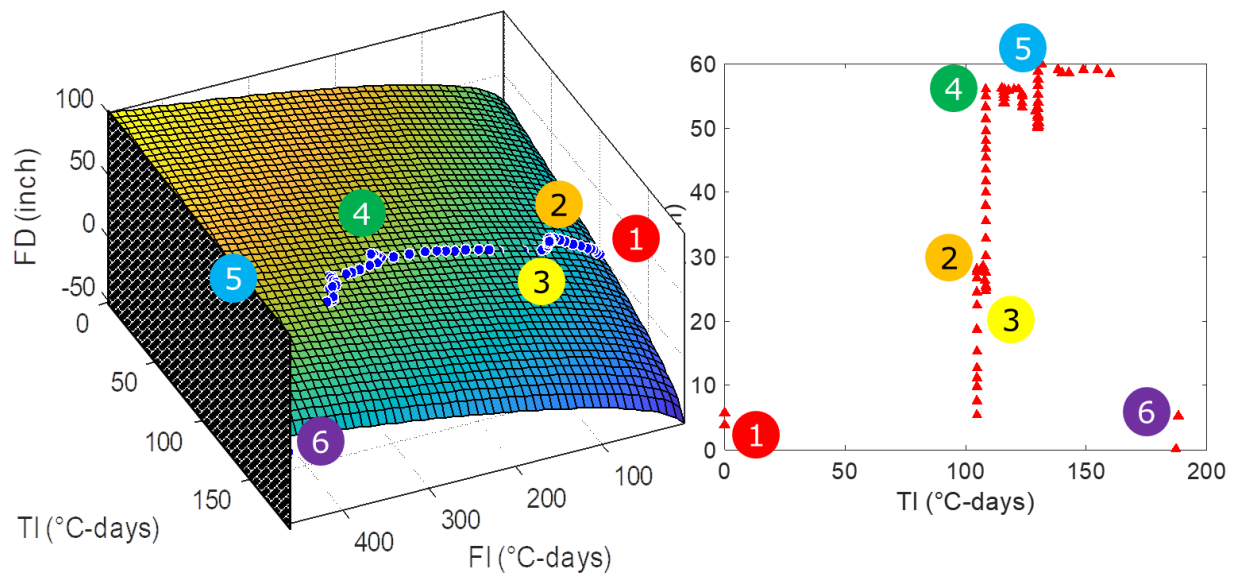


Figure 4.4 Schematic of 3D model and its project on the TD plane

#### 4.4 Prediction and Evaluation of Freezing-Thawing Depth Model

FDs and TDs presented in Figure 3.4 for all the selected sites were used for the statistical analyses based on the proposed model using FI and TI values calculated with the pavement surface temperature. **Error! Reference source not found.**a shows the fitting result of FD for Harvey. A curving surface for predicted FD is exhibited, in which FD increases as FI increases and decreases as TI increases. The maximum FD could be obtained when FI almost remains unchanged and TI significantly increases. The predicted FD surface is in good agreement with the measured FDs and the coefficient of determination is found to be 0.94. Therefore, the proposed FD model performs well in predicting FD with high accuracy.

Fig. 10b presents the surface fitting result of TD formulated by TI and FIT for Harvey. We can clearly see that the predicted TD surface is very close to the measured TDs. TD increases with an increase in TI. However, it is difficult to observe how TD changes with FIT from **Error! Reference source not found.**b, as Point A does not belong to TD data in the thawing period. This point appears before February 2018 due to the occurrence of some warm days in the freezing period (see Figure 3.4a). As our goal is to predict TD in the thawing period for applying SLR, Point A beyond the thawing cycle in Figure 3.4a can be removed. It can be seen in **Error! Reference source not found.**c that TD decreases as FIT increases when Point A is excluded. The predicted TD surface fitted to the measured TDs in the thawing cycle becomes more accurate and the coefficient of determination increases from 0.83 to 0.90 accordingly.

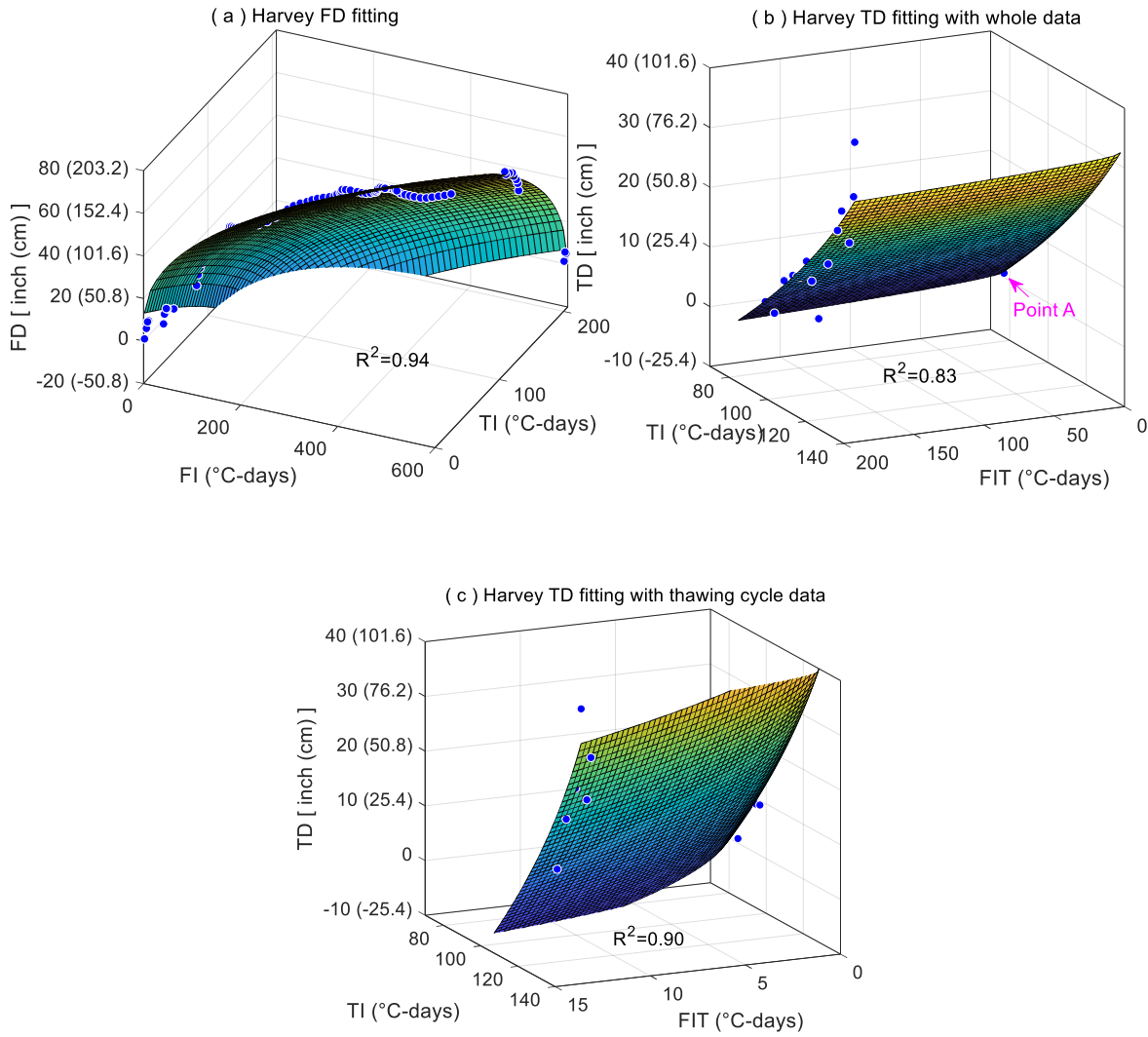
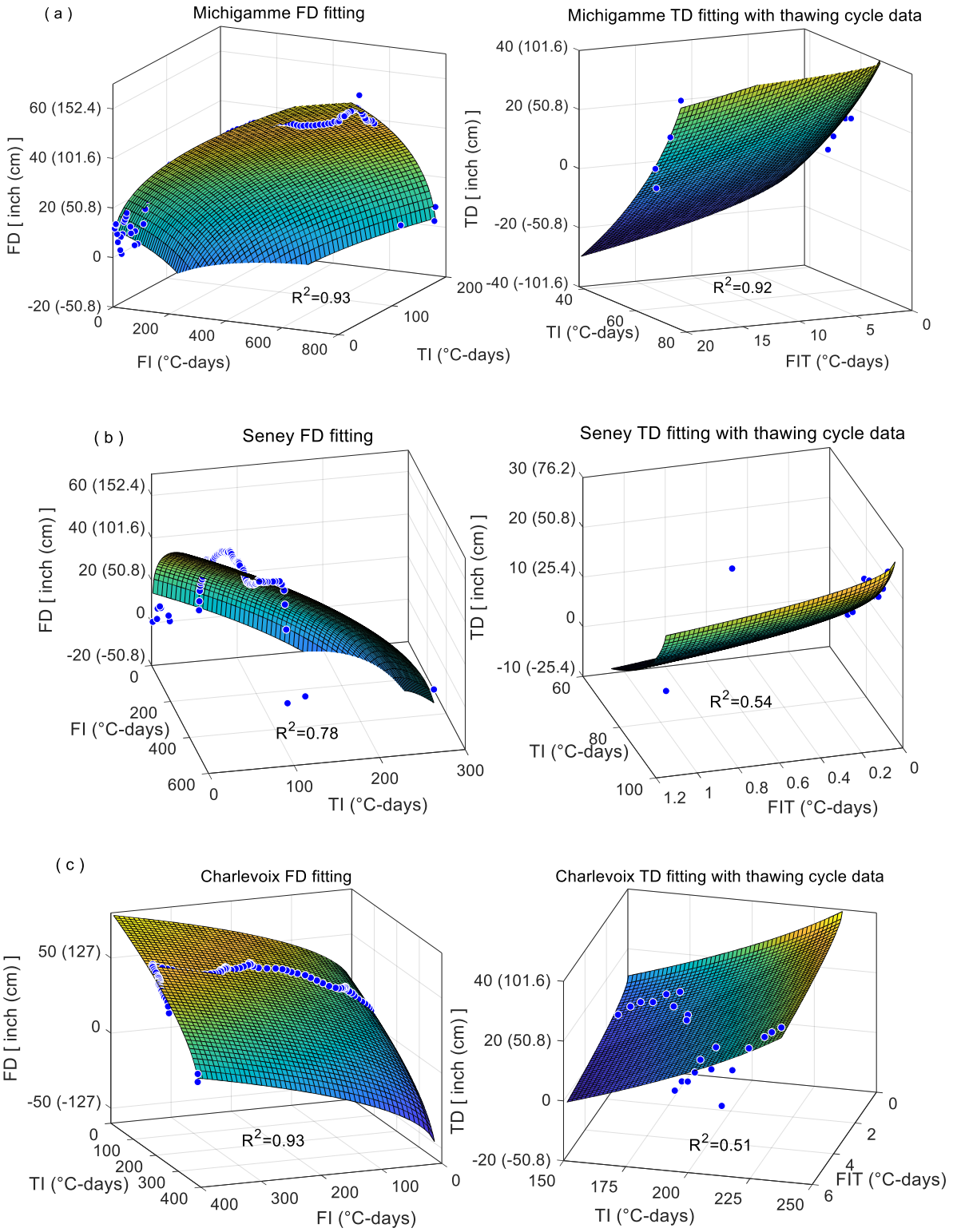


Figure 4.5 Fitting surfaces for Harvey: (a) FD fitting, (b) TD fitting with the whole TD data, (c) TD fitting with the thawing cycle data.

For the other four sites, **Error! Reference source not found.** presents the 3-dimensional fitting surfaces of FD and TD. The TD data in the thawing cycle in Fig. 8 were used for fitting TD for each site. It can be seen that the predicted FD surfaces for these sites match well with the measured FDs. The coefficient of determination for most sites is found to be as high as 0.93. For TD predictions, the predicted TD surfaces for Michigamme and Glennie are in good agreement with the measured TDs (see **Error! Reference source not found.a** and **Error! Reference source not found.d**). The predicted TD surfaces for the other two sites are not as good as those

for Harvey and Michigamme, as shown in **Error! Reference source not found.**b and **Error! Reference source not found.**c. The reason is that the measured TDs do not increase continuously, but rather, go up and down, for example, Charlevoix in Figure 3.4c. This makes it difficult to fit a 3-dimensional surface in the nonlinear regression analysis. However, the predicted TD surfaces for these two sites capture the key mechanism of the TD-TI-FIT relationship, i.e., TD nonlinearly increases with an increase in TI and a decrease in FIT. Also, from the fitting constants tabulated in Figure 4.6 Fitting surfaces for FD and TD: (a) Michigamme, (b) Seney, (c) Charlevoix, and (d) Glennie

, each fitting constant has the same sign for all the selected sites, regardless of FD and TD predictions. This implies that the FD-FI-TI relationship for all the five selected sites has the same trend, so is that of the TD-TI-FIT relationship. The proposed model was further assessed by additional sites shown in Figure 4.3. The 3-dimensional fitting surfaces for these additional sites are very similar to those in **Error! Reference source not found.**. The fitting results for these additional sites are tabulated in Table 3. It is seen that the coefficient of determination for FD and TD for most sites is higher than 0.8, which further confirms that the proposed model is adaptable to other sites. The above evaluation results clearly show the key varying mechanisms of both the FD-FI-TI relationship and the TD-TI-FIT relationship, and also demonstrate the high accuracy of the proposed model for predicting FD and TD for most sites. Comprehensive lists of the fitting constants for the RWIS sites, which are termed as FD/TD prediction models for these sites, were obtained based on the RWIS data in Year 2017-2018 and Year 2018-2019, and the lists are provided in the Appendix.



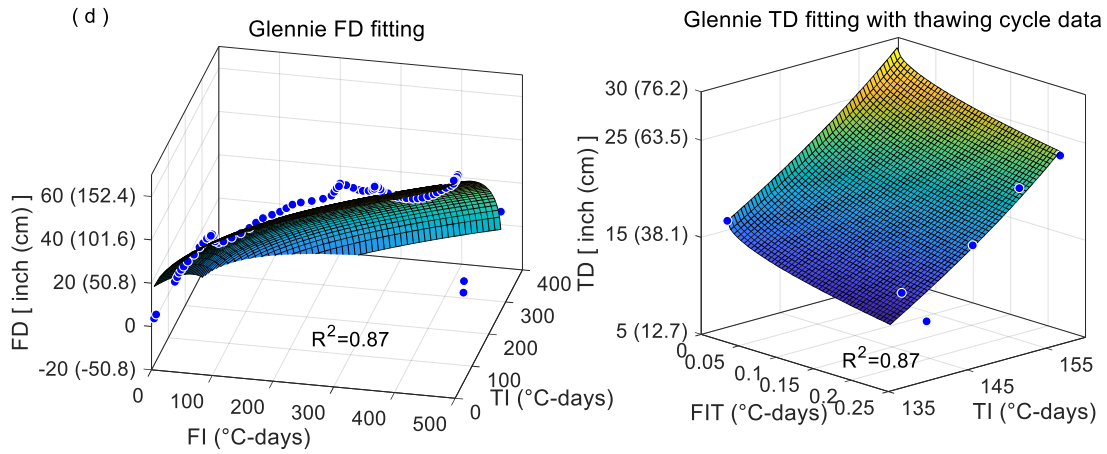


Figure 4.6 Fitting surfaces for FD and TD: (a) Michigamme, (b) Seney, (c) Charlevoix, and (d) Glennie

Table 4.2 Fitting results for the five selected sites

| Site       | Variable prediction   | Fitting constant                  |  |                   |          | $R^2$ |
|------------|-----------------------|-----------------------------------|--|-------------------|----------|-------|
|            |                       | unit: inch °C-day <sup>-0.5</sup> | inch <sup>2</sup> °C-day <sup>-1</sup> | inch <sup>2</sup> | inch     |       |
| Harvey     | FD                    | <i>a</i>                          | <i>b</i>                               | <i>c</i>          | <i>d</i> | $R^2$ |
|            |                       | 4.03                              | 69.24                                  | 14574             | -109.5   | 0.94  |
|            | TD                    | <i>e</i>                          | <i>f</i>                               | <i>g</i>          | <i>h</i> | $R^2$ |
|            |                       | 0.17                              | 56.59                                  | 1717.91           | 71.9     | 0.83  |
|            | TD with thawing cycle | 5.11                              | 120.3                                  | 18422.1           | 94.93    | 0.9   |
| Michigamme | FD                    | <i>a</i>                          | <i>b</i>                               | <i>c</i>          | <i>d</i> | $R^2$ |
|            |                       | 2.56                              | 36.84                                  | 6913.6            | -78.34   | 0.93  |
|            | TD with thawing cycle | <i>e</i>                          | <i>f</i>                               | <i>g</i>          | <i>h</i> | $R^2$ |
|            |                       | 6.31                              | 229.7                                  | 19071             | 100.1    | 0.92  |
| Seney      | FD                    | <i>a</i>                          | <i>b</i>                               | <i>c</i>          | <i>d</i> | $R^2$ |
|            |                       | 2.67                              | 29.06                                  | 8028.8            | -78.81   | 0.78  |
|            | TD with thawing cycle | <i>e</i>                          | <i>f</i>                               | <i>g</i>          | <i>h</i> | $R^2$ |
|            |                       | 8.16                              | 50.8                                   | 5410.8            | 42.27    | 0.54  |
| Charlevoix | FD                    | <i>a</i>                          | <i>b</i>                               | <i>c</i>          | <i>d</i> | $R^2$ |
|            |                       | 3.15                              | 17.09                                  | 528.36            | -65.47   | 0.93  |

|         |                       |          |          |          |          |                |
|---------|-----------------------|----------|----------|----------|----------|----------------|
|         | TD with thawing cycle | <i>e</i> | <i>f</i> | <i>g</i> | <i>h</i> | R <sup>2</sup> |
|         |                       | 5.43     | 29.03    | 1126.04  | 69.2     | 0.51           |
|         | FD                    | <i>a</i> | <i>b</i> | <i>c</i> | <i>d</i> | R <sup>2</sup> |
| Glennie |                       | 3.60     | 39.78    | 215.31   | -64.56   | 0.87           |
|         | TD with thawing cycle | <i>e</i> | <i>f</i> | <i>g</i> | <i>h</i> | R <sup>2</sup> |
|         |                       | 11.90    | 35.69    | 688.92   | 51.99    | 0.87           |

Note that 1 inch=2.54 cm



Figure 4.3 Locations of additional sites in Michigan

Table 4.2 Prediction results for additional sites

| Site     | Variable prediction   | Fitting constant                  |  |                   |          | R <sup>2</sup> |
|----------|-----------------------|-----------------------------------|--|-------------------|----------|----------------|
|          |                       | unit: inch °C-day <sup>-0.5</sup> | inch <sup>2</sup> °C-day <sup>-1</sup> | inch <sup>2</sup> | inch     |                |
| Rudyard  | FD                    | <i>a</i>                          | <i>b</i>                               | <i>c</i>          | <i>d</i> | R <sup>2</sup> |
|          |                       | 2.36                              | 7.08                                   | 2790.05           | -69.93   | 0.96           |
|          | TD with thawing cycle | <i>e</i>                          | <i>f</i>                               | <i>g</i>          | <i>h</i> | R <sup>2</sup> |
|          |                       | 1.19                              | 20.30                                  | 2033.04           | 83.42    | 0.83           |
| Eastport | FD                    | <i>a</i>                          | <i>b</i>                               | <i>c</i>          | <i>d</i> | R <sup>2</sup> |

|                |                       |          |          |          |          |                |
|----------------|-----------------------|----------|----------|----------|----------|----------------|
|                |                       | 3.37     | 13.39    | 460.14   | -65.84   | 0.83           |
|                |                       | <i>e</i> | <i>f</i> | <i>g</i> | <i>h</i> | R <sup>2</sup> |
|                | TD with thawing cycle | 0.56     | 70.37    | 1339.69  | 68.11    | 0.80           |
|                |                       | <i>a</i> | <i>b</i> | <i>c</i> | <i>d</i> | R <sup>2</sup> |
|                | FD                    | 3.16     | 51.25    | 427.50   | -76.16   | 0.84           |
| Au Train       |                       | <i>e</i> | <i>f</i> | <i>g</i> | <i>h</i> | R <sup>2</sup> |
|                | TD with thawing cycle | 2.70     | 11.11    | 204.37   | 36.92    | 0.54           |
|                |                       | <i>a</i> | <i>b</i> | <i>c</i> | <i>d</i> | R <sup>2</sup> |
|                | FD                    | 0.83     | 0.91     | 233.98   | -13.39   | 0.87           |
| Cadillac South |                       | <i>e</i> | <i>f</i> | <i>g</i> | <i>h</i> | R <sup>2</sup> |
|                | TD with thawing cycle | 0.32     | 1.70     | 210.58   | 22.88    | 0.85           |
|                |                       | <i>a</i> | <i>b</i> | <i>c</i> | <i>d</i> | R <sup>2</sup> |
|                | FD                    | 3.80     | 27.25    | 383.19   | -90.74   | 0.92           |
| Fife Lake      |                       | <i>e</i> | <i>f</i> | <i>g</i> | <i>h</i> | R <sup>2</sup> |
|                | TD with thawing cycle | 11.00    | 23.10    | 388.24   | 58.94    | 0.84           |

1 inch=2.54 cm

## 4.5 Discussions

### 4.5.1 Calculations of FI and TI via Surface Temperature Rather than Air Temperature

Calculations of FI and TI are needed to accurately predict FD and TD. To obtain appropriate FI and TI, the pavement surface temperature was used in this study. This is different from most existing models (e.g., Baiz et al. (2008) and Chapin et al. (2012)) that adopt the average air temperature to calculate FI and TI. To illustrate the advantage of using the pavement surface temperature, Figure 4.4 shows the comparisons of FI and TI calculated with the pavement surface temperature and those calculated with the average air temperature for Harvey and Michigamme, in which the corresponding FD and TD are also plotted.

It is clearly seen in Figure 4.4 that when the thawing starts from March 2018, FI calculated with the average air temperature (dashed blue line) still increases. At the same time, FD significantly decreases and TD continuously increases. Starting from March 2018, it is also seen that TI calculated with the air temperature (dashed red line) almost remains unchanged, which does not

appear reasonable. When the thawing starts, TI should increase accordingly and FI should decrease, as the increase in TD is mainly attributed to the continuous thaw penetration in the pavement base. This causes the accumulated frost in the base to thaw and accordingly, FD should decrease significantly. FI and TI calculated with the air temperature, however, fail to match the changes in TD and FD in a realistic way. When the pavement surface temperature is applied, as shown in Figure 4.4, FI (solid blue line) almost remains unchanged and TI (solid red line) increases starting from March 2018, which matches very well with the corresponding changes in TD and FD. In addition to the above two sites, FI and TI calculated with the pavement surface temperature for the rest of the three sites also match quite well with the trends of FD and TD. Therefore, the pavement surface temperature is more suitable to calculate FI and TI for predicting FD and TD than the average air temperature.

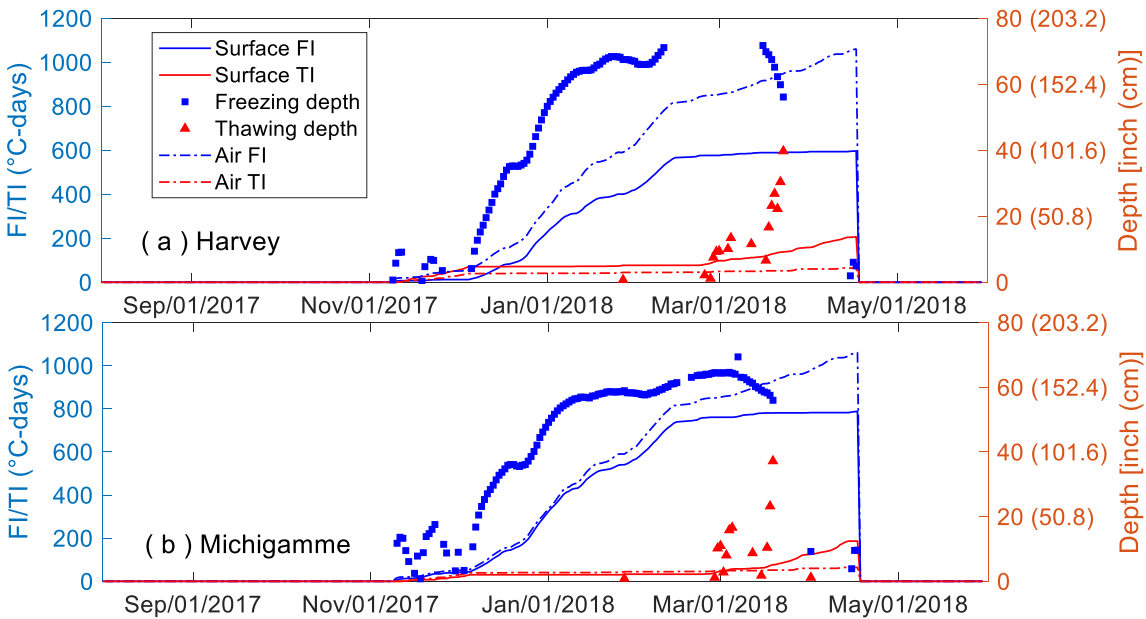


Figure 4.4 Comparisons of FI/TI calculated with the pavement surface temperature and the average air temperature: (a) Harvey and (b) Michigamme

## 4.5.2 Prediction Improvement

Good predictions for both FD and TD, especially the latter one, can be obtained with the proposed model. The 3D fitted surfaces hide the underneath measured data, causing a difficulty in visually evaluating the prediction accuracy. To clearly see the predictions, taking the Harvey site for example, Figure 4.5 shows the fitted line instead of fitted surfaces for both FD and TD. We can see in Figure 4.5 that the fitted line for FD agrees well with the measured FDs in a 3D space. The fitted line for TD in Fig. 14b is also very close to the measured TDs, in which the “staircase shape” is observed. This is due to the fact that TI keeps unchanged and in the meantime FIT increases if there have a few freezing days during the thawing period, and vice versa.

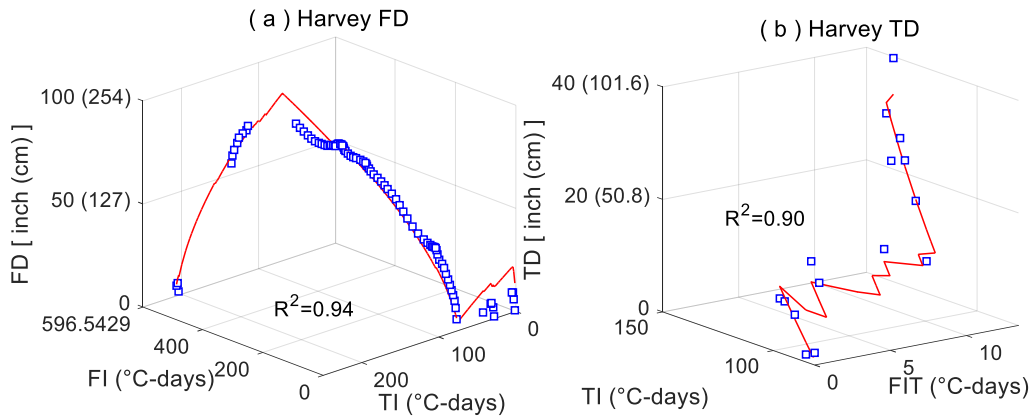


Figure 4.5 Fitting lines for Harvey: (a) FD fitting, (b) TD fitting with the thawing cycle data

The good predictions with the proposed model are primarily attributable to three reasons. First, the pavement surface temperature is used to reflect more realistic pavement thermal conditions than the air temperature, as explained in Section 4.5.1. Second, the proposed model adopts the mathematical form of  $-\sqrt{g - fTI}$  for TD predictions rather than the general form of  $f\sqrt{TI}$  used in the existing studies (e.g., Baiz et al. (2008)). The latter one may be only suitable for a specific site, while the former one has been confirmed by many different sites shown in Figure 4.3. Third, the proposed model adopts FIT rather than FI for predicting TD. The selection of FIT is more reasonable because the value of FI also determines the TD prediction accuracy in addition to its

mathematical form (i.e., square root). Therefore, FIT is better than FI for the TD prediction by appropriately considering the cumulative freezing index when the thawing starts.

Though the FD and TD predictions are promising for most sites in this study, there are still deviations for a few sites, e.g., Seney in **Error! Reference source not found.**. The possible reason is that factors, such as solar radiation and thermal properties of pavement materials, are not considered directly, but instead, considered via a constant  $T_{ref}$ . The effect of the solar radiation is believed to be significant as the solar radiation can significantly change both the pavement surface and air temperatures. However, the proposed model can predict both FD and TD with high accuracy for most sites even using a constant  $T_{ref}$ . Fig. 15 presents the comparison between the previous TD predictions (Baladi and Rajaei 2015) in Michigan and those with the proposed model. In addition to the selected five typical sites, three additional sites were also analyzed to evaluate the predicted maximum TDs. We can clearly see that the TD predictions in this study are very close to the measured TDs and much better than the previous TD predictions (Baladi and Rajaei 2015). Therefore, the TD predictions have been significantly improved.

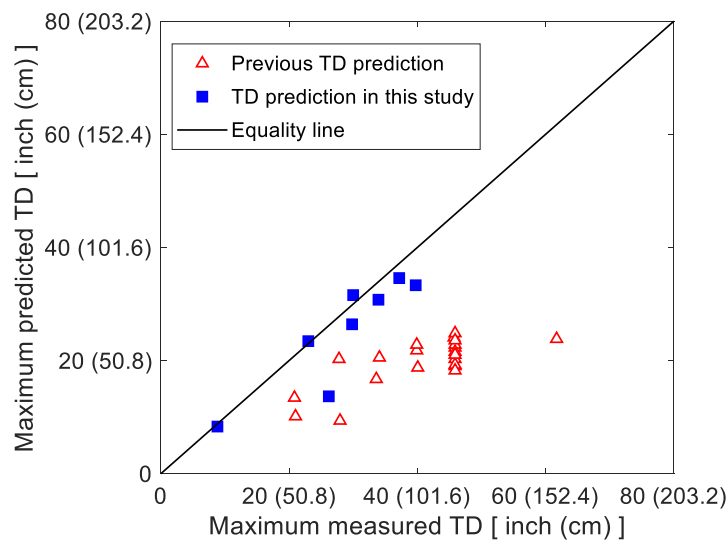


Figure 4.6 Comparison of the maximum measured TDs and predicted TDs

## 4.6 Conclusions

This study proposes a new multivariate model for predicting FD and TD to support SLR decision-making. The model can give a curving surface of FD and TD in a 3-dimensional space by considering both the freezing and thawing indices. For the model evaluation, yearly field data measured at five typical sites from 104 sites in Michigan were used. The results indicated that the use of the pavement surface temperature gives reasonable FI and TI and better results than the average air temperature. FI and TI calculated with the pavement surface temperature match well with the corresponding changes in FD and TD with time. Therefore, the pavement surface temperature is more appropriate to calculate FI and TI for FD and TD predictions.

Evaluation of the results from the proposed model revealed that FD can be predicted with high accuracy for all the selected sites. For the FD-FI-TI relationship, the 3-dimensional surface clearly demonstrated that FD increases as FI increases and decreases as TI increases in the freeze-thaw cycle. The predicted TDs for three selected sites are very close to the measured TDs. There are deviations in the TD predictions for the other two sites, which is possibly due to the fact that factors, e.g., solar radiation and thermal properties of pavement materials, are not considered directly during the thawing period. However, the TD predictions have been significantly improved when compared to the previous TD predictions. Therefore, the proposed model is a capable tool for practice for roadways in cold regions in support of SLR decision-making. In addition, the present study provides field data that have not been reported earlier in the literature and that can be used for validating other prediction models.

## **Chapter 5 Freezing-Thawing Depth Prediction with Constrained Optimization for Applications of Spring Load Restriction**

### **5.1 Overview**

Spring Load Restriction (SLR) has been widely implemented in many countries to reduce the cost of road repair for freeze-thaw induced damages in cold regions occurring in the spring thawing season. In most SLR policies, accurate predictions of the Freezing Depth (FD) and Thawing Depth (TD) are very critical because both FD and TD directly determine the dates for the SLR placement and removal. In this study, we propose a new constrained optimization approach to predict FD and TD and evaluate this approach for making SLR decisions with field measurements collected at four sites during two adjacent year cycles. The evaluation results showed that constrained optimization can not only accurately predict FD and TD with the determination coefficient of higher than 0.91 for most sites, but enable FD to meet TD in the thawing season for accurate SLR-decision making, which, however, cannot be achieved using non-constrained optimization widely adopted in the literature. We also discuss the accuracy of using a Thawing Index (TI)/Freezing Index (FI) ratio of 0.3 that still has been used by several agencies in the U.S. to determine the removal date of SLR. Our results indicated that on the true dates of the SLR removal, a TI/FI ratio is not equal even close to 0.3 for most sites. By comparison, a TI/FI ratio of 0.3 will be less accurate than the FD and TD prediction model for SLR decision-making. The methodology reported in this study is easy to use and implement for road engineers and the insights will help make accurate SLR decisions to prevent roads in cold regions from freeze-thaw induced damages.

### **5.2 Introduction**

Many FD and TD prediction models have been proposed in the literature based on 1D heat transfer in a semi-infinite soil. The typical one is the Neumann' empirical model (Jiji and Ganatos 2009), where FD is predicted in terms of the square root of FI and soil properties (e.g., thermal conductivity). The following models make some modifications by only keeping FI and lumping all the other terms for soil properties into one or two fitting constants (Asefzadeh et al. 2016; Baiz et al. 2008; Marquis 2008; Miller et al. 2012). To obtain these fitting constants, nonlinear

regression of the measured data is usually employed. For TD predictions, two major types of prediction models are available in the literature, but each contains 2-4 fitting constants that need to be determined by nonlinear regression as well. The first type is to predict TD via TI only using a power function. Chapin et al. (2012), for instance, used this type to predict TD with the measured data, where the obtained determination coefficient was 0.59-0.83. For the second type, TD is assumed to share the same mathematical function as that of FD, i.e., the square root of both FI and TI (see Figure 5.1). In comparison, the determination coefficient obtained based upon the second type (Baiz et al. 2008) is higher than of the first type and about 0.99. However, Baiz et al. (2008) predicted TD in the freezing and thawing seasons separately using a piecewise function, which is inconvenient in practice. Bao et al. (2019) thus suggested using an integrated approach to predict TD in the whole freeze-thaw cycle using a multivariate model (i.e., a variation of the second type), in which the obtained determination coefficient is in a range of 0.8-0.94 and the pavement surface temperature is confirmed to be better than the air temperature for calculating FI and TI.

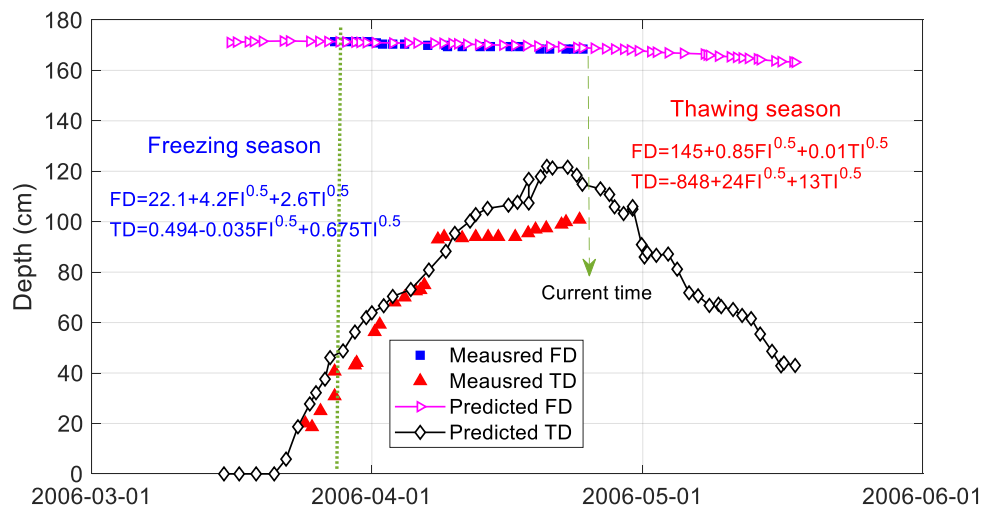


Figure 5.1 Measured vs predicted data for FD and TD [data is from (Baiz et al. 2008)]. Note that predicted TD and FD trends are obtained using the thawing season fitting constants.

Though either TI or an FD/TD prediction model has been extensively applied for SLR decision-making, two issues are still unclear. Firstly, several agencies in the U.S. still use a ratio of 0.3 between TI and FI proposed by Mahoney et al. (1987) to determine the removal date of SLR

because of its simplicity. However, it is still uncertain how accurately the TI/FI ratio method performs for SLR decision-making when compared to an FD/TD prediction model. Secondly, the essential step in SLR decision-making with an FD/TD prediction model is to determine a date for the SLR removal when FD meets TD (see Fig. 4 for details) in the thawing season (Baiz et al. 2008). However, FD and TD predicted via the existing model (Baiz et al. 2008) cannot meet with each other, as shown in Figure 5.1, which hinders the application of the FD and TD prediction model in practice for SLR decision-making. In addition, when both FI and TI are equal to zero, FD and TD in the thawing season in Figure 5.1 are 145 and -848 cm, respectively (22.1 and 0.494 cm in the freezing season). These numbers, in fact, should be identical and have the physical meaning that is related to the pavement surface thickness (see details in Section 5.3.2). Therefore, the fitting constants in Baiz et al. (2008) are only statistical numbers without clarifying their physical meaning, which fail to reflect realistic pavement FD and TD conditions.

In this study, we address the above issues using the multivariate FD/TD prediction model adopted from our previous study (Bao et al. 2019). Though the prediction model used in this study is the same as that of Bao et al. (2019), there are two distinct differences in the model application. First, we clearly clarify the physical meaning of all fitting constants in the prediction model. Second, we propose a new constrained optimization approach for obtaining fitting constants to reflect realistic pavement FD and TD conditions. We evaluate FD and TD predictions with constrained optimization via site measurements collected during two adjacent year cycles in Michigan. Discussion is also made to shed light on the advantages of constrained optimization newly proposed in this study and how accurate the FD/TD prediction model or a TI/FI ratio is for SLR decision-making.

## **5.3 Theory and Method**

### **5.3.1 Field Measurements and SLR Determination Method**

Field measurements for road pavements in Michigan are adopted in this study. A Road Weather Information System (RWIS) deployed in Michigan measures and transmits weather and road conditions in real-time via various sensors (Figure 5.2). Meteorological sensors record weather

conditions, e.g., air temperature, relative humidity, and precipitation. Pavement sensors measure road conditions, e.g., pavement surface and subsurface temperatures. There are 105 sites in total and we adopt four typical sites of Michigamme and Seney in the Upper Peninsula and Eastport and Fife Lake in the Lower Peninsula for analyses.

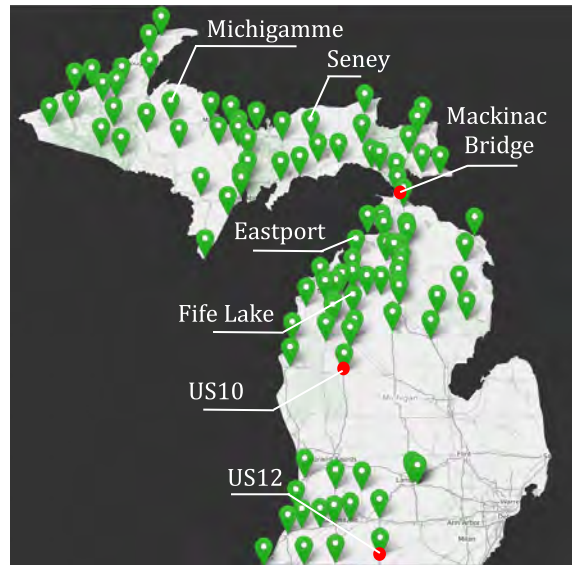


Figure 5.2 Monitoring sites in Michigan and selected sites location for analyses. Data is from the Michigan SLR website (<https://mdotslr.org>)

Figure 5.3 shows the cross-section of the test road pavements. The asphalt/concrete pavement surface has a thickness of about 25 cm, which is the same as that of roads in Asefzadeh et al. (2016). Base and subgrade soils are beneath the surface, where the base thickness is about 17 cm. The major soil type in the four sites is different, i.e., clayey soils in Eastport and Fife Lake and sandy soils in Michigamme and Seney. FD and TD are not measured directly, but rather calculated based on the measured subsurface temperatures starting from the base surface to subgrade soils. The measured locations are 0, 3 (7.62), 6 (15.24), 9 (22.86), 12 (30.48), 18 (45.72), 24 (60.96), 30 (76.2), 36 (91.44), 42 (106.68), 48 (121.92), 54 (137.16), 60 (152.4), 66 (167.64), and 72 inches (182.88 cm). To calculate FD and TD, two adjacent measured temperatures are compared and the linear interpolation is used. The base surface in Figure 5.3 is assumed as a datum, below which FD and TD are positive.

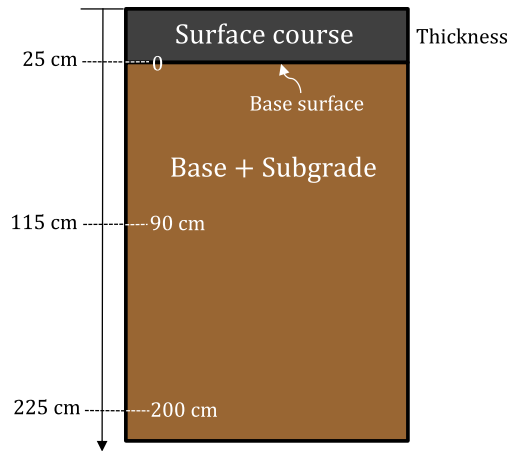


Figure 5.3 Schematic of a test road pavement cross section

The placement and removal of SLR are determined according to the suggested theory by Baiz et al. (2008) and Chapin et al. (2012). As shown in Figure 5.4, the SLR placement takes place if there are continuous TDs (red square); SLR ends after TD meets FD (purple square). At this time, a yearly freeze-thaw cycle can be assumed to be complete.

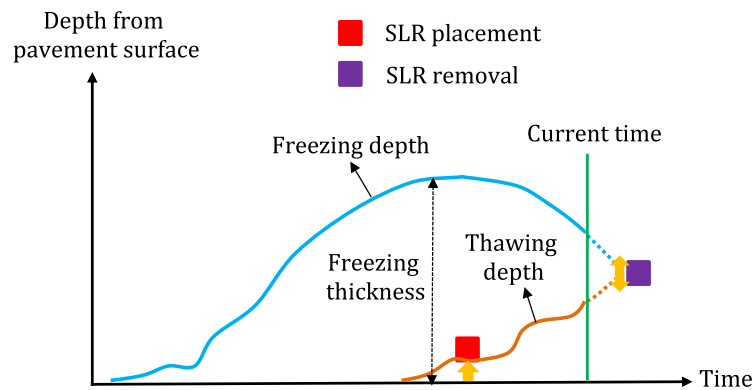


Figure 5.4 SLR decision-making based on the theory proposed by (Baiz et al. 2008)

In general, agencies require a notice at least 5 days prior to the placement and removal of SLR. To apply the FD/TD prediction model to practical SLR decision-making, Figure 5.5 presents a brief flowchart suggesting how this could be done. Based on the real-time field data, FD and TD can be calculated. When the thawing starts and TD continuously increases to a predefined threshold, SLR

can be set. SLR will be removed when FD meets TD or reaches other pre-specified thresholds. The decision to remove SLR can be easily made by observing the FD and TD graphs obtained by the prediction model. At each site, SLR decisions can be made based on the present FD/TD prediction models.

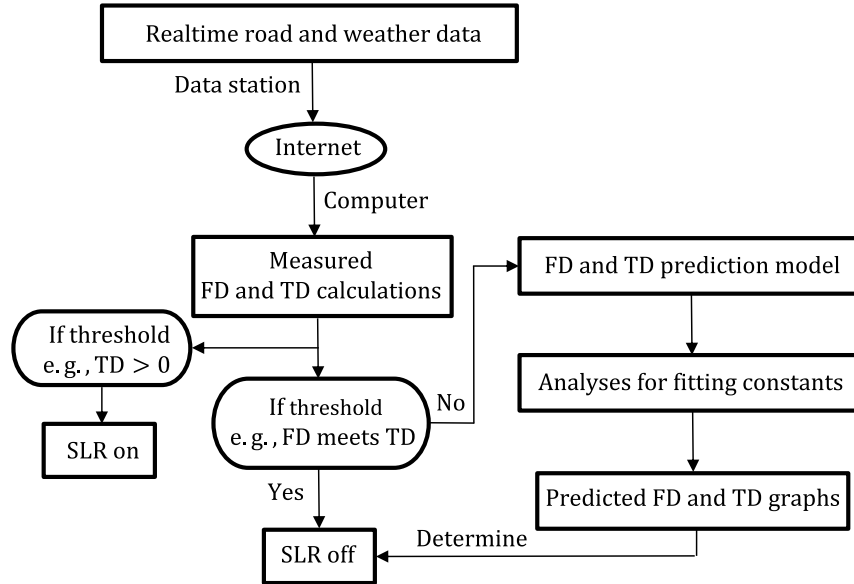


Figure 5.5 Conceptual flowchart of the FD/TD prediction model implementation for SLR

### 5.3.2 Freeze-Thaw Depth Prediction Model with Constrained Optimization

Accurate predictions of FD and TD are very significant for SLR decision-making to notify the public of SLR postings at least 3 to 5 days in advance for avoiding the economic loss of road users due to an unnecessarily long SLR period. In this chapter, we adopt the multivariate FD/TD prediction model that presents high-accuracy predictions of FD and TD explained in the previous chapter (Bao et al. 2019). This model assumes that FD is a function of the square root of both FI and TI as

$$FD = a\sqrt{FI} + \sqrt{c - bTI} - d \quad \text{Eq. 5.1}$$

where  $a$ ,  $b$ ,  $c$ , and  $d$  are fitting constants, all are always positive. The mathematical formulation for TD uses the square root function using the following expression by assuming that freezing and thawing processes in soils are similar (Konrad 1989)

$$TD = -e\sqrt{FIT} - \sqrt{g - fTI} + h \quad \text{Eq. 5.2}$$

where  $e$ ,  $g$ ,  $f$ , and  $h$  are fitting constants, all are always positive. FIT is the cumulative freezing index in the thawing period only, which is calculated starting from the first TD data point. Detailed calculations of FI, FIT, and TI can be found in Section 3.2.4.

Each of Eq. 5.1 and Eq. 5.2 has four fitting constants. For FD,  $a$  and  $b$  are the lumped parameters in the freezing and thawing seasons, respectively, to consider the volumetric latent heat of fusion, the conversion from the air temperature to the surface temperature, and the initial freezing depression (Aldrich and Paynter 1953; Berg et al. 2006). These two lumped fitting constants reflect the real situation for the depth and duration of the freeze and thaw penetration in the base and subgrade soils. Similarly,  $e$  and  $f$  for TD are also the lumped parameters that have a similar physical meaning to that of  $a$  and  $b$ .

The physical meaning of  $c$  and  $d$  in Eq. 5.1 is related to the pavement surface thickness. Before the freezing season starts, it is known that both FI and TI are equal to zero. Eq. 5.1 thus can be rewritten as

$$FD_{ini} = \sqrt{c} - d \quad \text{Eq. 5.3}$$

where  $FD_{ini}$  the initial freezing depth to represent the pavement surface thickness. In Figure 5.3, the base surface is the datum. FD starts from zero in the early freezing stage when FI is slightly greater than zero and TI is equal to zero. FD only occurs in base and subgrade soils beneath the pavement surface (Figure 5.3). Under the condition of FI=TI=0,  $FD_{ini}$  needs to be equal to 25 cm such that realistic pavement structure conditions can be physically described using Eq. 5.1. Similarly, Eq. 5.2 for TD can be written as

$$TD_{ini} = -\sqrt{g} + h \quad \text{Eq. 5.4}$$

Because of the same pavement road,  $FD_{ini} = TD_{ini}$  is required. The above explanations give the physical meaning of all the fitting constants in Eq. 5.1 and Eq. 5.2 in the multivariate FD/TD model. This is different from the existing prediction models that conduct regression analyses directly to have fitting constants that are far from realistic conditions (e.g., Baiz et al. (2008) and Chapin et al. (2012), see an example in Figure 5.1).

Non-constrained nonlinear regression of measured data is widely used to find fitting constants in the FD/TD prediction models (Asefzadeh et al. 2016; Baiz et al. 2008; Marquis 2008; Miller et al. 2012). However, non-constrained nonlinear regression cannot satisfy the requirements of Eq. 5.3 and Eq. 5.4 in this study. We thus propose a new constrained optimization approach to satisfy such requirements. In theory, the minimum of a nonlinear multivariable function  $f(\mathbf{x})$  can be expressed as (Bertsekas 2014)

$$\min_{\mathbf{x}} f(\mathbf{x}) \text{ such that } \begin{cases} \mathbf{x} \geq 0 \\ ceq(\mathbf{x}) = 0 \end{cases} \quad \text{Eq. 5.5}$$

where  $\mathbf{x}$  is the fitting constant vector and  $ceq(\mathbf{x})$  is the equality constraints that need to be satisfied. Take FD for example,  $\mathbf{x}$  contains  $a$ ,  $b$ ,  $c$ , and  $d$ .  $f(\mathbf{x})$  and  $ceq(\mathbf{x})$  can be expressed as

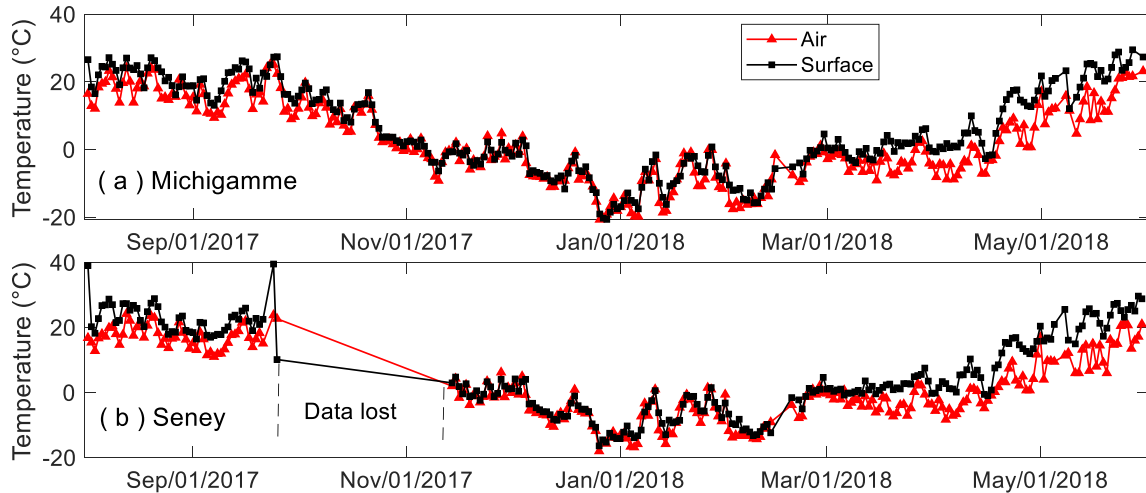
$$\begin{cases} f(\mathbf{x}) = FD(\mathbf{x}) - g(\mathbf{x}) \\ ceq(\mathbf{x}) = \sqrt{c} - d - FD_{ini} \end{cases} \quad \text{Eq. 5.6}$$

where  $g(\mathbf{x})$  is the measured data vector. In this study,  $FD_{ini} = TD_{ini} = -25$  is used (Figure 5.3). We utilize the negative sign here because the base surface is the datum. The sequential quadratic programming method (Gill and Wong 2012) is adopted for constrained nonlinear optimization. The randomly generated  $\mathbf{x}$  is used to start the optimization process and the termination tolerance is  $10^{-12}$ .

## 5.4 Results

### 5.4.1 Site Measurements

Two year-cycle field data for the four sites are available to evaluate the FD/TD model performance with constrained optimization. Figure 5.6 and Figure 5.7 show the daily average air and pavement surface temperatures collected from August 1<sup>st</sup>, 2017 to June 1<sup>st</sup>, 2018 for the first year cycle and August 1<sup>st</sup>, 2018 to April 1<sup>st</sup>, 2019 for the second year cycle. The second year cycle has less data than the first year cycle primarily due to problems caused by the data transmission. In general, the surface temperature is slightly higher than the air temperature. Also, the temperature range for the two year cycles is almost the same from -20 °C to 40 °C. In Figure 5.6b and Figure 5.7c, some data are missing in a short period probably because of the sensor connection and data transmission problems. This, however, does not affect TD predictions and may only slightly affect FD predictions in the early stage. We can see the continuous data after about November 15<sup>th</sup>, 2017. Thus, TD predictions are negligibly affected by those missing data for SLR decision-making.



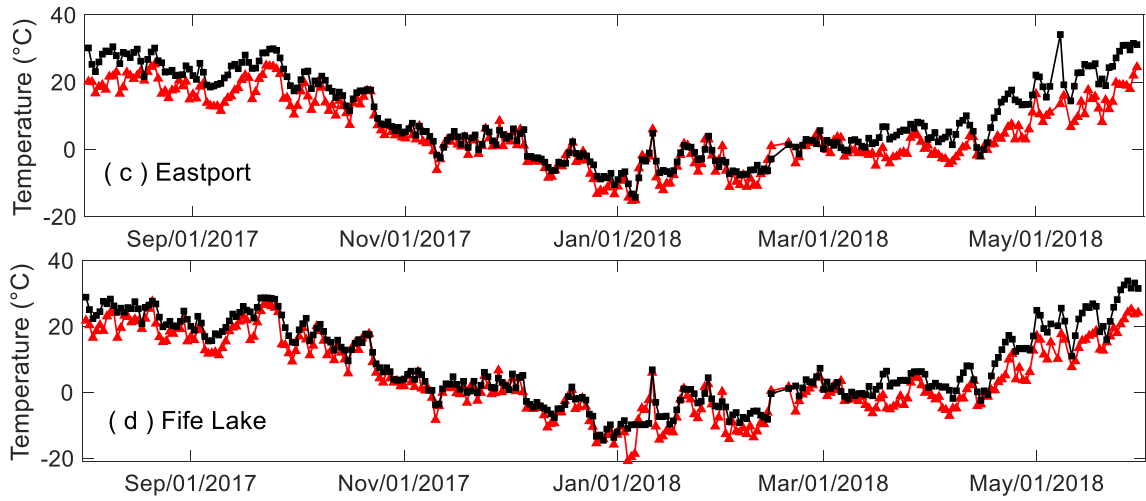
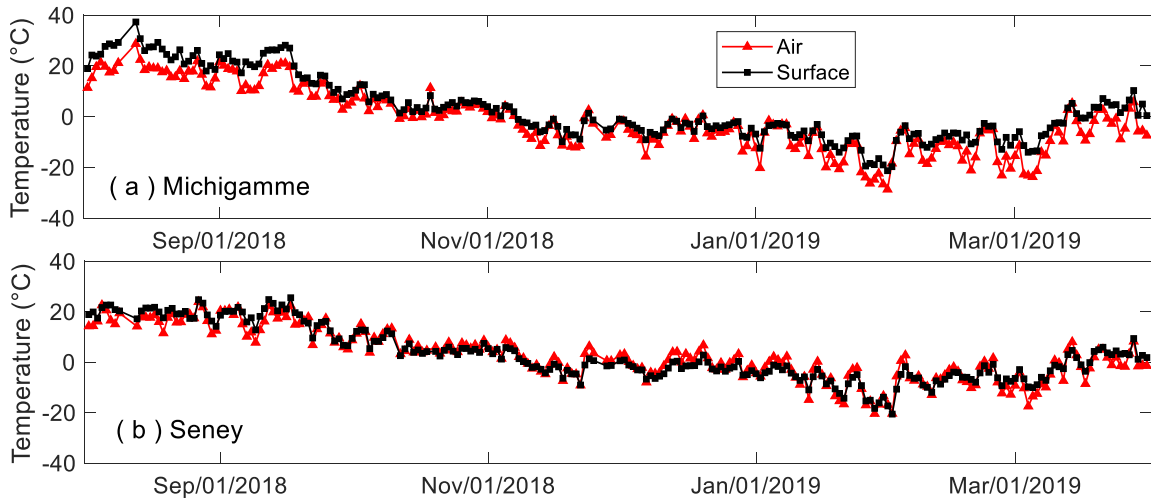


Figure 5.6 Measured air and pavement surface temperatures for Year Cycle 2017-2018



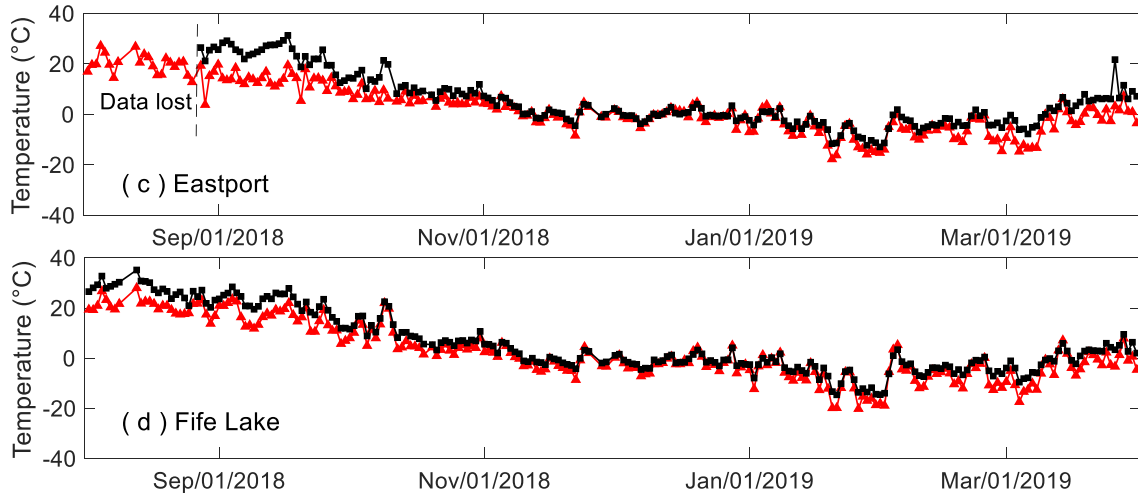
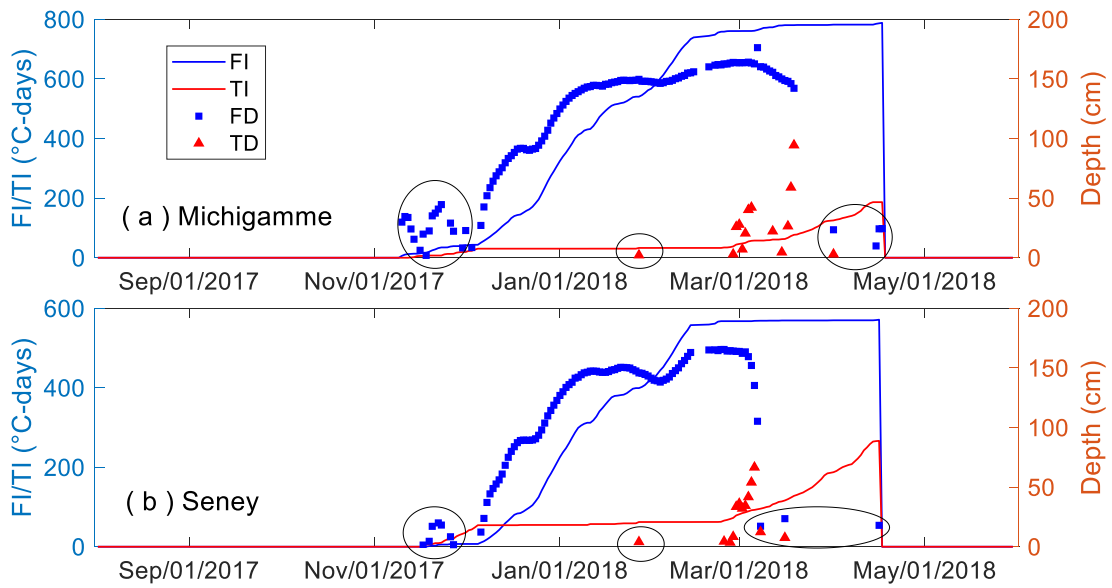


Figure 5.7 Measured air and pavement surface temperatures for Year Cycle 2018-2019



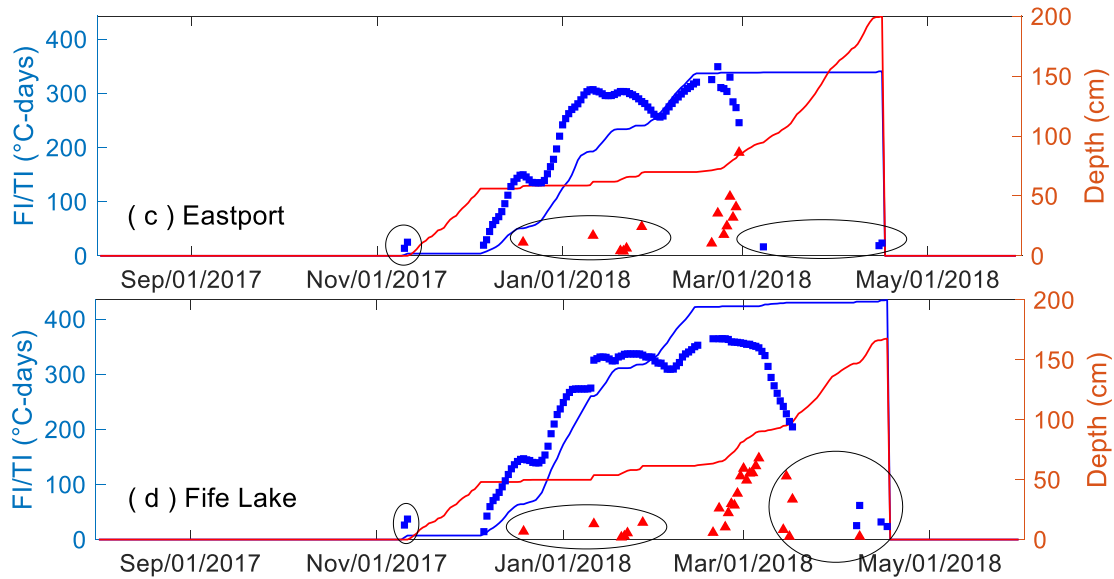


Figure 5.8 Measured FDs and TDs with FI/TI calculated using the pavement surface temperature for Year Cycle 2017-2018. Data within circles will be excluded in the fitting analysis

The measured FDs and TDs for the four sites for the two year cycles are shown in Figure 5.8 and Figure 5.9. FI and TI are also plotted, which are calculated starting from the first FD data point with the pavement surface temperature using Eq. 3.1 and Eq. 3.2. At all the sites, FD takes place around November 15<sup>th</sup> for each year cycle. The thawing season for the first year cycle is earlier than that of the second year cycle. Because we can see that FD starts decreasing around the beginning of March in Figure 5.8 but around the middle of March in Figure 5.9. This can also be supported by TD prediction trends. TD continuously increases around the beginning of March for the first year cycle but around the middle of March for the second year cycle. For all the sites in Figure 5.8 and Figure 5.9, there are some data points marked with circles. This can be explained in terms of two seasons. In the freezing season, several warm days may occur to thaw the base and subgrade soils, as a result, FD decreases somewhat, especially at the beginning of the freezing season. In the thawing season after the freeze-thaw cycle ends where FD meets TD, there have some cold days to freeze the soils close to the base surface, leading to some FDs after the freeze-thaw cycle ends.

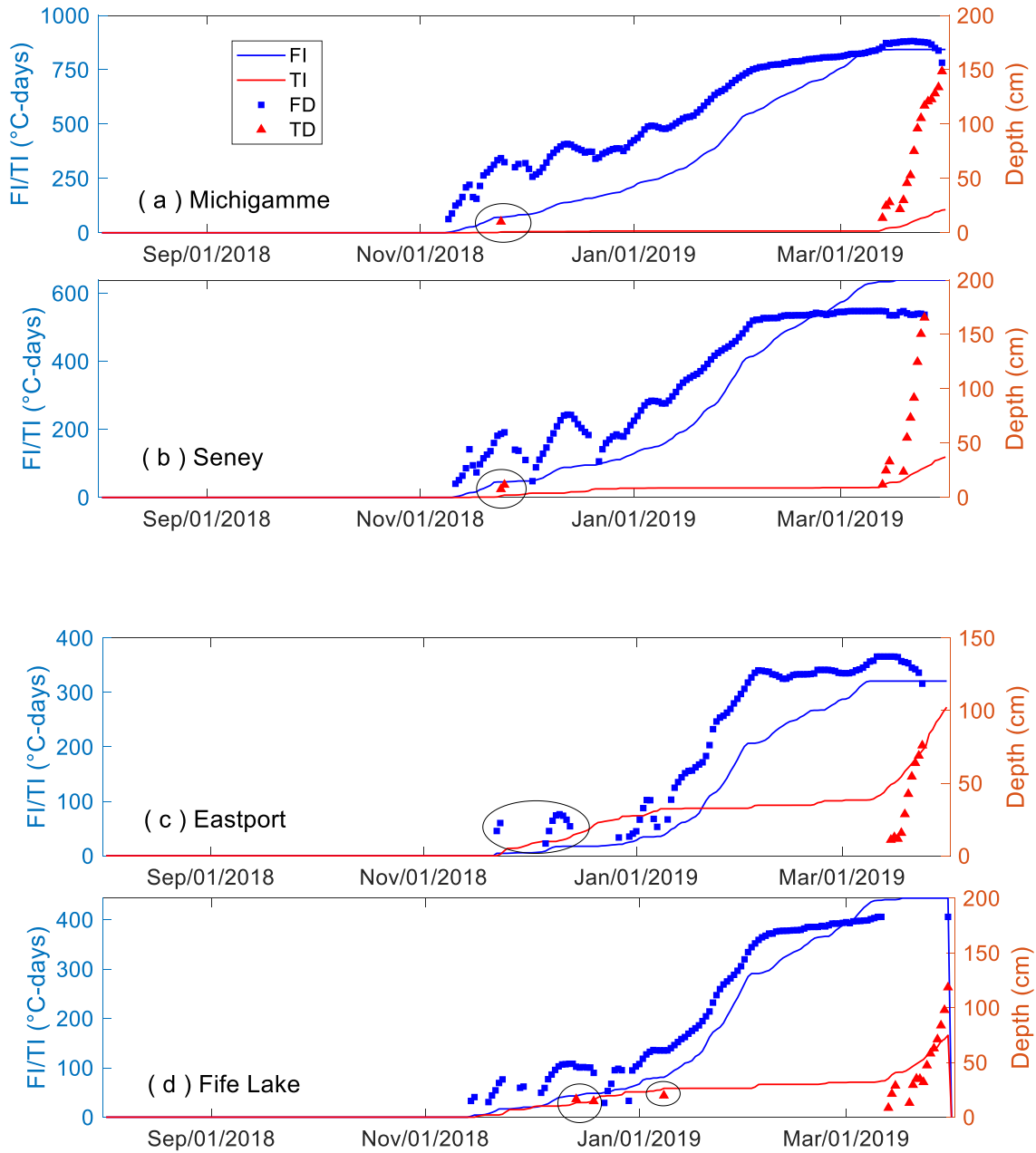


Figure 5.9 Measured FDs and TDs with FI/TI calculated using the pavement surface temperature for Year Cycle 2018-2019. Data within circles will be excluded in the fitting analysis

### 5.4.2 Application of Constrained Optimization for FD/TD Predictions

Predictions of FD and TD via constrained optimization for the two year cycles are shown in Figure 5.10 and Figure 5.11. In this constrained optimization, the circled data marked in Figure 5.8 and Figure 5.9 are excluded. The major consideration is that these circled data appear either at the beginning of the freezing season or after the thawing season due to the occurrence of some warm and/or cold days. The primary aim of this study is to predict TD and FD trends in the thawing season for accurately making SLR decisions. It is thus reasonable to exclude the circled data for statistical analyses to obtain high prediction accuracy in the thawing season.

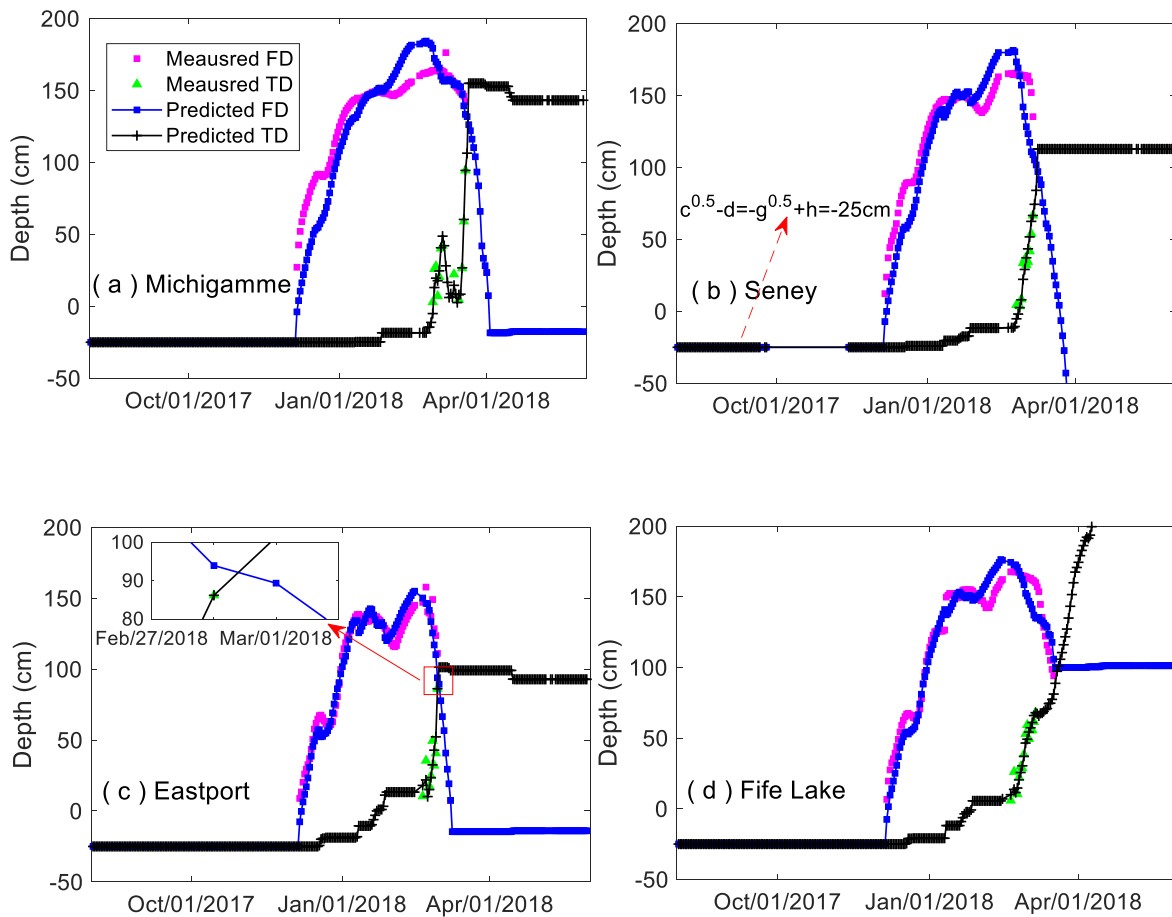


Figure 5.10 Predictions of FD and TD with the measured data for Year Cycle 2017-2018. Circled data Fig. 7 are excluded

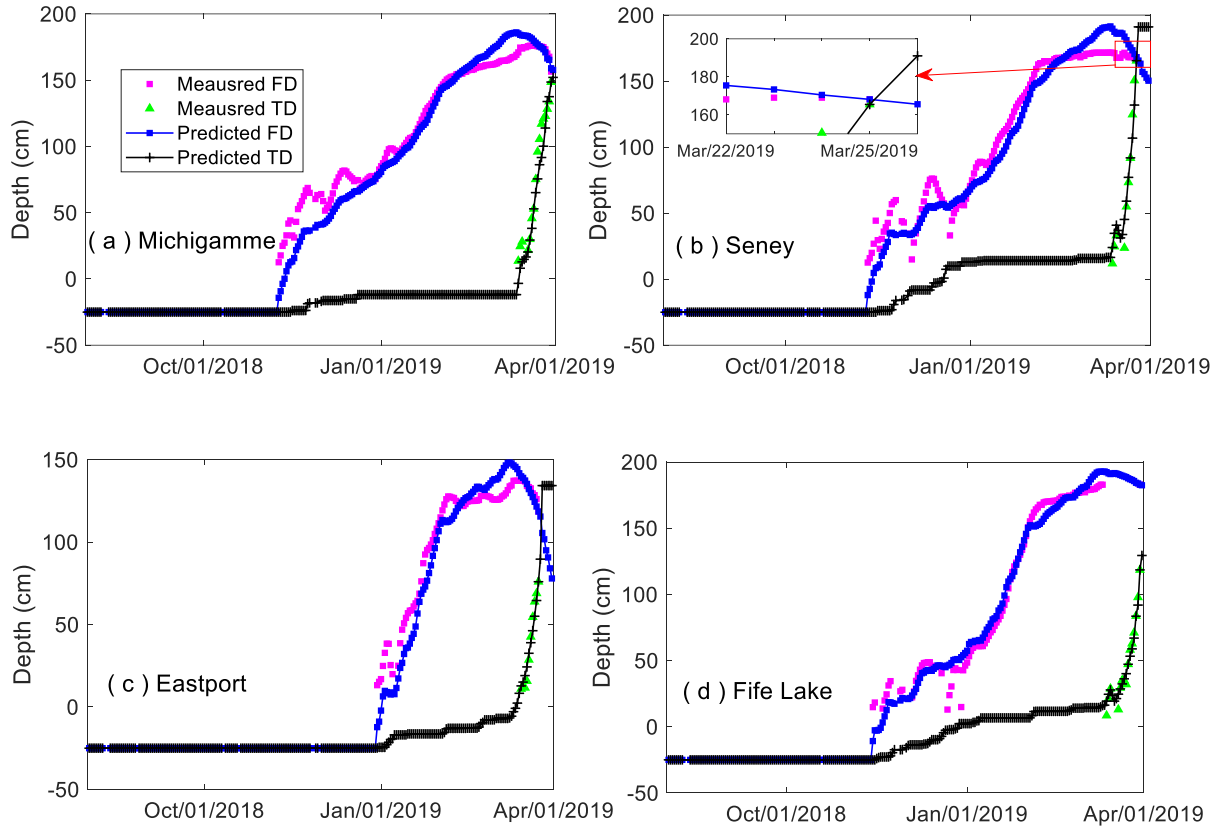


Figure 5.11 Predictions of FD and TD with the measured data for Year Cycle 2018-2019.

Circled data Fig. 8 are excluded

We can see in Figure 5.10 and Figure 5.11 that the predicted data for both FD and TD are in good agreement with the measured data. In general, the predicted FD trends match well with the measured FD trends, where FD increases in the freezing season and decreases when thawing starts. Slight deviations for FD can be observed in Figure 5.11 in a few days at the beginning of the freezing season because of the occurrence of some warm and/or cold days. This, however, has a negligible effect because the predicted FDs in the thawing season, which are key for determining the removal of SLR, are very close to the measured FDs. It is also seen that FD and/or TD is a horizontal line after FD meets TD because imaginary numbers are obtained using Eq. 5.1 and Eq. 5.2. This, however, is not an issue because the freeze-thaw cycle ends already, thus, these FD and/or TD values have no meaning.

Table 5.1 Fitting results for FD and TD

| Site       | Year cycle | Fitting constant for FD        |   |                      |             |                |
|------------|------------|--------------------------------|---|----------------------|-------------|----------------|
|            |            | a (cm °C-day <sup>-0.5</sup> ) | b (cm <sup>2</sup> °C-day <sup>-1</sup> ) | c (cm <sup>2</sup> ) | d (cm)      | R <sup>2</sup> |
| Michigamme | 2017-2018  | 7.9288                         | 441.6752                                  | 43671.3354           | 233.9769    | 0.9454         |
|            | 2018-2019  | 7.3565                         | 37.6986                                   | 5942.0144            | 102.1103    | 0.9826         |
| Seney      | 2017-2018  | 9.5470                         | 1129212.3434                              | 55527423258.9767     | 235667.5752 | 0.9175         |
|            | 2018-2019  | 8.9973                         | 66.8873                                   | 10452.0518           | 127.2441    | 0.9667         |
| Eastport   | 2017-2018  | 12.2351                        | 765988.3734                               | 77196409094.8204     | 277867.4177 | 0.9695         |
|            | 2018-2019  | 10.5288                        | 64.5584                                   | 14750.2992           | 146.4523    | 0.9738         |
| Fife Lake  | 2017-2018  | 10.5395                        | 77.0313                                   | 8406.6067            | 116.6875    | 0.9460         |
|            | 2018-2019  | 10.7898                        | 35597.0232                                | 23217827654.8394     | 152398.9745 | 0.9764         |
|            |            | Fitting constant for TD        |   |                      |             |                |
|            |            | e (cm °C-day <sup>-0.5</sup> ) | f (cm <sup>2</sup> °C-day <sup>-1</sup> ) | g (cm <sup>2</sup> ) | h (cm)      | R <sup>2</sup> |
| Michigamme | 2017-2018  | 16.0829                        | 1289.2506                                 | 63770.7833           | 227.5288    | 0.9337         |
|            | 2018-2019  | 0.0005                         | 2234315.8950                              | 448425887174.6080    | 669621.0911 | 0.9601         |
| Seney      | 2017-2018  | 0.0000                         | 437.2053                                  | 18992.6215           | 112.8137    | 0.9160         |
|            | 2018-2019  | 5.0099                         | 583.8922                                  | 51533.6769           | 202.0103    | 0.9745         |
| Eastport   | 2017-2018  | 10.7031                        | 299.1526                                  | 19229.1109           | 113.6691    | 0.8085         |
|            | 2018-2019  | 0.6620                         | 182.2324                                  | 25366.3592           | 134.2682    | 0.9651         |
| Fife Lake  | 2017-2018  | 2.7082                         | 1714226.7505                              | 671747443635.2280    | 819577.0032 | 0.9212         |
|            | 2018-2019  | 5.0651                         | 160.1695                                  | 26692.4104           | 138.3781    | 0.9777         |

The fitting constants for TD and FD are tabulated in Table 5.1. All the fitting constants are positive, which satisfy the requirement of constrained optimization in Eq. 5.5. The determination coefficient for almost all the predictions is found to be higher than 0.91, which further confirms the high accuracy of predicting both FD and TD with constrained optimization. In Figure 5.10 and Figure 5.11, we also can see FD and TD are overlapped and equal to -25cm in the early freezing season when no measured FD data point appears. This satisfies Eq. 5.6 for the physical meaning of the fitting constants to reflect the pavement surface thickness. At the late stage of the thawing season, FD meets TD in the predictions for all the sites, except Fife Lake in the second year cycle because no more data is available after April 1<sup>st</sup>. However, it is expected that FD will meet TD later according to their current prediction trends in Figure 5.11d.

Table 5.2 Site SLR determination

| Site       | Year cycle | Model determined date |           |                 | Suggested date |                 |
|------------|------------|-----------------------|-----------|-----------------|----------------|-----------------|
|            |            | SLR on                | SLR off   | Duration (days) | SLR off        | Duration (days) |
| Michigamme | 2017-2018  | 2/27/2018             | 3/20/2018 | 22              | 4/2/2018       | 35              |
|            | 2018-2019  | 3/13/2019             | 4/1/2019  | 20              | 4/1/2019       | 20              |
| Seney      | 2017-2018  | 2/24/2018             | 3/9/2018  | 17              | 3/16/2018      | 24              |
|            | 2018-2019  | 3/13/2019             | 3/25/2019 | 13              | 3/25/2019      | 13              |
| Eastport   | 2017-2018  | 2/19/2018             | 3/1/2018  | 10              | 3/1/2018       | 10              |
|            | 2018-2019  | 3/15/2019             | 3/25/2019 | 11              | 3/25/2019      | 11              |
| Fife Lake  | 2017-2018  | 2/19/2018             | 3/20/2018 | 29              | 4/8/2019       | 48              |
|            | 2018-2019  | 3/13/2019             | -         | -               | -              | -               |

The FD/TD predictions in Figure 5.10 and Figure 5.11 can be used to determine the placement and removal of SLR according to the suggested theory by Baiz et al. (2008) (see Figure 5.4). As shown in Table 5.2, all the sites in the first year cycle have an earlier date for the SLR placement and a later date for the SLR removal than the second year cycle. This is because the thawing season of the first year cycle came earlier (see Figure 5.8 and Figure 5.9). The FD/TD model suggests that the duration for SLR in Michigamme is 22 days for the first year cycle and 20 days for the second year cycle, where these two numbers are very close. For the other three sites, the SLR duration of the first year cycle is also close to that of the second year cycle. This implies that the SLR duration in different years at the same site seems similar. Considering that there are a few warm and/or cold days after FD meets TD when the freeze-thaw cycle ends (Figure 5.8), it is also suggested that the removal of SLR can take place when no more TD data point appears to eliminate any potential of thaw-weakening induced road damages. Such suggested dates for the SLR removal are shown in Table 5.2 and we can see that the SLR duration of the first year cycle increases over one or two weeks in Michigamme, Seney, and Fife Lake, while the SLR duration in Eastport keeps unchanged.

## 5.5 Discussions

### 5.5.1 Advantages of Using Constrained Optimization for FD/TD Predictions

Constrained optimization has two major advantages that make it more advanced than non-constrained optimization used in existing studies (Baiz et al. 2008; Bao et al. 2019) for statistical analyses of the measured data. First, as clearly shown in Figure 5.10 and Figure 5.11, constrained optimization can enable FD to meet TD in the thawing season. This can be further illustrated by comparing FD and TD predictions with non-constrained and constrained optimizations. Figure 5.12 shows such a comparison for the statistical analyses of the data collected during 2017-2018 in Seney. We can see that FD cannot meet TD in the thawing season if non-constrained optimization is employed, which has the same issue pointed out in Figure 5.1. However, constrained optimization can resolve this issue to enable the prediction model to work in practice in support of SLR decision-making.

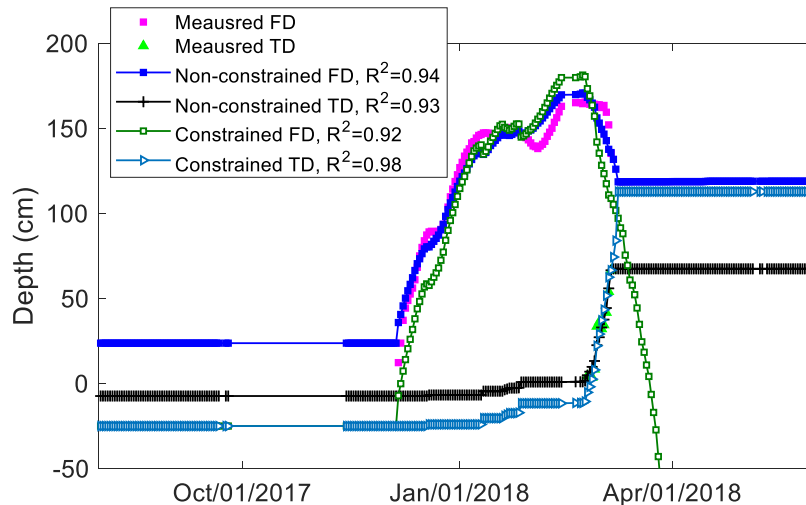


Figure 5.12 Comparison of FD/TD predictions with non-constrained and constrained optimization for Seney during 2017-2018

Second, when  $FI=TI=0$  in the early freezing season, non-constrained optimization yields about -5 cm and 25 cm (Figure 5.12) for TD and FD, respectively. The two numbers are different and also have a different sign simply resulting from the statistical analyses. They, however, cannot reflect

the realistic pavement FD and TD conditions. As explained in Section 5.3.2, these two number should be equal because they represent the pavement surface thickness. It is clearly seen in Figure 5.12 that FD is equal to TD when constrained optimization is used. Therefore, constrained optimization can yield not only satisfactory but more realistic results than those obtained with non-constrained optimization.

### **5.5.2 Feasibility of Using Year Cycle 1 Fitting Constants to Predict Year Cycle 2 FD/TD**

The FD/TD prediction model with constrained optimization can accurately predict the FD/TD trends for applying SLR in each year cycle. It is also very interesting to explore the feasibility of predicting the FD and TD trends in the current year cycle by directly employing the fitting constants from the previous year cycle at the same site. This feasibility can further facilitate the application of the prediction model in practice because it makes the model application more convenient for road engineers for making SLR decisions without needing further measurements in later year cycles.

To examine this feasibility, we predict the FD and TD trends during 2018-2019 in Michigamme and Seney, respectively, using the fitting constants obtained during 2017-2018 from Table 5.1. As shown in Figure 5.13, the predictions for both FD and TD lag behind and do not match the measured data. The removal of SLR for Michigamme is determined on 3/21/2019, which is earlier than the correct date of 4/1/2019. The SLR removal for Seney is also earlier and incorrect. The major reason for causing the earlier predictions is that the thawing season during 2017-2018 is earlier than that during 2018-2019 (see Figure 5.8 and Figure 5.9). Therefore, it is not feasible to predict the FD and TD trends in the current year cycle using the fitting constants from the previous year cycle. Though at the same site, the accuracy of the TD and FD predictions is also time-dependent and significantly influenced by FI and TI accumulated during each year cycle.

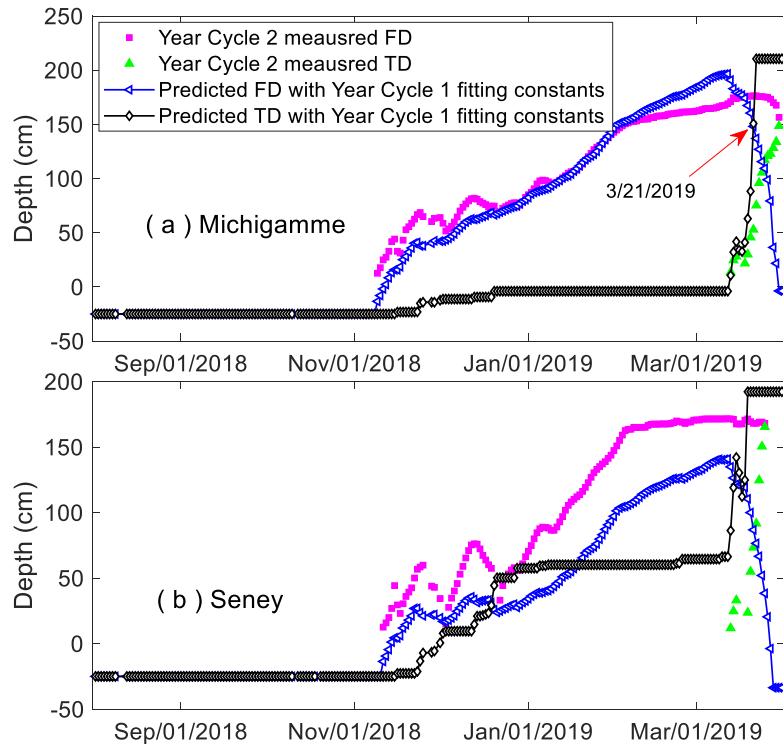


Figure 5.13 Comparison of FD/TD predictions with non-constrained and constrained optimization in Michigamme and Seney for Year Cycle 2017-2018

### 5.5.3 FD/TD Prediction Models are Better than a TI/FI Ratio for SLR Decision-Making

As mentioned in the introduction, a TI/FI ratio of 0.3 proposed by Mahoney et al. (1987) is still used by several agencies in the U.S. to determine the removal date of SLR, e.g., those in Washington (Mahoney et al. 1987; McBane and Hanek 1986). In this section, we evaluate the accuracy of using this TI/FI ratio for SLR decision-making.

Table 5.3 shows TI/FI ratios calculated by TI and FI obtained on the SLR removal dates. The removal dates are determined based upon the measured data in Figure 5.10 and Figure 5.11 when FD either already or nearly meets TD. These dates can be considered as the true solutions for removing SLR because the field measurements directly reflect pavement freezing and thawing conditions. TI/FI ratios for Eastport and Fife Lake are not either fully or partially shown in Table 5.3. The reason is that the last FD and TD data points at these two sites in Figure 5.10 and Figure 5.11 are still far from each other; therefore, it is difficult to determine the correct SLR removal

dates. The SLR removal dates determined by the FD/TD prediction model are also presented for comparison. We can see in Table 5.3 that the TI/FI ratios are not equal and/or very close to 0.3. Even at the same site, the ratio is obviously different in two year cycles. This might be caused by two possible reasons. First, FI and TI in Table 5.3 are calculated in terms of the pavement surface temperature. This differs from the air temperature used in Mahoney et al. (1987) for obtaining a TI/FI ratio of 0.3. Second, Mahoney et al. (1987) used “°F” for the temperature unit while “°C” is utilized here.

Table 5.3 Ratios between TI and FI on the SLR removal date

| Site       | Year circle | FI (°C-day) | TI (°C-day) | TI/FI ratio | SLR off     |             |
|------------|-------------|-------------|-------------|-------------|-------------|-------------|
|            |             |             |             |             | Measurement | FD/TD model |
| Michigamme | 2017-2018   | 737.68      | 47.64       | 0.06        | 3/19/2018   | 3/20/2018   |
|            | 2018-2019   | 843.32      | 106.13      | 0.13        | 4/1/2019    | 4/1/2019    |
| Seney      | 2017-2018   | 561.87      | 43.46       | 0.08        | 3/6/2018    | 3/9/2018    |
|            | 2018-2019   | 638.67      | 87.14       | 0.14        | 3/25/2019   | 3/25/2019   |
| Eastport   | 2017-2018   | 334.25      | 65.38       | 0.20        | 2/28/2018   | 3/1/2018    |
|            | 2018-2019   | -           | -           | -           | -           | 3/25/2019   |
| Fife Lake  | 2017-2018   | -           | -           | -           | -           | 3/20/2018   |
|            | 2018-2019   | -           | -           | -           | -           | -           |

To further examine the accuracy of using the TI/FI ratio, we calculate the TI/FI ratios for three additional sites of Mackinac Bridge, US-10, and US-12 in the Superior region in Michigan (see Figure 5.2). In the calculation, we adopt the air temperature to compute FI and TI using both “°F” and “°C” temperature units. The removal dates of SLR are determined based upon the field measurements when FD meets TD. It is clearly seen in Figure 5.4 that the TI/FI ratio is not equal to 0.3, no matter “°F” or “°C” is utilized. The TI/FI ratio is in a range of 0.26-2.37 when “°F” is used.

Table 5.4 SLR removal dates at three additional sites in the Superior region in Michigan

| Site            | Year | Date SLR off | FI     |        | TI     |        | TI/FI ratio |       |
|-----------------|------|--------------|--------|--------|--------|--------|-------------|-------|
|                 |      |              | °F-day | °C-day | °F-day | °C-day | if °F       | if °C |
| Mackinac Bridge | 2017 | 4/5/2017     | 694.00 | 477.22 | 362.00 | 201.33 | 0.52        | 0.42  |

|       |      |           |         |         |         |        |      |      |
|-------|------|-----------|---------|---------|---------|--------|------|------|
|       | 2014 | 5/4/2014  | 2024.00 | 1267.80 | 528.00  | 293.56 | 0.26 | 0.23 |
|       | 2011 | 4/18/2011 | 1062.00 | 711.67  | 1180.00 | 655.92 | 1.11 | 0.92 |
| US-10 | 2017 | 3/23/2017 | 471.00  | 330.56  | 498.00  | 276.90 | 1.06 | 0.84 |
| US-12 | 2017 | 3/8/2017  | 298.00  | 211.11  | 706.00  | 392.48 | 2.37 | 1.86 |

The results in Table 5.3 and Table 5.4 show that adopting a TI/FI ratio of 0.3 is not accurate for SLR decision-making. Even at the same site of Mackinac Bridge, the TI/FI ratio is significantly different in three years (Table 5.4). However, the SLR removal dates determined by the FD/TD prediction model are almost the same as those by the measurements (Table 5.3). According to Mahoney et al. (1987), a TI/FI ratio of 0.3, in fact, is an approximate solution under cases based upon fine-grained soils with a moisture content of 0.15. This approximate solution, however, can vary significantly site-by-site or year-by-year though at the same site. Using this approximate TI/FI ratio will yield an SLR removal date either earlier or later than a true date. This will cause the repair cost for freeze-thaw-induced road damages occurring in the thawing season or the economic loss of road users due to an unnecessarily long SLR period. Our results reveal that the FD and TD prediction model can yield more accurate results than a TI/FI ratio for SLR decision-making.

## 5.6 Conclusions

This study proposes constrained optimization to predict FD and TD in support of making SLR decisions. The physical meanings of all fitting constants in the multivariate FD/TD prediction model are clearly clarified, which can reflect realistic pavement FD and TD conditions but are neglected in existing studies. We evaluate constrained optimization with field measurements collected at four sites during two year cycles. The evaluation results showed that the constrained optimization approach can provide accurate predictions of FD and TD with the determination coefficient of higher than 0.91 for almost all sites. Most importantly, this approach makes the predicted FD and TD trends cross in the thawing season so that the removal date of SLR can be determined, which addresses the critical but resolved issue in most existing prediction models that FD cannot meet TD in the thawing season to enable such prediction models to work in practice for SLR decision-making.

From the discussion, we confirmed that it is not feasible to predict the FD and TD trends in the current year cycle by directly employing the fitting constants from the previous year cycle at the same site. Our results also revealed that the FD and TD prediction model is more accurate for SLR decision-making than a TI/FI ratio of 0.3 that still has been used in several agencies in the U.S. The TI/FI ratio can vary significantly site-by-site or year-by-year though at the same site. Therefore, the FD and TD prediction model with constrained optimization reported in this study is reliable and highly recommended for making SLR decisions for roadways in cold regions.

## **Chapter 6 Development of Web-Based Spring Load Restriction Decision Support Tool**

### **6.1 Abstract**

Thaw-weakening is a major cause of pavement damage in seasonally-frozen areas covering half of the U.S., leading to huge financial costs for taxpayers. In recent years, the damage has lessened due to improving practice with Spring Load Restriction (SLR) policies. However, even the most advanced SLR date prediction methods/tools are still primitive from the perspective of information technology. Such methods/tools are obtained and/or implemented manually with a small amount of data or even directly based on experience. The chapter reports what has been learned from an ongoing project supported by the Michigan Department of Transportation for the development of a web-based SLR decision support tool, i.e., a web-based app called MDOTSLR. MDOTSLR provides the access to much more data with little latency and automates data acquisition, processing, and decision making. In this chapter, the models and data supporting the functions of the tool will be first introduced. Next, the major functions (or services) of the app will be detailed. Followed will be the software engineering details for the development of the app. Compared with traditional tools without web delivery, this web-based tool automates the acquisition and processing of weather data, GIS data, and road weather information in real time and thus enables more accurate and convenient SLR predictions. In the accomplished automatic mode, no labor is required to keep the data up to date. The tool can be easily extended or modified for most state DOTs for immediate financial savings in road maintenance and less disturbance to the local economy.

The main purpose of this chapter is to detail the development of a web-based tool that uses the freeze-thaw model for assisting in SLR decision making to allow MDOT, local road agencies, and road users to better predict the dates for SLR placement and lifting. The web-based tool we are developing is accessible from any electronic device with Internet access and a web browser, which will be more convenient for users. Compared with traditional tools without web-based delivery the web-based tool we are developing can collect the data more timely and more comprehensively, as it can always acquire the latest data, including the weather data, Geographic Information System (GIS) data, and Road Weather Information Station (RWIS) data.

The remainder of the chapter is arranged as follows. First, an overview of the development goals for the web-based tool is presented. Then, the models and data employed for the web-based tool are introduced. This is followed by an explanation of the organization and functionality of the web-based SLR decision support tool that we have already developed. Next, software engineering details, especially the two major services in the app, will be given. Finally, conclusions are drawn as a summary of the whole chapter.

## **6.2 Goals for the App Development**

### **6.2.1 Objectives**

The objective of the project MDOT OR 16-009 is to establish how the web-based tool for setting and removing Seasonal Load Restrictions (SLR) will be set up as its development continues. The desired end state is a tool which will give industries the most amount of time to prepare for the restrictions and minimize the time to lift the restrictions. To be specific, recommendations will be made for the users of the tool to predict the accurate time to post and remove SLR signs so that the pavement structures can be protected from excessive damage during the spring thaw season and hauling industries can minimize losses. In addition, a user-friendly decision support tool is being developed, which will provide all the relevant data used by the recommendation algorithm to the user. This way the data could be easily utilized by the public and private sector in estimating potential thaw conditions using their own methods and in developing their own models for SLR. The work that has been accomplished has produced a tool called MDOTSLR at [mdotslr.org](http://mdotslr.org).

### **6.2.2 Features and Benefits**

This tool can not only be applied in Michigan but also other states in the U.S. Minnesota DOT (MnDOT) once published a web-based tool similar to ours. However, MnDOT's tool divides Minnesota into only 4 parts to help make the SLR decision, which is far less precise than the web-based tool that we are developing. Also, MnDOT's tool mostly relies on air temperature for predictions while there is not GIS and RWIS data for predictions or validations.

In our web-based tool, the users can retrieve the information of every specific district by inputting a zip code. For instance, if a user enters a zip code of 49931, then all the information for Houghton, MI, will be presented to the user. In addition to Michigan zip codes, the tool also supports Wisconsin and Minnesota zip codes. Furthermore, MDOTSLR will be able to provide a prolonged prediction, i.e., one month, which is much longer than that can be offered in the other existing tools, though as of now it only supports ten-day predictions. This will give users more time to prepare, with the caveat that weather forecasts are always associated with uncertainties that increase with time; a prediction for a time far from now is associated with more uncertainties. In addition, many more services are provided in the web-based tool we are developing than the one developed by MnDOT. Finally, MDOTSLR uses a variety of data types rather than merely air temperature. Function details in methods, data, and functions will be provided in later sections.

Compared with traditional non-web SLR decision support tools, the web-based tool we are developing has a series of benefits:

- ❖ A powerful tool for SLR practice is provided for the MDOT, local road agencies, and public road users in Michigan, currently based on freezing/thawing index values.
- ❖ MDOT and local road agencies can better determine the dates for placing the removing the SLR with this tool. The tool can provide the users with a much more accurate, convenient, and automated SLR decisions, which can effectively save the investment in repairing the road damage induced during the spring thaw season and effectively prolong the service life of the pavement.
- ❖ Since this process is automated, less labor would be required for determining SLR since all a road engineer has to do is quickly validate the data instead of doing all the calculations themselves.
- ❖ The road users, especially those seriously affected by the SLR policy, such as trucking companies and industries that rely on hauling services will also benefit from this tool. More time, in fact, much more than other states, i.e. one month instead of several days, will be given by the tool, once the forecast range is increased, for the users to prepare for the SLR placement or removal. Both the road users and the economy of Michigan will benefit a lot from this tool.
- ❖ The tool will change the current practice in Michigan and make the SLR practice better guided by scientific and engineering principles and benefit from the digital infrastructure, which will enhance the current web services provided by MDOT.

- ❖ This tool will also provide suggestions and information for future RWIS sites and help refine the pavement design so that it can better consider frost effects.

- ❖ This tool can be easily extended or modified for most states in the U.S. as well as other places around the world. Its use could lead to an incalculable save in the budget of state DOTs, local road agencies, and road users.

## **6.3 Models and Data**

### **6.3.1 Models**

Seasonal Load Restrictions have been used for a long time. In the past, traditional methods usually rely on engineers' experience and visual observations in situ. For example, in Michigan, as described on the CRA website, the road commissions employ licensed Professional Engineers to make these decisions and also consult neighboring road agencies.

Despite the historical statistics, more and more agencies are turning to use quantitative SLR decision algorithms. After a lot of efforts, several popular methods have been produced to determine the placement and removal dates or the duration of the SLR.

Previous analytical models often use the parameters including air freezing, thawing indices and cumulative thawing index (CTI) and so on, to determine the SLR application and removal dates. The current version of the tool uses these models to recommend SLR. However, it has been found that the predictions of freezing and thawing depths, especially the latter one, are the key to better determine the placement and removal dates of SLR, as the depth and thickness of the frost in the pavement determine the seasonal fluctuations in the bearing capacity of the road.

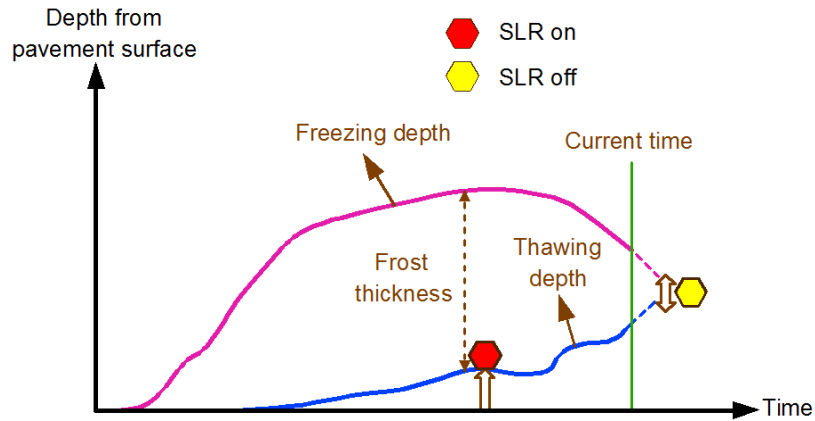


Figure 6.1 SLR decisions with freezing/thawing depth predictions (Baiz et al. 2008)

The correlation between freezing/thawing depths and the spring thaw period has been studied. As illustrated in Figure 6.1, the time for SLR placement corresponds to the time when the continuous thawing starts in the subgrade soils. After the thawing depth (moving downward) meets the frost depth (moving upward) in the thaw season, SLR should be removed.

Accurate SLR decisions made using the predictions of freezing/thawing depths are highly desirable. This is because most agencies are required to notify the public of SLR postings at least 3 to 5 days in advance. Therefore, the freezing/thawing depth predictions already available in the depth-curve service will be implemented in the SLR recommendation service which will allow for this advanced notice. Note that either extensive damage to the pavement owing to late placement or early removal of the SLR, or economic loss of road users due to an unnecessarily long period for SLR will be caused by the inaccurate predictions of these depths.

There are several different types of procedures (methods or criteria) for SLR decision making based on freezing/thawing depth predictions. These include the Mahoney et al. (1986) model (Mahoney et al. 1987) for WSDOT and FHWA, the Berg model (Berg et al. 2006) for the US Forest Service which was initially used by the NH DOT, the MnDOT Models (Van Deusen et al. 1998), and the MIT method (Manitoba Department of Infrastructure and Transportation, (Bradley et al. 2012)). Although these models were developed based on field experience and long-term observations and have been tested by for years, they cannot be directly applied to Michigan due to

different weather, soil, and pavement conditions. Therefore, new models which have been adjusted with Michigan-specific data are used in this web-based tool. The models are generated with RWIS-site-specific data via multivariate statistical analysis using the following two equations. For the predictions of SLR dates, we currently adopted the FHWA model. However, we will make the predictions site-specific in the next stage.

$$FD = a\sqrt{FI} + \sqrt{c - bTI} + d \quad \text{Eq. 6.1}$$

where  $a$ ,  $b$ ,  $c$ , and  $d$  are fitting constants, the first three always positive. Mainstream viewpoint is that freezing and thawing have similar processes, thus the mathematical formulation for TD and FD are similar:

$$TD = -e\sqrt{FIT} - \sqrt{g - fTI} + h \quad \text{Eq. 6.2}$$

where  $e$ ,  $g$ ,  $f$ , and  $h$  are fitting constants, in which the first three always positive.  $FIT$  is the cumulative freezing index in the thawing period only.

### 6.3.2 Composite Data Mapping Service

Composite data refers to all three categories of data being displayed for one geographical area, in the case of [mdotslr.org/services/data-map](https://mdotslr.org/services/data-map) points are used. The purpose of this service is to provide the composite data of each RWIS station, that is RWIS, soil and weather data at the geographical coordinates of each station. The current limitation of the RWIS data is a small number of data points. Without interpolation, we only have one hundred and five data points to work with whereas the weather and soil data span the state. Until a good method of interpolation is put into place we are limited to these points. The method used to map the RWIS stations to a zip code and map unit is as follows: make a call to the google maps API to get the zip code and county for the station. Since we have the zip code right off the bat that mapping is done. As for the county, each legend area, larger areas that contain individual map units, happens to be broken down by county with a few exceptions that were controlled for. We take the county name and make a call to the soil database for all map units and their geographical polygons in that legend area and then check each polygon using a point in polygon algorithm, provided by the turf.js library, to find which map unit

the station is in. We then save the map unit and zip code as properties of the station in the database so we do not have to do another time-consuming search for it when we actually pull the data. This process worked for all but two of the RWIS stations. Further investigation would be needed to figure out why but it would be much faster to find these two stations map units visually, show the stations and show the possible map units on an actual map and then pick and save the correct map unit. This is on the to-do list. Since each RWIS station is mapped to a map unit and a zip code all we have to do is make calls for their data and we can quickly provide the composite data to the users of the website. The front end formatting of the table is somewhat trivial, though time-consuming to set up, and to some extent arbitrary so we will omit that part of the service.

### **6.3.3 Optimization of MongoDB Queries**

The MongoDB queries were sped up using the standard practice of only selecting relevant data from the database. This seems obvious since we do not want to waste time pulling information from the database we do not need but it was not intuitive. By default, when you make a MongoDB query it pulls the entire object of each record but you can select just the fields you want by passing the names of these fields to the query call. It gets slightly more complicated when dealing with relational information but for the most part uses the same process. We had not learned about this method until recently since all our previous projects were small proof of concept stuff that did not deal with huge amounts of data but at least we are now running at the proper speed. Extra care should be taken in the future by anyone contributing to the project to read and understand how to make these selective queries in order to keep all future services running fast.

## **6.4 Functions and Organization of the APP**

The tool aims to provide two modes for users: automatic and manual. In the automatic mode, the users do not need to provide input and they can receive an estimate based on the default values. In the manual mode, users can input site-specific information such as the pavement type for a better prediction. As of now, the automatic mode has been finished while the manual mode is still under development.

As shown in Figure 6.2, our web-based tool has four main services, including 1. Temperature, F/T indices & SLR prediction, 2. Map of freezing/thawing indices & RWIS station, 3. Freezing/thawing depth by ZIP code, and 4. Freezing/thawing depth by RWIS station.

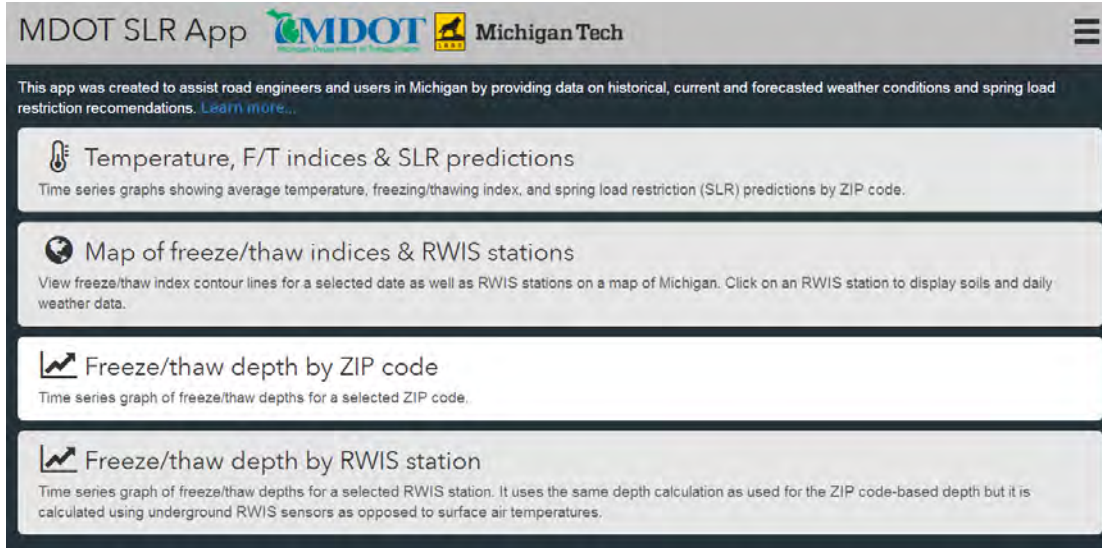


Figure 6.2 Homepage of MDOT SLR App

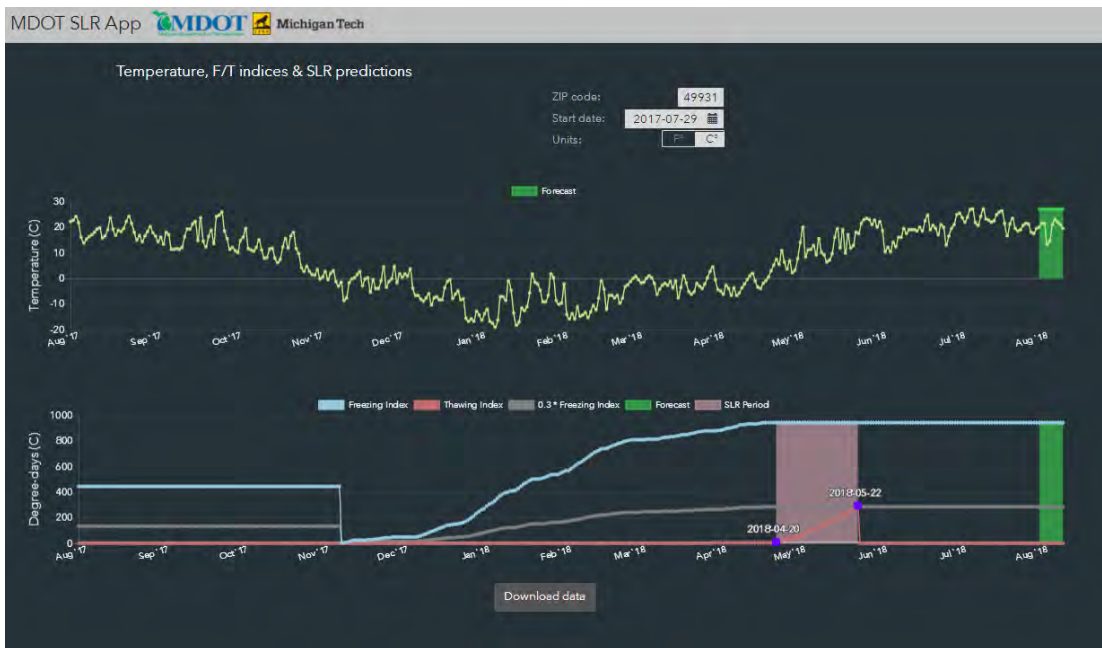


Figure 6.3 Page of temperature, F/T indices & SLR prediction

By clicking the first service in the homepage, it transfers to the page as illustrated in Figure 6.3, in which users can input the ZIP code to get the time series graphs of temperature, freezing/thawing indices and SLR prediction of a specific area in Michigan. The start date and unit of measure also can be chosen in this page. Note that the SLR starts when thawing index reaches 5.6 degrees·days and stops when thawing index reaches  $0.3 \times$  freezing index. The green part at the end of the two graphs represents the forecast. It is worth mentioning that a prolonged prediction is provided in MDOTSLR compared with other DOTs and other existing tools that lack this feature. All the data are downloadable via a “Download data” button at bottom of this page.

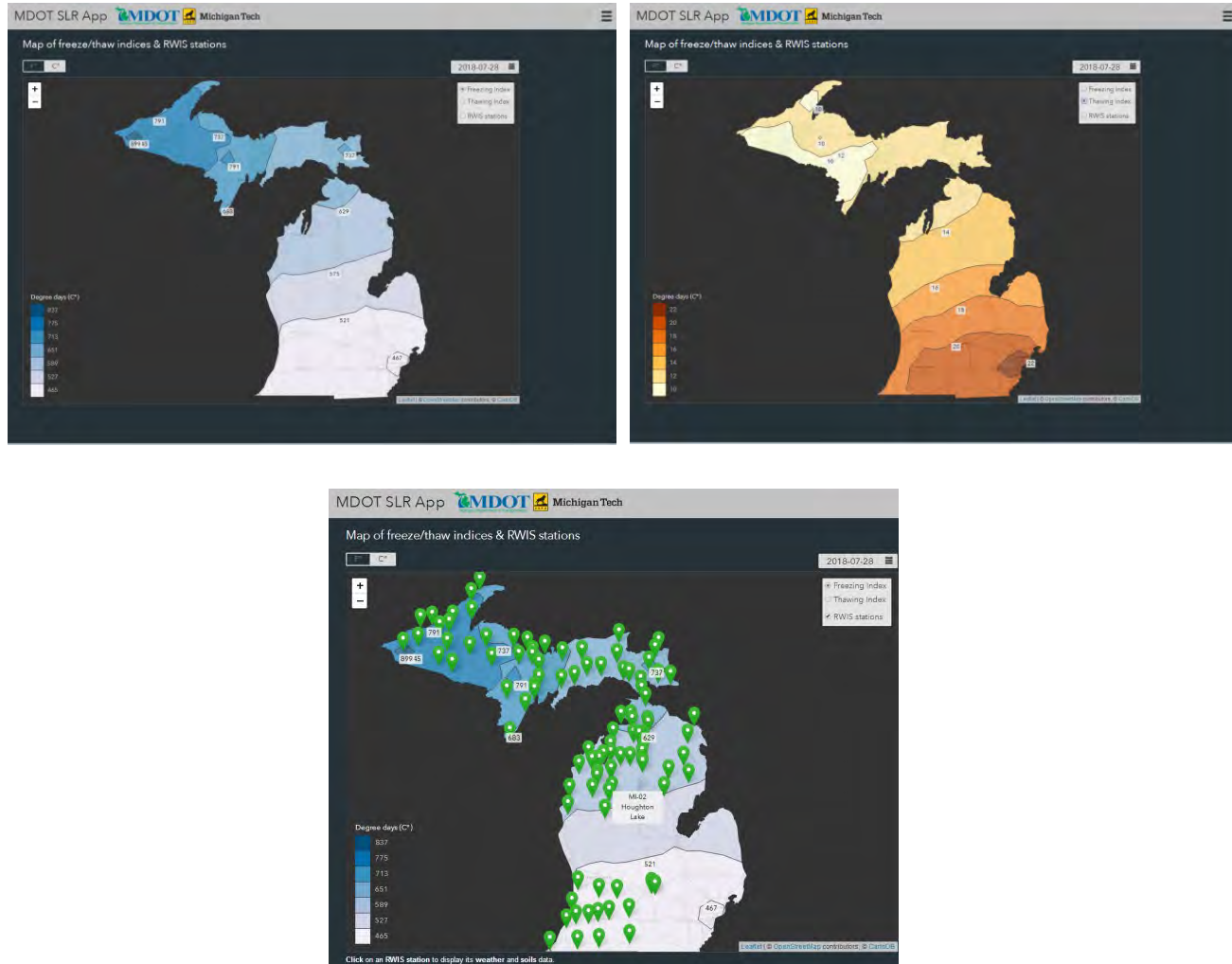


Figure 6.4 Maps of freezing indices (a), thawing indices (b), and RWIS stations (c)

In the second service, a map of freezing/thawing indices and all three categories of data, i.e., weather, GIS, and RWIS, which are indexed using RWIS sites, are provided. Users can choose to see the freezing/thawing index contour lines intuitively from this map (Figure 6.4a and Figure 6.4b). Additionally, all the RWIS stations for Michigan are presented in the map (Figure 6.4c), thus the users can view the soil data and daily weather data of each station by clicking a green marker which represents a station on the map.

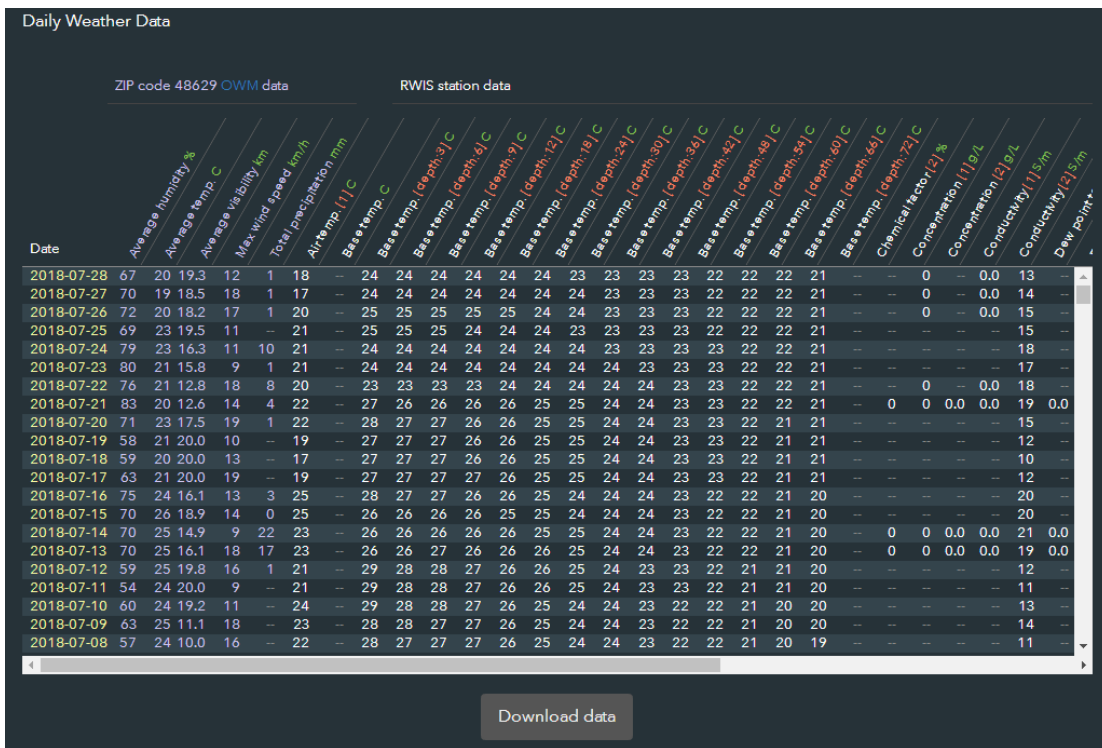
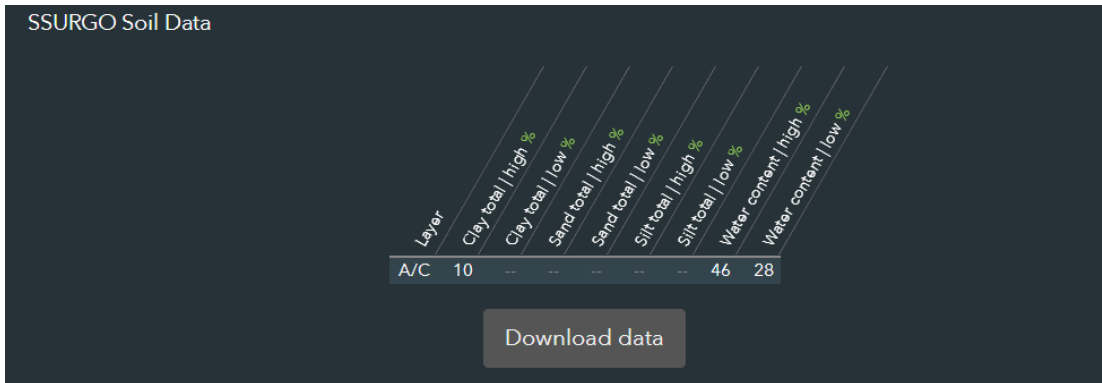


Figure 6.5 SSURGO soil data of the selected station (a) and daily weather data of the selected station (b)

For example, if the user clicks the green marker which represents the MI-02 Houghton Lake as shown in Figure 6.4c, the information of this station will be displayed as shown in Figure 6.5. Figure 6.5a shows a table of SSURGO soil data including the layer, clay total, sand total, silt total and water content. Users can also find a table of daily weather and RWIS data as shown in Figure 6.5b, which includes the parameters of average humidity, average temperature, average visibility, max wind speed, total precipitation, maximum air temperature, minimum air temperature, base temperatures at different depths, and chemical factor and so on.

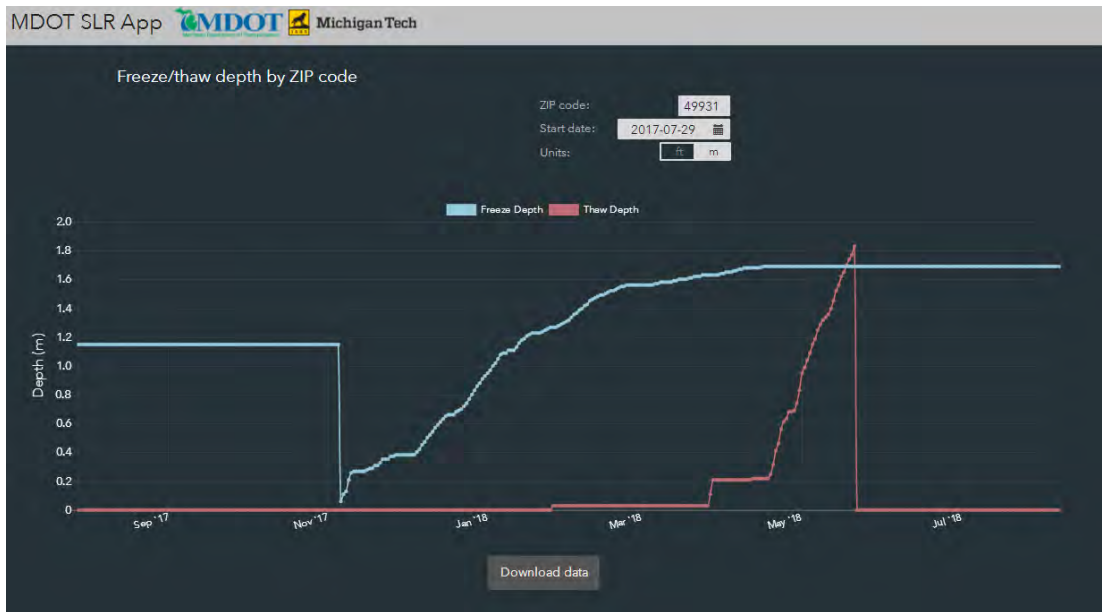


Figure 6.6 Predicted variation of freezing/thawing depth

The third main function of MDOTSLR (Figure 6.6) is that the users can view the time series graph of freezing/thawing depths of a specific area once they select a ZIP code. The start date and units can be assigned as well.

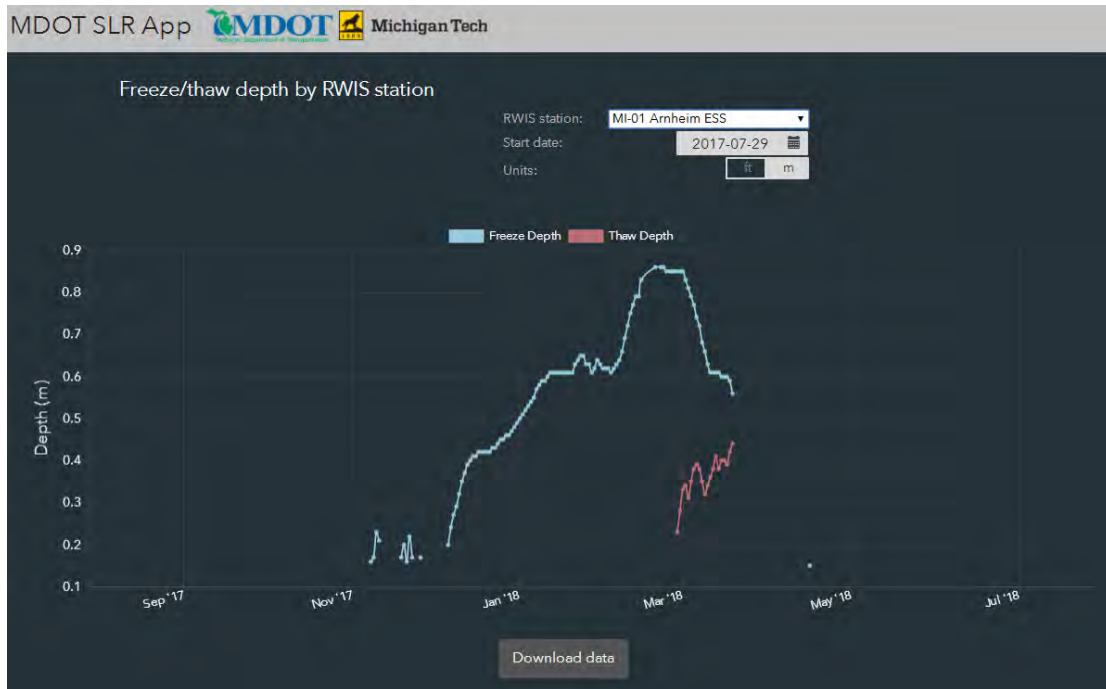


Figure 6.7 Measured variation of freezing/thawing depth

In the last service, users can view the time series graph of freezing/thawing depth for a selected RWIS station (see Figure 6.7). Note that the same depth calculations are used in this part as for the ZIP code-based depth, however, the underground RWIS sensors are used to calculate the depth rather than the surface air temperatures. As mentioned before, there is a difference between the air temperature and the pavement surface temperature, so that they are taken into consideration respectively.

## 6.5 Construction of the App

### 6.5.1 Data Transfer and Workflow

In the default automatic mode, the users just need to enter the zip code for the area of interest to obtain the temperature and SLR predictions, freezing/thawing depth predictions, and measured freezing/thawing depth. With further development, the users will also be able to draw a line (either straight line or polyline) or click one point in a map on a web page to select a road or road segment

that he/she is interested in. As shown in Figure 6.8, the request from the user is sent to the server and translated into accurate location information. The main program on the server will then request weather and GIS information from NOAA/Accuweather and WebSoilSurvey/GeoWebFace. This information will be used to calculate the freezing/thawing depth as well as the SLR recommendations. Both the freezing/thawing depths and SLR recommendations will be sent back to the front-end, that is, the user's electronic device. The web browser on the user's side will process the data and show predicted freezing and thawing depths vs. location lines for the next 30 days. A potential SLR placing or lifting sign will be shown if it is predicted as possible (should or must level) during the time range. Given the current progress made, once extrapolation of the RWIS data has been completed, this functionality will be easy to implement since we already have the work for setting up and taking input from the map taken care of.

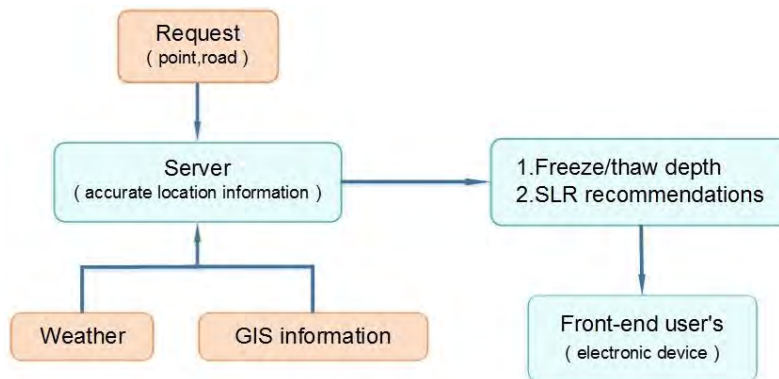


Figure 6.8 The calculation framework of the web-based tool

## 6.5.2 Development of the Web-Based App

The web-based app is essentially a dynamic website. For the front-end design, the web pages are written using HTML5 and CSS3 compiled from SASS. The responsive web design approach is adopted to make sure the website can be optimally accessed with all major types of electronic devices, i.e., desktops, tablets, and mobile phones. jQuery, a JavaScript library, is used to enhance the functionality and user-friendliness of the front-end pages. The mapping and location fetching are achieved with OpenStreetMap and Leaflet.js. Data transfer between the front-end and the server is conducted via JSON. Nodejs (a JavaScript-based programming platform) is used to

manage the retrieval of data from the weather and RWIS sites while MongoDB (a noSQL database technology) is used to store the data locally. Though SQL has traditionally been used as the go-to database for web app's, MongoDB was used for its high speed and ease of use. Even though MongoDB is not fully atomic, meaning all documents are protected in case one query fails, this is not an issue since queries are almost always read-only, with the exception of the automatic data retrieval that occurs once a day. For serving the app, Express, a Node.js website framework, is used to deliver HTML documents and the actual data earlier detailed. The calculation process is programmed on the server side using Node.js to shorten the development cycle, though the calculations were developed using separate technologies. Weather and GIS information is obtained via APIs made available from the sources listed previously. The calculation results are shown as charts and tables on the web pages. This plotting functionality is developed using the free software charting library, Chart.js.

### **6.5.3 Freezing/Thawing Index Acquisition on Backend**

Every service of the app uses a number of different data sources from the database, each doing their assigned job but the easiest place to start in this process would be the data routes as that is where the data is pulled in from MongoDB, processed and then sent off to the client. All data served by the app is served from a subroute of <https://mdotslr.org/data>, though only its subroutes actually serve data, i.e., <https://mdotslr.org/data/tempCurve/49931>, serves the temperature and freezing/thawing index data for Houghton. Though the data is only one portion of the app, it serves as a good starting point as each data sub route relates directly to one of the services.

The temperature curve data route, <https://mdotslr.org/data/tempCurve/>, is the first sub route and serves data to the first service developed last quarter (<https://mdotslr.org/services/temp-curve>), though many changes have been made this quarter including the addition of two new states weather data, Minnesota and Wisconsin. The route takes a zip code in a GET request and returns the temperature, freezing/thawing index and SLR recommendations in JSON format. Thus, for the link <https://mdotslr.org/data/tempCurve/49931>, the zip code we are selecting is 49931 and the data returned will be for that zip code.

The first step is to retrieve the past and forecasted average temperature from MongoDB and the wunderground API respectively. This is done through a query to the database which returns the past data and another HTTP GET request made by the server to the wunderground API which returns the forecasted data. Both of these requests are handled asynchronously meaning we make a request for this data without blocking the thread our server runs on. This is the default behavior of Node.js and this non-blocking paradigm allows us to handle multiple requests and calculations pseudo-concurrently as opposed to sequentially, which makes serving data to multiple users at the same time much faster.

The data is stored on the server in a JSON-like format, which makes it very straightforward for Node.js to handle and for express to send to the client. The JSON format is predefined in a model so we know exactly what fields we have to work with, in this case, we are just using the average temperature of each day but other data fields are available. The data that comes in from the wunderground API is also in JSON format and is organized very similarly to our data, so joining the two together is simple.

With that, we have all the past weather data and the next 10 days forecast. Originally the plan was to also store the 10-day forecast into the database but since the forecast is likely to change it was changed to make live API calls at each request. With that, we have all of our average temperature data that would be returned to the client. Returning the data to the client is handled by Express which simply takes our JSON and sends it off.

However, before the request is returned we must use the temperature data to calculate our freezing and thawing indices and include that in our response to the client.

In short, the function that calculates the freezing index follows this equation:

$$FI = \sum_{i=1}^N (0 - T_i) \tag{Eq. 6.3}$$

and the thawing index is calculated using the following equation:

$$TI = \sum_{i=1}^N (T_i - T_{ref}) \tag{Eq. 6.4}$$

With the difference being the app does this all in JavaScript as opposed to mathematical notation so the actual code and process are slightly different.

For these equations,  $i$  represents the current day in the sigma equation, or in JavaScript the current iteration of the loop that processes each day, and  $N$  is the total number of days in the collection.  $T_i$  is the average temperature of the current day being iterated through, and  $T_{ref}$  is the offset used to account for the temperature difference between the pavement in the air, though it is not 100% successful and this discrepancy is the main flaw in this model. Using these equations, the freezing and thawing indices are calculated, and each step of the summation is also saved so we can show the changes over time where:

$$FI_i = \sum_{j=1}^i (0 - T_j) \quad \text{Eq. 6.5}$$

and

$$TI_i = \sum_{j=1}^i (T_j - T_{ref}) \quad \text{Eq. 6.6}$$

which gives us the indices for each day as well as the final day.

During this summation, or looping through the data, we also mark which dates, or which  $i$ , should be the start and end of SLR. If  $TI_i > 5.6$ , we mark  $i$  as an SLR start date or if SLRs have already started, a continuation of the SLR period. If  $TI_i \geq 0.3 * FI_i$ , we mark  $i$  as an SLR end date. In addition to these calculations, there are also some simple fuzzy rules for determining when the freeze-thaw cycle is and when to reset the values for a new freeze-thaw cycle. Since we're using a programming language and not just doing each of these calculations separately, all of these calculations and the SLR classification can be done in  $O(N)$  operations,  $N$  being our total number of days in the collection. With the calculations are finished, the data is sent off to the front end by Express to be graphed by the client.

#### 6.5.4 Freezing/Thawing Depth Acquisition on Backend

The other main service of the app is the RWIS based freezing and thawing depth calculator, found at <https://mdotslr.org/services/road-depth-curve>. It uses RWIS data provided by the Vaisala API

to calculate the freezing and thawing depth using underground temperature sensors. The temperature data is reported from several RWIS stations set up throughout Michigan that have these sensors installed. Just like with the last service, the data returned from this API is stored locally in MongoDB, organized by each station's unique id in the database. Getting back to the sub route itself, this service starts at the <https://mdotslr.org/data/stations> data route. Unlike the freezing and thawing indices service, this service uses a drop-down menu to select the station you want to see the data for. When you select a station from the drop down, an additional GET request is made via jQuery's ajax function to our sub route, i.e., <https://mdotslr.org/data/roadIndices/11760> where 11760 is a unique station id.

Once the data request has been made to the server, Node.js retrieves the underground temperature data for every day recorded from MongoDB. Each day returned follows a set format, just like with the weather data, where the multiple sensors that each RWIS station reports are organized in JSON format. This data route is only concerned with the underground temperature data for each day since we are trying to determine the freezing/thawing depth, so that is the only field retrieved from MongoDB.

With the temperature data retrieved, we use it to determine the freezing and thawing depth either by direct observation or by interpolation. We are essentially working with a tuple of tuples that hold depth, temperature pairs:

$[[D_1, T_1], [D_2, T_2], \dots [D_N, T_N]]$

where  $N$  is the total number of sensors. Each sensor is ordered by the depth, so the interpolation is fairly straightforward. We just need to iterate over each sensor and apply the following rules:

if  $T_i = 0$

    if  $F$  is not set,  $F = D_i$

    else,  $T = F$  and  $F = D_i$

else if 0 is between  $T_i$  and  $T_{i-1}$

    if  $F$  is not set,  $F =$  interpolated depth between  $D_i$  and  $D_{i-1}$

else,  $T = F$  and  $F =$  interpolated depth between  $D_i$  and  $D_{i-1}$

where,

$D_i =$  current iteration depth

$D_{i-1} =$  last iteration depth

$T_i =$  current iteration temperature

$T_{i-1} =$  last iteration temperature

$F =$  freezing depth

$T =$  thawing depth

Using these rules as we iterate through each tuple, we are looking for the freezing point, or where the sensors report 0 degrees Celsius. This depth is either a freezing depth or a thawing depth. If the sensors don't directly report where 0 is, we need to use linear interpolation to determine where 0 lies between two sensors. This interpolation is done using the following equation:

$$D_{int} = (0 - T_{i-1}) \times (D_i - D_{i-1}) / (T_i - T_{i-1}) + D_{i-1} \quad (7)$$

The above equation is just a standard linear interpolation. The reason we set  $F$  and then switch it out if a new 0 point is found is that we assume that for two 0 points, the one occurring higher in the soil, or for lower  $D_i$  values, is the thawing depth since thawing occurs faster from the surface downwards than from the subgrade upwards.

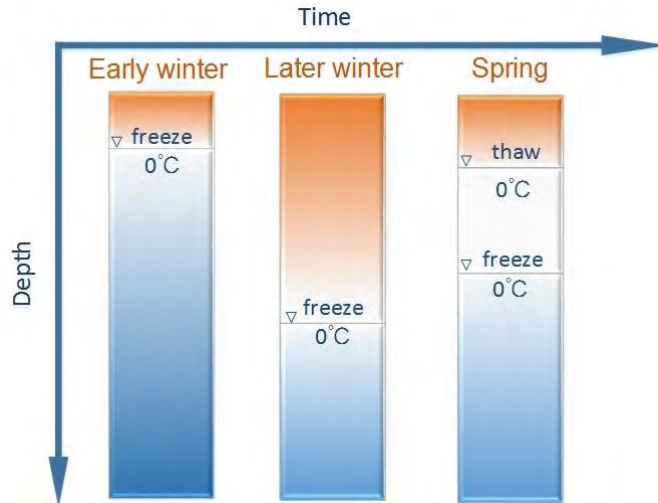


Figure 6.9 Variation of freezing and thawing depth with time

As shown in Figure 6.9, this same process is repeated for every day in our collection of days and the freezing/thawing depths are stored in their own collection of days which we return to the client using Express where it is graphed. For one station the calculation process takes  $O(D*N)$  where  $D$  is the number of days in the collection and  $N$  is the number of depth sensors the station has.

### 6.5.5 Refactoring

In early versions of the app, the entire project was written using callback functions. Callback functions refer to the fact that certain resources, pulling data from a website or making a database call, don't take a predictable amount of time. We call this asynchronous programming, async for short, were not all of the code is run in the order written. One way to deal with this is to pass callback functions to the resource you're pulling from. When the resource is ready it fills your callback function with the data you requested and execution of the script can continue. The only problem with this is that every time you write a function you have to indent the file and after passing upwards of 3 callback functions the code starts to get hard to follow and code that's hard to follow is hard to maintain. To combat this problem, Javascript has special functions called async functions that return a Promise object. Async functions have special rules that let them pause execution to wait for a resource using the await keyword. This means async code can be written

all within the same indent making everything look nice and easy to understand. With all that in mind, we recently went back and refactored much of the code to implement async functions. The hope is that since the code isn't a huge indented mess anymore it will be easier to work on and updates can be made faster.

```
File Edit Selection Find View Goto Tools Project Preferences Help
data.js
14 getTempAverages: function( zip, callback ) {
    var averages = {};
    var currentDate = new Date();

    // get the forecast days for the given zip, this portion is for getting past dates
    ZipCode.findOne( { zip: zip } ).populate( 'forecastDays.id' ).exec( function( err, zipCode ) {
        // if there is an error or no zipcode object is found then return an error
        if ( err ) {
            console.log( err );
            return callback( { status: 500, title: 'An error has occurred', error: err } );
        }
        if ( !zipCode ) {
            return callback( { status: 500, title: 'An error has occurred', error: { message: 'Zipcode not found' } } );
        }

        // go through each forecast day and add its average temperature to the averages object
        zipCode.forecastDays.forEach( function( day ) {
            averages[ day.id.date ] = day.id.day.avgtemp_c;
        } );

        // get the city and state information for the zipcode, this portion is for future dates
        request( 'http://maps.googleapis.com/maps/api/geocode/json?address=' + zip + '&sensor=false' )
        // if there is an error getting future dates return the past dates
        if ( err ) {
            callback( { status: 200, message: 'Found data', averages: averages } );
        }
    } );
}
```

```
File Edit Selection Find View Goto Tools Project Preferences Help
data.js
22 getTempAverages: async function( zip, testing ) {
    // setup variables
    var averages = {}, currentDate = new Date(new Date().toLocaleDateString());
    var err, zipCode, city, state, location;

    // get the weather data stored in the database, handle any errors
    [err, zipCode] = await to( ZipCode.findOne( { zip: zip }, 'forecastDays' ).lean().populate( 'forecastDays.id' ) );
    if ( err ) throw { status: 500, error: err };
    if ( !zipCode ) throw { status: 404, error: { message: 'No ZipCode Found' } };

    // put the weather data into the averages variable
    zipCode.forecastDays.forEach( function( day ) {
        averages[ day.id.date ] = day.id.day.avgtemp_c;
    } );

    if ( testing ) return averages;

    // get the location data for the ZipCode, return on error
    [err, location] = await to( request( { uri: 'http://maps.googleapis.com/maps/api/geocode/json?address=' + zip + '&sensor=false' } ) );
    if ( err ) return averages;
    if ( !location ) return averages;

    // find the city and state values and save them to their variables
    for ( var i = 0; i < location.results.length; i++ ) {
        for ( var j = 0; j < location.results[i].address_components.length; j++ ) {
            if ( location.results[i].address_components[j].types[0] == 'locality' || location.results[i].address_components[j].types[0] == 'administrative_area_level_1' ) {
                if ( location.results[i].address_components[j].types[0] == 'locality' ) {
                    city = location.results[i].address_components[j].short_name;
                } else {
                    state = location.results[i].address_components[j].short_name;
                }
            }
        }
    }
}
```

Figure 6.10 The first picture shows the re-factored code, it is all on one indent and uses await calls instead of callbacks

### 6.5.6 Map Binary Search

This section presents the effort that we made to address the challenge to map the GIS data from the websoilsurvey to any location associated with a zip code, county, or RWIS site. To start we have a map full of zip codes and map units, for the sake of this example we have only illustrated one of each but in reality there would be many.



Figure 6.11 Schematic of map binary search: original map

We start with a box around the entirety of Michigan, working with one peninsula at a time. We then divide the box in two over and over until the box is small enough to only be in one map unit and one zip code.



Figure 6.12 Schematic of map binary search: one box

We have only illustrated one divide but in reality every box would continue to make divides until they are in the same state as the one illustrated. This chain of divides is saved to the database. Now when we have a point we want to find:



Figure 6.13 Schematic of map binary search: refined boxes

We can keep track of the divides we made and use that to identify which box the point belongs in and in turn which map unit and zip code the point has. There will be an enormous number of divide

chains saved to the database but they can be encoded very efficiently as binary data. We can represent each new box as either a one or a zero, zero for the first box made by the divide and one for the other. This binary data will be very small so storage shouldn't get too large. Another advantage of this method is that the point in polygon algorithm is extremely efficient for rectangles. So the loading time, in theory, should be short.

## 6.6 Conclusions

The development progress and future development plans for the MDOT web-based SLR prediction tool, i.e., MDOTSLR, have been detailed in this chapter. This tool is for the benefit of MDOT, road agencies, and road users since they will be able to make better decisions about when SLR should be started and ended. Freezing/thawing depth prediction models, which are considered a key factor to the prediction of SLR, will be used by this tool to provide more accurate results and will replace the current freezing/thawing indices model in place now. RWIS information, significant Weather, and GIS soil data are automatically collected by MDOTSLR to make SLR decisions with plans to expand the current database to include solar radiation data and a longer date range of all data types.

To conclude, the web-based tool we developed has functions and advantages as follow:

- ❖ Automatic SLR prediction accompanied by the data used to predict SLR so users may calculate it manually with a different model or develop their own models from the data.
- ❖ Searching by ZIP code, the users can get the time series graphs of average temperature, freezing/thawing index and SLR prediction.
- ❖ Users can view freezing/thawing index contour lines for any date as well as RWIS stations on the map of Michigan. By clicking on an RWIS station, the users can get the information of soils and daily weather. (<https://mdotslr.org/services/map>)
- ❖ Both searching by the ZIP code and RWIS station, the users can get the time series graphs of the freezing/thawing depth. Note that the freezing/thawing depth by ZIP code is calculated by the air temperature (<https://mdotslr.org/services/depth-curve>) while the freezing/thawing depth by RWIS station is calculated by the pavement surface temperature (<https://mdotslr.org/services/road-depth-curve>).

- ❖ Compared with other existing tools, the web-based tool we developed is more accurate, convenient, user-friendly, automatic and feature rich. With the implementation of a longer forecast, it will provide a much longer prediction than other tools.
- ❖ The tool will significantly enhance the current web services provided by MDOT. Studies that use the tool as a resource will help refine the pavement design to better consider frost effects and provide suggestions and information for future RWIS sites.

## Appendix

### FD/TD Prediction Models Obtained with RWIS Data 2017-2018

|  |                |                          |   |                           |                  |             |                |
|--|----------------|--------------------------|---|---------------------------|------------------|-------------|----------------|
| <b>Important Notes</b>   | Note A         | Fitting function for FD: | $FD = a * FI^{0.2} + (c - b * TI)^{0.5} - d$  |                           |                  |             |                |
|  |                | Fitting function for TD: | $TD = -e * FI^{0.5} - (g - f * TI)^{0.5} + h$ |                           |                  |             |                |
|  |                | Fitting constraints      | FD: $c^{0.5} - d = 0.25$                      | TD: $-g^{0.5} + h = 0.25$ |                  |             |                |
| Measured situation 1: depth=[0;3;6;9;12;18;24;30;36;42;48;54;60;66;72] |                |                          |   |                           |                  |             |                |
| Measured situation 1   | Site           | Fitting parameter        | Fitting constant                              |                           |                  |             |                |
|  |                |                          | FD a (TD e)                                   | FD b (TD f)               | FD c (TD g)      | FD d (TD h) | r <sup>2</sup> |
|  | Charlevoix     | FD with freezing cycle   | 10.46   | 3398479.01                | 8329021367327.90 | 2886029.39  | 0.96           |
|  |                | TD with thawing cycle    | 12.62   | 6729249.71                | 9098417670462.76 | 3016333.35  | 0.46           |
|  | Glennie        | FD with freezing cycle   | 9.01  | 1049235.17                | 1027864588018.50 | 1013861.57  | 0.76           |
|  |                | TD with thawing cycle    | 38.93   | 1798820.29                | 239192937999.03  | 489048.55   | 0.86           |
|  | Cadillac South | FD with freezing cycle   | 4.29  | 28087.87                  | 5140425402.13    | 71721.76    | 0.86           |
|  |                | TD with thawing cycle    | 0.00  | 349807.28                 | 239137715029.24  | 488992.09   | 0.66           |
|  | Eastport       | FD with freezing cycle   | 12.16   | 521.44                    | 44940.40         | 236.99      | 0.97           |
|  |                | TD with thawing cycle    | 10.70   | 299.15                    | 19229.11         | 113.67      | 0.81           |
|  | Fife Lake      | FD with freezing cycle   | 10.79   | 1511.04                   | 1309376.37       | 1169.29     | 0.93           |
|  |                | TD with thawing cycle    | 36.87   | 6831142.56                | 5351199864511.11 | 2313241.07  | 0.57           |
|  | Wolverine      | FD with freezing cycle   | 12.74   | 1927272.28                | 147084221172.63  | 383540.61   | 0.43           |
|  |                | TD with thawing cycle    | 27.06   | 606.17                    | 40378.04         | 175.94      | 0.72           |
|  | Williamsburg   | FD with freezing cycle   | 5.02  | 75.74                     | 4706.63          | 93.60       | 0.74           |
|  |                | TD with thawing cycle    | Only 1 data point                             |                           |                  |             |                |
|  | West Branch    | FD with freezing cycle   | 8.91  | 2302.26                   | 318871.91        | 589.69      | 0.96           |
|  |                | TD with thawing cycle    | 0.32  | 349.50                    | 13208.83         | 89.93       | 0.96           |
|  | Wellston       | FD with freezing cycle   | Need TD data to calculate TI                  |                           |                  |             |                |

|               |                        |               |             |                    |             |          |
|---------------|------------------------|---------------|-------------|--------------------|-------------|----------|
|               | TD with thawing cycle  | No data point |             |                    |             |          |
| Waters        | FD with freezing cycle | 8.26          | 38.59       | 5909.32            | 101.87      | 0.96     |
|               | TD with thawing cycle  | 2.62E+00      | 16841557.51 | 214932656724285.00 | 14660561.84 | 0.51     |
| Walloon Lake  | FD with freezing cycle | 5.65          | 91241.80    | 24908181751.87     | 157848.26   | 0.89     |
|               | TD with thawing cycle  | 0.00          | 242716.56   | 146353610036.38    | 382536.90   | 0.50     |
| Sherman       | FD with freezing cycle | 5.73          | 458458.28   | 274551215053.46    | 524001.35   | 0.92     |
|               | TD with thawing cycle  | 0.13          | 1428859.23  | 1159236899600.87   | 1076653.64  | 0.70     |
| Rose City     | FD with freezing cycle | 5.45          | 175708.69   | 50301126130.76     | 224304.13   | 0.32     |
|               | TD with thawing cycle  | 0.00E+00      | 8.03E+04    | 13470726159.78     | 116038.46   | 2.60E-02 |
| Presque Isle  | FD with freezing cycle | 8.59          | 530014.81   | 27174946019.24     | 164873.25   | 0.82     |
|               | TD with thawing cycle  | 41.34         | 16601697.27 | 16311015628135.30  | 4038664.84  | 0.89     |
| Maple City    | FD with freezing cycle | 10.31         | 254.09      | 25259.46           | 183.93      | 0.88     |
|               | TD with thawing cycle  | 20.21         | 870.41      | 223043.28          | 447.27      | 0.93     |
| Manistee      | FD with freezing cycle | 10.29         | 774763.65   | 25058961907.79     | 158325.23   | 0.91     |
|               | TD with thawing cycle  | 9.70E-01      | 2.42E+06    | 182412237151.44    | 427072.46   | 4.88E-01 |
| Mackinaw City | FD with freezing cycle | 8.17          | 2239190.08  | 3949456590587.00   | 1987348.98  | 0.91     |
|               | TD with thawing cycle  | 2.73E-04      | 15704549.20 | 49406917740286.80  | 7028980.46  | 0.22     |
| Ludington     | FD with freezing cycle | 7.99          | 0.00        | 2554.67            | 75.54       | 0.39     |
|               | TD with thawing cycle  | 3.58          | 58.60       | 12047.32           | 84.76       | 0.12     |
| Levering      | FD with freezing cycle | 4.77          | 5832.42     | 72445319.14        | 8536.48     | 0.89     |
|               | TD with thawing cycle  | 0.62          | 295993.52   | 138794422057.67    | 372528.50   | 0.39     |
| Lachine       | FD with freezing cycle | No data point |             |                    |             |          |
|               | TD with thawing cycle  | No data point |             |                    |             |          |
| Kalkaska      | FD with freezing cycle | 8.37          | 930237.04   | 451357885129.89    | 671856.74   | 0.95     |
|               | TD with thawing cycle  | 0.00          | 161400.15   | 265135410339.95    | 514888.01   | 0.00     |
| Houghton Lake | FD with freezing cycle | 5.83          | 10.21       | 1408.29            | 62.53       | 0.90     |
|               | TD with thawing cycle  | 10.90         | 316.75      | 85594.22           | 267.56      | 0.53     |
| Grayling      | FD with freezing cycle | 6.47          | 23.31       | 2896.22            | 78.82       | 0.94     |

|  |               |                        |                              |            |                  |            |      |
|--|---------------|------------------------|------------------------------|------------|------------------|------------|------|
|  |               | TD with thawing cycle  | Only 1 data point            |            |                  |            |      |
|  | Elmira ESS    | FD with freezing cycle | 8.35                         | 176.71     | 54000.19         | 257.38     | 0.90 |
|  |               | TD with thawing cycle  | Only 1 data point            |            |                  |            |      |
|  | Curran ESS    | FD with freezing cycle | 7.83                         | 702276.14  | 1046257704357.73 | 1022892.39 | 0.77 |
|  |               | TD with thawing cycle  | 0.003                        | 2018631.55 | 1124988234451.56 | 1060629.63 | 0.84 |
|  | Benzonia      | FD with freezing cycle | 6.20E+00                     | 97192.55   | 602132303625.07  | 775996.85  | 0.06 |
|  |               | TD with thawing cycle  | 0.000                        | 376.62     | 25317.30         | 134.11     | 0.26 |
| Measured situation 2: depth=[6;12;18;24;36;48;60;72] |               |                        |                              |            |                  |            |      |
|  | South Haven   | FD with freezing cycle | No data point                |            |                  |            |      |
|  |               | TD with thawing cycle  | No data point                |            |                  |            |      |
|  | Marshall      | FD with freezing cycle | No data point                |            |                  |            |      |
|  |               | TD with thawing cycle  | No data point                |            |                  |            |      |
|  | Paw Paw       | FD with freezing cycle | 7.62                         | 390066.96  | 129978156086.85  | 360549.83  | 0.29 |
|  |               | TD with thawing cycle  | Only 1 data point            |            |                  |            |      |
|  | Kalamazoo     | FD with freezing cycle | 7.01                         | 64037.48   | 11528602715.76   | 107396.33  | 0.14 |
|  |               | TD with thawing cycle  | Only 1 data point            |            |                  |            |      |
|  | Hartford      | FD with freezing cycle | No data point                |            |                  |            |      |
|  |               | TD with thawing cycle  | No data point                |            |                  |            |      |
| Measured situation 2                                 | Galesburg     | FD with freezing cycle | No data point                |            |                  |            |      |
|  |               | TD with thawing cycle  | No data point                |            |                  |            |      |
|  | Edwardsburg   | FD with freezing cycle | No data point                |            |                  |            |      |
|  |               | TD with thawing cycle  | No data point                |            |                  |            |      |
|  | Coldwater     | FD with freezing cycle | 6.82                         | 86508.98   | 13112721800.46   | 114535.79  | 0.18 |
|  |               | TD with thawing cycle  | Only 1 data point            |            |                  |            |      |
|  | Benton Harbor | FD with freezing cycle | No data point                |            |                  |            |      |
|  |               | TD with thawing cycle  | No data point                |            |                  |            |      |
|  | New Buffalo   | FD with freezing cycle | Need TD data to calculate TI |            |                  |            |      |
|  |               | TD with thawing cycle  | No data point                |            |                  |            |      |
|  | Wayland       | FD with freezing cycle | No data point                |            |                  |            |      |

|             |                        |                   |           |                 |           |      |
|-------------|------------------------|-------------------|-----------|-----------------|-----------|------|
|             | TD with thawing cycle  | No data point     |           |                 |           |      |
| Holland     | FD with freezing cycle | No data point     |           |                 |           |      |
|             | TD with thawing cycle  | No data point     |           |                 |           |      |
| Hastings    | FD with freezing cycle | 7.56              | 0.00      | 3297.11         | 82.42     | 0.81 |
|             | TD with thawing cycle  | Only 1 data point |           |                 |           |      |
| Constantine | FD with freezing cycle | 7.36              | 152450.12 | 77429790971.16  | 278287.09 | 0.32 |
|             | TD with thawing cycle  | 0.002             | 813705.78 | 286888814597.40 | 535595.03 | 0.06 |

The following sites have various data problems

| Site                  | Problem detail             |
|-----------------------|----------------------------|
| Cadillac              |                            |
| I75BL_M93_M72_Lake    |                            |
| I75MM2638             |                            |
| Mesick                |                            |
| US31_Ames-Dexter      | No RWIS data               |
| US31_M37_Beitner      |                            |
| US31_M72_3 Mile       |                            |
| US131_US31_Charlevoix |                            |
| Charles Brink         |                            |
| Gaylord North         |                            |
| I75_Trowbridge        |                            |
| Interlochen           |                            |
| Kalkaska East         |                            |
| M32_Hallock           | No sub-surface temperature |
| Reed City             |                            |
| Dunckel Rd            |                            |
| I96 E at US127        |                            |
| Okemos Rd             |                            |
| Trowbridge Rd         |                            |
| Lachine               | No freezing depth          |

FD/TD Prediction Models Obtained with RWIS Data 2018-2019

|  |                        |                          |                                    |                       |                      |               |                |
|--|------------------------|--------------------------|------------------------------------|-----------------------|----------------------|---------------|----------------|
| <b>Important Notes</b>   | <b>Note A</b>          | Fitting function for FD: | $FD=a*FI^{0.2}+(c-b*TI)^{0.5}+d$   |                       |                      |               |                |
|  |                        | Fitting function for TD: | $TD=-e*FIT^{0.5}-(g-f*TI)^{0.5}+h$ |                       |                      |               |                |
|  |                        | Fitting constraints      | FD: $c^{0.5}-d=0.25$               | TD: $-g^{0.5}+h=0.25$ |                      |               |                |
| Measured situation 1: depth=[3;6;9;12;18;24;30;36;42;48;54;60;66;72] |                        |                          |                                    |                       |                      |               |                |
| Measured situation 1   | Site                   | Fitting parameter        | Fitting constant                   |                       |                      |               |                |
|  |                        |                          | FD a (TD e)                        | FD b (TD f)           | FD c (TD g)          | FD d (TD h)   | r <sup>2</sup> |
|  | Michigamme             | FD with freezing cycle   | 7.31                               | 8.40                  | 875.78               | 54.59         | 0.99           |
|  |                        | TD with thawing cycle    | 0.0016                             | 81698974.2360         | 599403088830328.0000 | 24482684.9977 | 0.9601         |
|  | Seney                  | FD with freezing cycle   | 8.94                               | 35.64                 | 4052.38              | 88.66         | 0.97           |
|  |                        | TD with thawing cycle    | 5.01                               | 583.89                | 51533.67             | 202.01        | 0.97           |
|  | Rudyard                | FD with freezing cycle   | 8.52                               | 82067.02              | 90801819794.21       | 301358.40     | 0.99           |
|  |                        | TD with thawing cycle    | 0.00                               | 1981514.47            | 3113369394659.51     | 1764449.25    | 0.77           |
|  | Au Train               | FD with freezing cycle   | 9.70                               | 7.48                  | 667.51               | 50.84         | 0.97           |
|  |                        | TD with thawing cycle    | 0.68                               | 340.36                | 42067.95             | 180.10        | 0.73           |
|  | Twin Lakes             | FD with freezing cycle   | 4.85                               | 6.70E+02              | 1144874.32           | 1094.99       | 0.70           |
|  |                        | TD with thawing cycle    | Only 2 data points                 |                       |                      |               |                |
|  | St. Ignace             | FD with freezing cycle   | 5.65                               | 16.54                 | 2372.56              | 73.71         | 0.88           |
|  |                        | TD with thawing cycle    | Only 2 data points                 |                       |                      |               |                |
|  | Gwin                   | FD with freezing cycle   | Straight line for FD data          |                       |                      |               |                |
|  |                        | TD with thawing cycle    | Straight line for TD data          |                       |                      |               |                |
|  | Engadine               | FD with freezing cycle   | 8.16                               | 15.31                 | 8107.48              | 115.05        | 0.98           |
|  |                        | TD with thawing cycle    | 1.88E-14                           | 557.31                | 111666.64            | 309.17        | 0.92           |
|  | Cooks                  | FD with freezing cycle   | 8.35                               | 62.31                 | 5891.30              | 101.75        | 0.04           |
|  |                        | TD with thawing cycle    | 0.00                               | 1609144.64            | 742156590242.99      | 861460.11     | 0.03           |
| Brevort  | FD with freezing cycle | 2.39                     | 0.06                               | 7.28                  | 27.70                | 0.47          |                |
|  | TD with thawing cycle  | 0.00                     | 1128752.03                         | 2460335715843.00      | 1568520.73           | 0.00          |                |

| Measured situation 2: depth=[6;12;18;24;36;48;60;72] |              |                        |                                    |             |                    |             |          |
|--|--------------|------------------------|------------------------------------|-------------|--------------------|-------------|----------|
| Measured situation 2                                 | Arnheim      | FD with freezing cycle | 5.00                               | 0.71        | 68.65              | 33.30       | 0.96     |
|  |              | TD with thawing cycle  | 6.89E-01                           | 605279.73   | 118839710281.94    | 344706.36   | 0.93     |
|  | Dafter       | FD with freezing cycle | 0.08                               | 0.00        | 36707788.96        | 5959.09     | 0.85     |
|  |              | TD with thawing cycle  | 0.15                               | 1607.78     | 473442576.81       | 21733.74    | 0.03     |
|  | Detour       | FD with freezing cycle | 7.9241276                          | 2.557680113 | 357.5769635        | 43.93543195 | 0.991099 |
|  |              | TD with thawing cycle  | 0.1066528                          | 147.2217094 | 21724.35322        | 122.3918357 | 0.930869 |
|  | Golden Lake  | FD with freezing cycle | 4.69                               | 0.08        | 72.43              | 33.51       | 0.84     |
|  |              | TD with thawing cycle  | Four equal TD data (Straight line) |             |                    |             |          |
|  | Hermansville | FD with freezing cycle | 7.16                               | 4.31        | 741.00             | 52.22       | 0.96     |
|  |              | TD with thawing cycle  | 0.18                               | 370.31      | 116442.69          | 316.24      | 0.85     |
|  | Ontonagon    | FD with freezing cycle | 5.96                               | 0.00        | 72.23              | 33.50       | 0.97     |
|  |              | TD with thawing cycle  | Only 1 data point                  |             |                    |             |          |
|  | Republic     | FD with freezing cycle | 9.05                               | 326910.07   | 17701784967.06     | 133073.06   | 0.47     |
|  |              | TD with thawing cycle  | 5.13E-05                           | 41653997.54 | 271802057354251.00 | 16486395.39 | 0.78     |
|  | Sundell      | FD with freezing cycle | 5.79                               | 20059.25    | 7957372391.35      | 89229.11    | 0.93     |
|  |              | TD with thawing cycle  | 5.90E-04                           | 4753832.17  | 4966095969833.44   | 2228448.91  | 0.91     |
|  | Trenary      | FD with freezing cycle | 0.34                               | 0.00        | 9923301420136.17   | 3149964.41  | 0.82     |
|  |              | TD with thawing cycle  | Straight line for TD data          |             |                    |             |          |
|  | Trout Creek  | FD with freezing cycle | 6.88                               | 206.39      | 97452.53           | 337.17      | 0.85     |
|  |              | TD with thawing cycle  | 9.78E-16                           | 3025553.71  | 871775274788.18    | 933664.07   | 0.64     |
|  | Wakefield    | FD with freezing cycle | 6.93                               | 247.16      | 23800.50           | 179.27      | 0.45     |
|  |              | TD with thawing cycle  | 180.55                             | 1280345.78  | 357204545157.36    | 597640.92   | 0.12     |
|  | Paradise     | FD with freezing cycle | No TD data point caused problems   |             |                    |             |          |
|  |              | TD with thawing cycle  | No TD data point                   |             |                    |             |          |
|  | Nisula       | FD with freezing cycle | Straight line for FD data          |             |                    |             |          |
|  |              | TD with thawing cycle  | Straight line for TD data          |             |                    |             |          |
| Measured situation 3: depth=[18;24;36;48;60;72]      |              |                        |                                    |             |                    |             |          |
|  | Cedar River  | FD with freezing cycle | Up and down FD data                |             |                    |             |          |

|  |                    |                            |                     |        |          |        |      |
|--|--------------------|----------------------------|---------------------|--------|----------|--------|------|
| Measured situation 3                           |                    | TD with thawing cycle      | Up and down TD data |        |          |        |      |
|  | Calumet            | FD with freezing cycle     | 7.88                | 54.90  | 18480.32 | 160.95 | 0.90 |
|  |                    | TD with thawing cycle      | 0.73                | 850.89 | 82291.55 | 261.87 | 0.86 |
| The following sites have various data problems |                    |                            |                     |        |          |        |      |
| Problem sites                                  | Site               | Problem detail             |                     |        |          |        |      |
|  | Sault_Ste._Marie   | No RWIS data               |                     |        |          |        |      |
|  | Menominee          |                            |                     |        |          |        |      |
|  | Manistique         |                            |                     |        |          |        |      |
|  | Negaunee           |                            |                     |        |          |        |      |
|  | Escanaba           |                            |                     |        |          |        |      |
|  | Blaney_Park        | No sub-surface temperature |                     |        |          |        |      |
|  | Covington          |                            |                     |        |          |        |      |
|  | Cut_River_Bridge   |                            |                     |        |          |        |      |
|  | Escanaba           |                            |                     |        |          |        |      |
|  | Rapid_River        | No surface temperature     |                     |        |          |        |      |
|  | Silver_City        |                            |                     |        |          |        |      |
|  | Harvey             |                            |                     |        |          |        |      |
|  | Kiva               | No air temperature         |                     |        |          |        |      |
|  | Merriweather       |                            |                     |        |          |        |      |
|  | Rockland           |                            |                     |        |          |        |      |
| Cedarville                                     | No air temperature |                            |                     |        |          |        |      |
| Newberry                                       |                    |                            |                     |        |          |        |      |
| Phoenix  |                    |                            |                     |        |          |        |      |
| Shingleton                                     |                    |                            |                     |        |          |        |      |
| Watersmeet                                     |                    |                            |                     |        |          |        |      |

## References

- ACE-US (1984). "Pavement criteria for seasonal frost conditions." Department of the Army Technical Manual, U.S. Army Corps of Engineers.
- Aldrich, H. P. J., and Paynter, H. M. (1953). "Analytical studies of freezing and thawing of soils." Arctic Construction and Frost Effects Lab, Boston, MA.
- Asefzadeh, A., Hashemian, L., Haghi, N. T., and Bayat, A. (2016). "Evaluation of spring load restrictions and winter weight premium duration prediction methods in cold regions according to field data." *Canadian Journal of Civil Engineering*, 43(7), 667-674.
- Asefzadeh, A., Hashemian, L., Tavafzadeh Haghi, N., and Bayat, A. (2016). "Evaluation of Spring Load Restrictions and Winter Weight Premium Duration Prediction Methods in Cold Regions according to Field Data." *Canadian Journal of Civil Engineering*(ja).
- Baiz, S., Tighe, S., Haas, C., Mills, B., and Perchanok, M. "Development and Calibration of Frost and Thaw Depth Predictors for Use in Variable Load Restrictions Decision-Making On Flexible Low Volume Roads." *Proc., Transportation Research Board Annual Meeting, Washington, DC*.
- Baiz, S., Tighe, S., Haas, C., Mills, B., and Perchanok, M. (2008). "Development of frost and thaw depth predictors for decision making about variable load restrictions." *Transportation Research Record: Journal of the Transportation Research Board*(2053), 1-8.
- Baladi, G. Y., and Rajaei, P. (2015). "Predictive modeling of freezing and thawing of frost-susceptible soils." Michigan State University, Department of Civil & Environmental Engineering, Lansing, MI.
- Bao, T., Bland, J., and Liu, Z. (2019). "A multivariate freezing-thawing depth prediction model for spring load restriction." *Cold Regions Science and Technology*.
- Berg, R. L., Kestler, M. A., Eaton, R. A., and Benda, C. C. "Estimating when to apply and remove spring load restrictions." *Proc., Current Practices in Cold Regions Engineering*, American Society of Civil Engineers, 1-11.

- Bertsekas, D. P. (2014). *Constrained optimization and Lagrange multiplier methods*, Academic press.
- Bradley, A., Ahammed, M., Hilderman, S., and Kass, S. (2012). "Responding to climate change with rational approaches for managing seasonal weight programs in Manitoba." *Cold Regions Engineering 2012: Sustainable Infrastructure Development in a Changing Cold Environment*, 391-401.
- C-SHRP (2000). "seasonal load restrictions in canada and around the world." *C\_SHRP Technical Brief #21*.
- Chapin, J., Kjartanson, B. H., and Pernia, J. (2012). "Comparison of two methods for applying spring load restrictions on low volume roads." *Canadian Journal of Civil Engineering*, 39(6), 599-609.
- Chisholm, R., and Phang, W. (1983). "Measurement and Prediction of Frost Penetration in highways." *Transportation Research Record*(918).
- Cluett, C., Gopalakrishna, D., and Middleton, D. (2011). "Clarus Multi-State Regional Demonstrations, Evaluation of Use Case# 2: Seasonal Load Restriction Tool."
- CRAM (2019). "County Road Association of Michigan." <<http://micountyroads.org/Doing-Business/Seasonal-Weight-Restriction>>.
- Eaton, R., Hanscom, A., Kestler, M., Hall, A., and Berg, R. (2009). "Spring Thaw Predictor and Development of Real Time Spring Load Restrictions."
- Eaton, R. A., Berg, R. L., Hall, A., Miller, H. J., and Kestler, M. A. "Initial Analysis of the New Hampshire Spring Load Restriction Procedure." *Proc., Proceedings of the American Society of Civil Engineers 14th International Conference on Cold Regions Engineering, Duluth, MN*.
- Embacher, R. (2006). "Duration of spring thaw recovery for aggregate-surfaced roads." *Transportation Research Record: Journal of the Transportation Research Board*(1967), 27-35.
- Fayer, M. J. (2000). "UNSAT-H version 3.0: Unsaturated soil water and heat flow model. Theory,

- user manual, and examples." *Pacific Northwest National Laboratory*, 13249.
- Fayer, M. J., and Jones, T. (1990). "UNSAT-H Version 2. 0: unsaturated soil water and heat flow model." Pacific Northwest Lab., Richland, WA (USA), Richland, Washington.
- FHWA (1990). "Pavement Newsletter No. 17." *FHWA, US Department of Transportation*.
- Gill, P. E., and Wong, E. (2012). "Sequential quadratic programming methods." *Mixed integer nonlinear programming*, Springer, 147-224.
- Hanek, G. L., Truebe, M. A., and Kestler, M. A. (2001). *Using Time Domain Reflectometry (TDR) and Radio Frequency (RF) Devices to Monitor Seasonal Moisture Variation in Forest Road Subgrade and Base Materials*, Technology & Development Program.
- Isotalo, J. (1993). "Seasonal Truck-Load Restrictions and Road Maintenance in Countries with Cold Climate." *Infrastructure Notes: Transportation, Water and Urban Development Department*.
- Jiji, L. M., and Ganatos, P. (2009). "Approximate analytical solution for one-dimensional tissue freezing around cylindrical cryoprobes." *International Journal of Thermal Sciences*, 48(3), 547-553.
- Kestler, M., Berg, R., Steinert, B., Hanek, G., Truebe, M., and Humphrey, D. (2007). "Determining when to place and remove spring load restrictions on low-volume roads: Three low-cost techniques." *Transportation Research Record: Journal of the Transportation Research Board*(1989), 219-229.
- Kestler, M. A., Knight, T., and Krat, A. "Thaw weakening on low volume roads and load restriction practices." *Proc., Transportation Research Board Conference Proceedings*.
- Konrad, J.-M. (1989). "Physical processes during freeze-thaw cycles in clayey silts." *Cold Regions Science and Technology*, 16(3), 291-303.
- Konrad, J.-M., and Morgenstern, N. (1982). "Prediction of frost heave in the laboratory during transient freezing." *Canadian Geotechnical Journal*, 19(3), 250-259.

- Konrad, J.-M., and Shen, M. (1996). "2-D frost action modeling using the segregation potential of soils." *Cold regions science and technology*, 24(3), 263-278.
- Liu, Z., Sun, Y., and Yu, X. B. (2012). "Theoretical basis for modeling porous geomaterials under frost actions: A review." *Soil Science Society of America Journal*, 76(2), 313-330.
- Liu, Z., and Yu, X. (2011). "Coupled thermo-hydro-mechanical model for porous materials under frost action: theory and implementation." *Acta Geotechnica*, 6(2), 51-65.
- Liu, Z., Yu, X., Sun, Y., and Zhang, B. (2012). "Formulation and characterization of freezing saturated soils." *Journal of Cold Regions Engineering*, 27(2), 94-107.
- Liu, Z., Yu, X. B., Tao, J.-l., and Sun, Y. (2012). "Multiphysics extension to physically based analyses of pipes with emphasis on frost actions." *Journal of Zhejiang University SCIENCE A*, 13(11), 877-887.
- Liu, Z., Zhang, B., Yu, X., Tao, J., Sun, Y., and Gao, Q. (2013). "Thermally induced water flux in soils." *Transportation Research Record: Journal of the Transportation Research Board*(2349), 63-71.
- Mahoney, J., Rutherford, M., and Hicks, R. (1987). "Guidelines for spring highway use restrictions."
- Mahoney, J., Rutherford, M., and Hicks, R. (1987). "Guidelines for spring highway use restrictions." Federal Highway Administration, 1-15.
- Marquis, B. (2008). "Mechanistic Approach to Determine Spring Load Restrictions in Maine." Technical Report.
- McBane, J. A., and Hanek, G. (1986). *Determination of the critical thaw-weakened period in asphalt pavement structures*.
- michigan.gov                      "Michigan                      Legislature                      Section                      257.722."  
 <[http://www.legislature.mi.gov/\(S\(wneqcopxuijfkjhkwkvw42nt\)\)/mileg.aspx?page=GetObject&objectname=mcl-257-722](http://www.legislature.mi.gov/(S(wneqcopxuijfkjhkwkvw42nt))/mileg.aspx?page=GetObject&objectname=mcl-257-722)>.

- Miller, H., Cabral, C., Kestler, M., Berg, R., and Eaton, R. (2012). "Calibration of a Freeze-Thaw Prediction Model for Spring Load Restriction Timing in Northern New England." *Cold Regions Engineering 2012: Sustainable Infrastructure Development in a Changing Cold Environment*, ASCE Publications, 369-379.
- Miller, H., Cabral, C., Kestler, M., Berg, R., and Eaton, R. "Comparative Analyses of Methods for Posting Spring Load Restrictions." *Proc., Proceedings of the 10th International Symposium on Cold Regions Development, Anchorage, Alaska June, 2-5.*
- Ovik, J. M., Siekmeier, J. A., and Van Deusen, D. A. (2000). "Improved Spring Load Restriction Guidelines Using Mechanistic Analysis."
- Ray, M., Thriscutt, S., Guerin, M., and Mason, M. (1992). "Road rehabilitation and maintenance in Central and Eastern Europe."
- Rutherford, M. S., Mahoney, J. P., and Hicks, R. G. (1985). *Guidelines for spring highway use restrictions*, Washington State Department of Transportation, Planning, Research and Public Transportation Division.
- Smalkoski, B., and Levinson, D. M. (2003). "Value of time for commercial vehicle operators in Minnesota." *Available at SSRN 1091828.*
- Tighe, S. L., Mills, B., Haas, C. T., and Baiz, S. (2007). "Using Road Weather Information Systems (RWIS) to control load restrictions on gravel and surface-treated highways." Ontario Ministry of Transportation, Downsview, Ontario Canada.
- Tighe, S. L., Mills, B., Haas, C. T., and Baiz, S. (2007). "Using Road Weather Information Systems (RWIS) to control load restrictions on gravel and surface-treated highways."
- Van Deusen, D., Schrader, C., Bullock, D., and Worel, B. (1998). "Springtime thaw weakening and load restrictions in Minnesota." *Transportation Research Record: Journal of the Transportation Research Board*(1615), 21-28.
- Yesiller, N., Benson, C. H., and Bosscher, P. J. (1996). "Comparison of load restriction timings determined using FHWA guidelines and frost tubes." *Journal of cold regions engineering*,

10(1), 6-24.

Zarrillo, M., Miller, H., Balasubramanian, R., Wang, H., Berg, R., Eaton, R., and Kestler, M. (2012). "Preliminary Development of a Real Time Seasonal Load Restriction System for Remote Sites." *Cold Regions Engineering 2012: Sustainable Infrastructure Development in a Changing Cold Environment*, ASCE Publications, 380-390.